Degree PhD Year 2008 Name of Author AL-HO
Hel

COPYRIGHT

This is a thesis accepted for a Higher Degree of the University of London. unpublished typescript and the copyright is held by the author. All consulting this thesis must read and abide by the Copyright Declaration belo

COPYRIGHT DECLARATION

I recognise that the copyright of the above-described thesis rests with th and that no quotation from it or information derived from it may be published the prior written consent of the author.

LOANS

Theses may not be lent to individuals, but the Senate House Library ma copy to approved libraries within the United Kingdom, for consultation solel premises of those libraries. Application should be made to: Inter-Library Senate House Library, Senate House, Malet Street, London WC1E 7HU.

REPRODUCTION

University of London theses may not be reproduced without explicit permission from the Senate House Library. Enquiries should be addresse Theses Section of the Library. Regulations concerning reproduction vary a to the date of acceptance of the thesis and are listed below as guidelines.

A. Before 1962. Permission granted only upon the prior written conse author. (The Senate House Library will provide addresses where possi

B. 1962-1974. In many cases the author has agreed to permit copyi completion of a Copyright Declaration.

C. 1975-1988. Most theses may be copied upon completion of a C Declaration.

D. 1989 onwards. Most theses may be copied.

This thesis comes within category D.

☑ This copy has been deposited in the Library of _____

☐ This copy has been deposited in the Senate House Library, Senate House, Malet Street, London WC1E 7HU.

Age-related changes in retinal pigment epithelium

Dr Heba Al-Hosaini

Supervisor: Professor Glen Jeffery

Submitted for the Degree of Doctor of Philosophy

Institute of Ophthalmology

University College London

2008

ProQuest LLC
789 East Eisenhower Parkway
P.O. Box 1346
Ann Arbor, MI 48106-1346

Abstract

The retinal pigment epithelium (RPE) is a monolayer of hexagonal organized cells located between the choriocapillaris and the neurosensory retina. As the RPE is implicated in a range of eye diseases, an understanding of its structure and ability for self renewal is critical for therapeutic strategies.

Analysis of human RPE cells at the extreme periphery of the retina reveals a population larger in size than those in the centre, they are highly irregular and form an annulus of 4–5 mm. Although binucleation in humans is rare, 10% of these cells are binucleated. In the central region these large binucleated cells are only found adjacent to drusen, which are age-related lipid-rich deposits.

Compared with humans, rat RPE is relatively homogeneous, however, the majority of its cells are binucleated, particularly in the central region. Human and rat RPE also shows different patterns of aging. In humans, the centre of the retina shows a significant reduction in RPE cell density with age, which was not observed in aged rats.

The capacity of mature RPE cells to enter the cell cycle was investigated using a proliferative marker in rats. Here a subpopulation of mature peripheral RPE cells had the capacity to enter the cell cycle, and one-third of these cells completed cellular division. As RPE proliferation occur in response to retinal detachment, this was performed on rats and the patterns of gene expression in RPE examined. An increase was observed in nestin, PCNA and Ki67 expression, which was also confirmed at a protein level by immunohistochemistry. These results suggest that RPE cells have the capacity to proliferate and may possibly differentiate if subjected to appropriate stimuli in a normal retina.

List of abbreviations

- AMD age related macular degeneration.
- atRal all-trans-retinaldehyde
- B2M β-2-microglobulin
- Bp base pair
- **CB** cone bipolar cells
- CCD charge couple device
- CDK cyclic dependent kinase
- CMZ ciliary margine zone
- CNTF ciliary neurotrophic factors
- 11cRAL 11-cis-retinaldehyde
- Ct cycle threshold
- DA dark agouti rats
- DAPI 4, 6-diamidino-2-phenylindole dihydrochloride
- Dcx double cortin
- ERKs extracellular signal-regulated kinase
- FGF fibroblast growth factor
- GCL ganglion cell layer
- HPR1 hypoxanthine phosphoribosyl transferase 1
- IMH isomerohydrolase
- INL inner nuclear layer
- IPL inner plexiform layer
- MAPKS mitogen-activated protein kinase
- Mel melanopsin
- OPL outer plexiform layer
- PCR polymerase chain reaction
- PDGF platelets-derived growth factor
- PEGF pigment epithelium-derived factor

- PIS photoreceptor inner segments
- POS photoreceptor outer segment
- QRT quantitative real-time
- RGC retinal ganglion cells
- Rho rodopsin
- ROS reactive oxygen species
- RPE retinal pigment epithelium
- SDS sequence detector soft ware
- Shh sonic hedgehog
- TBP TATA box binding protein
- VEGF vascular endothelial growth factor
- VZ ventricular zone

Table of Contents

Table of Figures.....9

Declaration.....12

List of collaborators.....13

Dedication.....14

Acknowledgements.....15

Chapter 1: General Introduction to the Eye

1.1 The mammalian eye..... 17

1.2 The retina..... .18

1.3 Comparison of central and peripheral retina.....23

1.4 Blood supply to the retina..... 24

1.5 Retinal pigment epithelium..... 25

1.5.1 General topography..... 26

1.5.2 RPE cell function..... 28

1.5.3 Phagocytosis..... 29

1.5.4 Transepithelial transport..... 31

1.5.5 Absorption of light and protection against photo-oxidation.....32

1.5.6 Secretion.....33

1.6 Phototransduction cascade.....34

1.7 RPE development.....35

1.8 Age-related changes in the retina.....37

Chapter 2: Methods and materials

2.1 Materials and methods for human tissue.....43

2.1.1 Tissue preparation.....43

2.1.2 Sampling method.....43

2.1.2a Single RPE strip analysis of human RPE cell size.....44

2.1.2b Analysis of RPE cell size and regularity from two donors

aged 17 & 58 years 45
2.1.2c Analysis of RPE cell size, matrix of regularity, and
binucleation in six human retina.....45
2.1.3 MatLab analysis.....47
2.1.4 Neural retinal rim analysis.....48
2.1.5 Central and equatorial RPE cell analysis.....48
2.1.6 RPE analysis around drusen 49
2.2 Material and methods for rat tissue.....51
2.1.1 Tissue source.....51
2.2.2 DAPI staining.....52
2.2.3 Morphometric analysis.....52
2.3 Statistical analysis.....53
2.4 Antibody introduction.....53
2.5 Tissue staining.....58
2.6 BrdU analysis.....61
2.7 L-DOPA affect on the cell cycle.....62
2.8 The adaptive state of the retina.....63
2.9 Retinal detachment 64
2.10 Retinal detachment analysis.....66
2.11Gene expression methods 66
2.11.1 Total RNA extraction.....66
2.11.2 Estimating concentration of RNA.....66
2.11.3 First strand cDNA synthesis.....67
2.11.4 Primer design.....68
2.11.5 Polymerase chain reaction.....70
2.11.6 Gel electrophoresis.....70
2.11.7 DNA gel extraction.....71
2.11.8 Sample sequencing.....71
2.11.9 Real-time quantitative RT-PCR.....73

2.11.10 Data analysis.....77
2.11.11 Normalization of data.....80
2.11.12 Statistical analysis.....81

Chapter 3: RPE cell topography in human and rat

3.1 Introduction to topographical variation in human RPE cells.....82
3.2 Results.....85
3.2.1 Central to peripheral variation in human RPE cells size.....85
3.2.2 Regional variation of RPE cell size and regularity
of the entre retinal surface.....88
3.2.3 Comparison of human and rat RPE.....91
3.2.4 Age-related changes in central and equatorial RPE.....96
3.2.5 Cone-rich retinal rim analysis.....99
3.3 Discussion.....100

Chapter 4: The lateral affect of drusen on human RPE

4.1 Introduction to drusen.....105
4.2 Results.....109
4.3 Discussion.....112

Chapter 5: Peripheral RPE cell entering the cell cycle in rats

5.1 Introduction.....116
5.2 Results.....118
5.2.1 Peripheral RPE cells entering the cell cycle.....118
5.2.2 RPE65 & Ki67 colocalization.....132
5.2.3 Effect of L-DOPA on RPE cell entering the cell cycle.....134
5.2.4 The light-adaptive state of the retina.....135
5.2.5 Discussion.....136

Chapter 6: Changes in RPE cell gene expression after retinal detachment

6.1 Introduction 144

6.1.1 Retinal detachment.....144

6.2 Results 153

6.2.1 Retinal detachment.....153

6.2.2 Changes in gene expression in retinal detachment.....157

6.3 Discussion 161

General discussion 167

Appendix.....169

Data analysis (Delaunay triangulation).....169

Cell size and regularity measurements.....170

Simulation.....171

References.....173

Figures

1. Gross anatomy of the eye.....19
2. Schematic diagram of the retina.....20
3. Schematic diagram of the photoreceptors.....21
4. Central and peripheral retina.....24
5. The retina's blood supply.....26
6. Schematic representation of the RPE/photoreceptor complex.....27
7. Cartoon of the retinal pigment epithelium function.....29
8. Phagocytosis.....31
9. Diagram of the visual cycle.....36
10. Scanned image of outline of RPE cells.....44
11. Outline diagram of the retina and sampling methods.....46
12. Triangulation used in Matlab analysis.....47
13. Concept of drusen analysis
14. DAPI labelling in RPE cells.....53
15. Cell-cycle distribution for immunocytochemical staining.....54
16. The proliferative and non-proliferative zone.....61
17. Induced retinal detachment.....
18. Method of analysis of Ki67 distribution in retinal detachment.....64
19. Agrose gel electrophoresis.....71
20. Melting peak for HPR.....74
21. Amplification plot.....78
22. Images of peripheral and equatorial RPE cells.....85
23. Drawing of a strip of RPE.....86
24. Analysis of a radial strip from peripheral to central retina.....87
25. Comprehensive retinal surface analysis.....89
26. RPE cell topography in humans.....93
27. Images of central and peripheral RPE cells in human and rat.....94

28. RPE cell topography in rats.....95
29. Age-related changes in central and equatorial RPE in humans.....97
30. Age-related changes in central and equatorial RPE cell in rats.....98
31. The peripheral RPE and corresponding neural retina.....99
32. Drusen.....106
33. Retinal changes in age-related macular degeneration.....108
34. Images of RPE surrounding drusen.....109
35. Effect of drusen on RPE cells.....111
36. RPE cell double labelled with Ki67 and CRALBP.....118
37. Labelling patterns in a whole-mounted retina in pigmented animals.....120
38. Labelling patterns in an albino rat's whole-mounted retina 121
39. The distribution and relative number of Ki67 cells in pigmented and albino retina 122
40. Effect of age on RPE cells in pigmented and albinos.....123
41. Ki67-positive cells in humans.....124
42. The distribution of binucleated cells in pigmented and albino rats.....125
43. The distribution of Ki67 positive cells during development.....126
44. The number of Ki67 positive cells during development.....127
45. Effect of age on peripheral RPE binucleated.....128
46. Formation of plasma membrane between dividing cells.....129
47. BrdU labelling in RPE cells.....130
48. Migration of BrdU labelled cell beyond the proliferative zone.....131
49. BrdU labelling in mononucleated and binucleated cells.....132
50. Central and peripheral density of RPE65.....133
51. Colocalization of Ki67 labelling and low density RPE65 labelling 134
52. Effect of L-DOPA on cell entering the cell cycle.....135
53. Effect of light on cell entering the cell cucle.....136
54. Retinal detachment.....144
55. Remodelling occurring in retinal detachment.....145

56. The cell cycle.....147
57. Ki67-labelled cells in retinal detachment.....153
58. The association between duration of retinal detachment and RPE cell proliferation.....154
59. The effect of retinal detachment and the monolayer sheet of the RPE under retinal detachment.....155
60. The relative density and distribution of Ki67 due to retinal detachment.....156
61. The effect of retinal detachment on the number of proliferative RPE cells.....157
62. Level of expression of PCNA.....158
63. Level of expression of Ki67.....159
64. Level of expression of Nestin.....160
65. Nestin labelling in RPE cells.....161
66. Delaunay triangulation.....172

Declaration

I declare that this thesis, submitted for the degree of Doctor of Philosophy, is of my own composition, and the data presented herein is my own original work, unless otherwise stated.

A list of collaborations, with details of experiments undertaken in conjunction with others, is provided on the following page.

List of collaborations

(1) Analysis of the lateral effect of drusen on RPE cells (Figure 35) was undertaken with the help of a BSc student, Matthew Schneiders.

(2) Collecting the data for the effect of aging on human RPE cells (Figure 29) was undertaken with the help of a Bsc student Golnaz Shahabi.

(3) The program used to analyse RPE cell sizes and matrix of regularity was designed by Peter Lundh.

(4) Retinal detachments were all undertaken by Robert McLaren (chapter 4).

Dedication

"To the soul of my mother.....

To my daughters Yasmeen and Jinan ...

Whose discipline and love gave me the eyes to see grace"

Acknowledgements

I would like to thank the University of Kuwait for sponsoring me and this work. I would like to thank my supervisor, Glen Jeffery, for his constant supervision throughout all stages of this project, in addition to supporting me in all the difficult times I have been through in this period. Many thanks also to Peter Lundh, Ma'ayan Semo, Anthony Vugler, Golnaz Shahabi, Jaimie Hoh Kam and Matthew Schneiders for their assistance during various parts of this project.

I would like to thank all my family, especially my sister Hana, and friends for their continuous support. Thanks especially to my friend Mariam who believed in me and encouraged me, Najla for putting up with me, and Manal who made me laugh when I am crying. Finally I would like to thank my parents, especially my mother who supported me through all my years of study but did not live long enough to see her dream come true. In conclusion, I would like to thank everyone who has helped me in any way to make this journey an enjoyable one.

Chapter 1

General Introduction to the Eye

1.1 The mammalian eye

The vertebrate eye develops from bulges that grow from the neural tube. These bulges, the optic vesicles, remain attached to the diencephalon by the optic stalks. When the vesicles reach the head ectoderm, this thickens to form the lens placodes. The optic vesicles invaginate to form optic cups, the outer layer of the cup ultimately developing into the melanin-containing pigment epithelium and the inner layer becoming the neural retina.

Figure 1 shows the structure of the human eye. The cornea is a curved transparent membrane and represents the first boundary between the air and the eye. The cornea does not contain blood vessels and is nourished by the aqueous humour (the watery fluid between the cornea and the lens). Posterior to the cornea is the iris, which is embedded with muscles that cause the pupil to enlarge or contract. Behind the pupil is the lens, which is suspended by ligaments to the ciliary muscles. The function of these muscles is to change the shape of the lens and help the eye to adjust focus to different viewing distances. The globe of the eye is filled with a viscous fluid (vitreous humour) which acts as a cushion for the eye and maintains its spherical shape.

The retina lines the innermost surface of the eye and contains two different kinds of light-sensitive cells; rods and cones. The fovea defines the centre of the retina which is the region of highest visual acuity. The area in and around the fovea has a pale yellow pigmentation and is called the macula.

Figure 1. Gross anatomy of the eye: saggital section through the adult human eye. RPE=retinal pigment epithelium; SR=sensory retina; CB=ciliary body. Adapted from W. Barry VanWinkle. (http://medic.med.uth.tmc.edu/Lecture/Main/eye.htm)

1.2 The Retina

The neural retina is a layered structure with three distinct cell body layers (Fig. 2), and two plexiform layers, which contain the neuronal processes and synaptic contacts. There are essentially five major cell types in the retina: photoreceptors; cells located in the outer retina; the bipolar amacrine and horizontal cells of the inner retina; and the ganglion cells in the ganglion cell layer (GCL).

In the simplest sense, photons of light are detected by the photoreceptors, which lie at the back of the retina furthest from the incoming rays of light. This information is passed to the second-order bipolar cells, which are connected to ganglion cells, whose axons pass out of the retina via the optic nerve and send visual information to the retinorecipient regions in the brain. The amacrine and

horizontal cells provide further processing of the light signal and enhance the function of the retina.

Figure 2. (left) Cross-section of an immunostained mouse retina. Photoreceptor immunolabelled with anti-cone arrestin (bluish-purple), amacrine and ganglion cells immunstained for calbindin (red) and bipolar cells immunstained for GFP (green). (right) Schematic diagram illustrates the distribution of retinal cell types in various layers. The adult vertebrate retina is a highly specialised, stratified tissue with distinctive nuclear and plexiform layers. Rod (R) and cone (C) photoreceptors form an outer nuclear layer that contact rod and cone bipolar cells (RB, CB) and horizontal cells (H); Bipolar cells relay information from the outer retina to the inner retina where they synapse onto retinal ganglion cells (G) cells and amacrine cells (A); OPL is the outer plexiform layer and IPL the inner plexiform layer. The left cross-section of an immunostained mature mouse retina shows lamination of cell bodies and synaptic photoreceptors. Adapted from Rachel Wong's website (http://wonglab.biostr.washington.edu/Research.html#Retina)

Photoreceptors are classified into three types; rods, cones and melanopsin photoreceptors, the latter being a small number of intrinsically photosensitive retinal ganglion cells (Bellingham *et al.*, 2006). In mammals there is only one type of rod, and usually two types of cones (M and S); primates however, have three classes of cones (L, M and S). These are distinguished by the wavelength

of light to which they are sensitive: L= long-wave sensitive; M= medium wave; and S= short wave.

The photoreceptor cells are highly specialized, polarized cells. The outer segments (OS) contain membranous stacks of discs packed with photosensitive visual pigment, opsin. The inner segments (IS) consist of myoid, ellipsoid and nuclear regions. The ellipsoid is densely packed with mitochondria, and the myoid contains the cell's rough endoplasmic reticulum and Golgi apparatus (Fig. 3), reviewed in Rodieck (1998). The cell bodies of the photoreceptors reside in the outer nuclear layer (ONL).

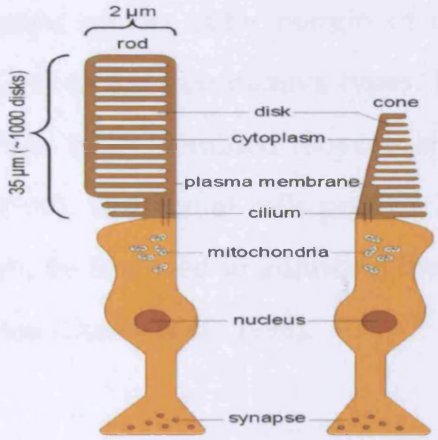

Figure 3. Schematic diagram of cone and rod photoreceptors. The outer segments contain membranous stacks of discs. The inner segments consist of myoid, ellipsoid and nuclear regions. The ellipsoid is densely packed with mitochondria, and the myoid contains the cell's rough endoplasmic reticulum and Golgi apparatus.

Photoreceptors are not distributed evenly throughout the retina. One of the characteristic features of a primate's retina is the high density of rods throughout the periphery. In humans, for example, rods outnumber cones by twenty-five to one in the midperiphery (Curcio *et al.*, 1990). On the other hand the fovea is exclusively occupied by cones, and they are at their highest density

there. However, Williams (1991) showed that cones also occupy the first 1 mm of the extreme peripheral retina (Williams, 1991). Rods are relevant for monochromatic vision and are very light sensitive, while cones enable colour vision and are relatively less sensitive.

The rods and cones synapse onto bipolar and horizontal cells in the outer plexiform layer (OPL). Bipolar cells receive inputs either from rods (rod bipolar) or cones (cone bipolar), but not from both. These cells then convey light information to the ganglion and amacrine cells, making contact in the inner plexiform layer (IPL).

Horizontal cells are situated on the outer margin of the inner nuclear layer (INL). In most mammals there are two distinct types, HI and HII, but in rats and mice only one type has been identified (Boycott *et al.*, 1987; Wassle *et al.*, 1989; Hack and Peichl, 1999). Horizontal cells provide feedback onto the rods and cones, and they might be involved in adjusting the retinal response to the overall level of illumination (Dacey *et al.*, 1996).

Amacrine cells make synaptic contacts onto ganglion cells and also make inhibitory contacts with the bipolar cells in the IPL. There are many different kinds of amacrine cells that seem to have diverse functions. For example, there are dopaminergic amacrine cells, whose dopamine release influences several processes in the retina that are involved in its adaptation under light and dark conditions (Masland, 2001).

In most mammals, retinal ganglion cells (RGCs) have been classified into three categories; I, II and III, based on morphology and projection (Dreher et al., 1985; Martin, 1986). In the mouse, type I cells have both large soma and large dendritic fields, type II cells have small to medium-sized soma with small

dendritic fields and type III have small to medium-sized soma and large dendritic fields (Matsuo *et al.*, 1993). It should be pointed out that the cell bodies of ganglion and amacrine cell types are not restricted to the GCL and INL, respectively. In rat and mouse retinae approximately 2% of ganglion cells have their cell bodies within the INL (Drager and Olsen, 1981), and ~59% of cells within the ganglion cell layer are displaced amacrine cells (Jeon *et al.*, 1998).

The retina also contains three types of glial cell; Müller cells, astrocytes and microglia. The Müller cells are the principal glial cells in the retina with their cell bodies positioned in the INL. The neural retina is entirely bounded by the highly resistant seals of the Müller cells. The microvilli of Müller cells project apically to surround the photoreceptor cell bodies, and distally to surround blood vessels within the retina. These cells carry out diverse metabolic support functions for the neural retina: they control homeostasis by the uptaking of K^+; they remove neurotransmitters from the extracellular space following release from synaptic terminals; they may also control extracellular pH by facilitating the removal of CO_2 by the production of the enzyme carbonic anhydrase; and also they nourish retinal neurons from glycogen stores (Newman and Reichenbach, 1996).

During development, the astrocytes of the retina migrate in from the brain via the optic nerve: they are mostly found within the optic nerve fibre layer where they envelop ganglion cell axons, they also cover blood vessels and may form part of the blood retinal barrier. Astrocytes may function in homeostasis by K^+ and neurotransmitter uptake (Chan-Ling, 1994). The microglia are mesodermal in origin and are found in every retinal layer. In response to retinal injury, they become macrophagic and phagocytose-degenerating neurons (Chan-Ling, 1994).

1.3 Comparison of central and peripheral retina

In humans, the thickness of the retina varies between central and peripheral (Fig. 4), this is due to the increased packing density of photoreceptors, particularly the cones, and their associated bipolar and ganglion cells. In the foveal region, the cones have oblique axons displacing their cell bodies from their synaptic pedicles in the OPL. These oblique axons have accompanying Müller cell processes from the Henle fibre layer, which is the layer of the inner cone fibres in the central area of the retina, which is absent in the peripheral retina.

Figure 4. (A) Light micrograph of a vertical section through the central retina and (B) peripheral retina showing an increase in central retinal thickness due to the increase in packing density of photoreceptors, particularly the cones, and their associated bipolar and ganglion cells. The arrow point to the location of Henle fibre layer, which is the layer of the inner cone fibres in the central area of the retina. (webvision.med.utah.edu/imageswhusect.jpeg)

The INL is also thicker in the central area of the retina compared with the peripheral retina; this is due to a greater density of cone-connecting second-order neurons (cone bipolar cells) and more closely-spaced horizontal and amacrine cells concerned with the cone pathways.

Another difference between the central and peripheral retina can be seen in the relative thicknesses of the IPL, GCL and nerve fibre layer (NFL). This is again due to the greater numbers and increased packing density of ganglion cells needed for the cone pathways in the cone-dominant foveal retina compared to the rod-dominant peripheral retina. The greater number of ganglion cells means more synaptic interaction in a thicker IPL and greater numbers of ganglion cell axons coursing to the optic nerve in the nerve fibre layer.

1.4 Blood supply to the retina

There are two sources of blood supply to the mammalian retina; the central retinal artery and the choroidal blood vessels. The choroid receives the greatest ocular blood flow (65–85%) and is vital for the maintenance of the outer retina (Henkind et al., 1979). The remaining 20-30% flows to the retina through the central retinal artery from the optic nerve head to nourish the inner retinal layers.

The central retinal artery has four main branches in the human retina. The choroidal arteries arise from long and short posterior ciliary arteries and branches of Zinn's circle (around the optic disc). Each of the posterior ciliary arteries breaks up into fan-shaped lobules of capillaries that supply localized regions of the choroid (Hayreh, 1975). The arteries pierce the sclera around the optic nerve and fan out to form the three vascular layers in the choroid; the outer, medial and inner layers of the blood vessels. This is clearly shown in the corrosion cast of a cut face of the human choroids in Figure 5 (Zhang, 1994). The corresponding venous lobules drain into the venules and veins that run anterior towards the equator of the eyeball to enter the vortex veins. One or two vortex

veins drain each of the four quadrants of the eyeball. The vortex veins penetrate the sclera and merge into the ophthalmic vein.

Figure 5. The three vascular layers in the choroid: outer arteries and veins (red/blue arrow), medial arterioles (red arrow) and inner capillary bed (yellow star). Corrosion cast of a cut-face of the human choroid. Adapted from Zhang 1994.

1.5 Retinal pigment epithelium

1.5.1 General topography

The retinal pigment epithelium (RPE) consists of a continuous hexagonal monolayer of cells beginning at the edge of the optic nerve head and extending peripherally to the ora serrata. There are around 3.6 million RPE cells in a human retina (Boulton and Dayhaw-Barker, 2001).

Figure 6 shows the general structure of an RPE cell. The apical membrane of the RPE is rich in two types of microvilli which project into the photoreceptor space (Hogan, 1971). The first type has long thin microvilli (5–7 nm), which lie between the outer segments of the photoreceptors and make no contact with them. The second type has a shorter, more specialized form of microvilli (3–4

nm), which form a sheath around the outer segments of the photoreceptors (Cardillo-Piccolino *et al.*, 1989). The basal membrane of the RPE faces the choriocapillaris and exhibits numerous invaginations which increase the overall membrane surface area (Hogan, 1971).

Two essential features of the RPE are its polarity and barrier properties. The RPE is polarized, because it separates the neural retina from the fenestrated capillaries in the choroid. The apical membrane of RPE interacts with the photoreceptors; the basal membrane interacts with the choroid. Like other epithelia, the apical and basolateral membranes have different protein compositions that enable each to interact with different environments reviewed in (Rizzolo, 1997; Strauss, 2005).

Figure 6. A schematic representation of the RPE/photoreceptor outer segment complex. The apical membrane of the RPE is rich in two types of microvilli (MV), long and short. The basal membrane of the RPE exhibit numerous basal invaginations (BI) and is separated from the choriocapillaris by Bruch's membrane. The cytoplasm of RPE cells contains a large number of organelles including a nucleus (N), melanin (M) and lipofuscin granules (L). Intercellular junctions like the gap junction (GAP), tight junction (TJ) and apical junction (AJ) form between neighbouring cells which extend in a continuous fashion around the entire lateral membrane of each cell. Adapted from Rizzolo 1997 (http://info.med.yale.edu/surgery/anatomy/Rizzolo/rizzolo%20fig1.html)

Human RPE is densely packed with melanin-containing pigment granules called melanosomes. Melanogenesis takes place in the early stages of the embryonic development of the RPE and is over by birth (Zinn KM, 1979). This involves the generation of premelanosomes in the smooth endoplasmic reticulum and synthesis of tyrosinase, an enzyme essential for melanogenesis. In the foetus, RPE cells of the macular area are less pigmented than in other RPE regions, whereas in adults, the highest concentration of melanin is recorded in the macular and mid-peripheral region (Ts'o and Friedman, 1968).

Melanin granules have two shapes; ellipsoid, located at the apical region, and spherical in the midpoint. The function of these cells is to attenuate the impinging radiation by light scattering. Melanin also has a role in regulation and maturation of the retina. In albinos the central retina is underdeveloped, the fovea fails to develop and there is a reduction in rod numbers more than for cones, due to the deficiency in melanin (Neveu *et al.*, 2003; Gimenez *et al.*, 2005).

Together with Bruch's membrane the RPE forms the retinal blood barrier. Bruch's membrane is about 2μm thick, formed by the basal laminae of the choriocapillaris and the RPE, with an intervening zone of collagen and elastic tissue forming a five-layered structure (Feeney and Hogan, 1961; Hogan, 1961). The five layers consist of: 1- The basement membrane of the retinal pigment epithelium; 2- The inner collagenous zone, which is a central band of elastic fibres of about 0.8 μm; 3- Central band of elastic fibers, 4- The outer collagenous zone, which is similar in structure to the inner collagenous zone; and 5- The basement membrane of the choriocapillaris.

1.5.2 RPE cell function

RPE cells have many complex functions such as light absorption, uptake, processing, and transport of retinoids that subserve vision, as well as phagocytosis of rod and cone outer segments (Fig. 7). Uptake and transport of retinol are mediated by receptors on the basolateral sides of the RPE and by cytosolic retinol- binding proteins that carry retinol to the interphotoreceptor matrix to be distributed to the photoreceptor.

Figure 7. A cartoon of the retinal-pigmented epithelium's function in vision. From left to right, the RPE's functions are: to absorb stray light; to transfer metabolites and waste to and from the photoreceptors; retinal glia (Müller) cells clear excess K+ ions; to recycle the retinal molecules involved in phototransduction; phagocytose optic disks and secrete angiogenic vascular endothelial growth factor (VEGF); and anti-angiogenic platelet-derived growth factor (PEDF). VEGF plays a naturally protective role of maintaining adequate blood flow to the RPE and photoreceptors. PEDF is an autocrine growth factor, which causes RPE cells to migrate and proliferate. The RPE cell microvilli extend towards the top of the diagram to wrap around the rod and cone photoreceptors. Situated below the RPE are BM and then the choroid vasculature. Figure adapted from Strauss 2005.

RPE cells also transport ions, water and metabolic end products from the subretinal space to the blood (Miller and Edelman, 1990) and take up nutrients such as glucose, retinol, and fatty acids from the blood and deliver these to photoreceptors (Strauss, 2005).

1.5.3 Phagocytosis

As time passes, the concentration of light-induced toxic substances increases inside the photoreceptors (Beatty *et al.*, 2000). Therefore, to maintain their function, the outer segment (Saari *et al.*) undergoes a constant renewal process (Bok, 1993). The tips of the POS photoreceptors are shed and phagocytosed by the RPE. Here the digested molecules and other important molecules, such as retinal or docosahexaenoic acid (DHA), are redelivered to photoreceptors in a manner comparable to the visual cycle (Bok, 1993). For recycling, DHA is removed from phospholipids and redelivered to photoreceptors as a fatty acid (Bazan *et al.*, 1992). Retinal undergoes the RPE-specific part of the visual cycle and is redelivered as 11-cis-retinal to photoreceptors.

The initial step in phagocytosis (Fig. 8) is the specific binding of POS at the apical membrane of the RPE (Thomson et al., 1998). The second step involves activation of a second-messenger cascade, which in turn activates the ingestion of bound POS (Thomson et al., 1998). CD36, MerTK and integrin receptors have all been described as regulators of POS phagocytosis. The macrophage scavenger receptor CD36 was found to regulate the rate of POS internalization (Ryeom *et al.*, 1996; Finnemann and Silverstein, 2001). Tyrosine kinase c-*mer* (MerTK) and $\alpha_v\beta_5$ –integrin receptors are involved in the initialization of phagocytosis (Finnemann, 2003). Cells lacking the MerTK receptor can bind POS but are unable to ingest them (Chaitin and Hall, 1983).

Figure 8. Phagocytosis: the binding of the photoreceptor outer segment (POS) leads to an increase in intracellular InsP3 which acts as an intercellular signal. Integrin is involved in binding POS and that is mediated by receptor tyrosine kinase MerTK. Ingestion involves the macrophage receptor CD36. Coordinate signal transduction occurs through the focal adhesion Kinase (FAK); CD36, macrophage phagocytosis receptor; FAK, focal adhesion kinase; Gas6, growth-arrest-specific protein 6; MerTK, receptor tyrosine kinase c-*mer*; PLC, phospholipase C; and POS, photoreceptor outer segment. Figure adapted from Strauss 2005.

The process of POS shedding and phagocytosis is under circadian control (LaVail, 1980, , 1983; Chen *et al.*, 1999). The major burst of the rods' outer segment phagocytosis takes place shortly after the beginning of the light period, and during the remainder of the light period, the membranes are degraded by the pigment epithelium. In contrast, the major burst of activity of the cones' outer segment takes place early in the dark period, and is then digested by the pigment epithelial cells during the subsequent hours of darkness (Young, 1978).

1.5.4 Transepithelial transport

The RPE has the structural properties of an ion-transporting epithelium, it transports ions and water from the subretinal space (apical side) to the blood (basolateral side). Both the apical and basal membranes contain pumps, facilitative transport systems and passive ion channels such as the electrogenic sodium-potassium pump on the apical membrane and the chloride-bicarbonate exchange transporter on the basal membrane. The net effect of these is to move water across the RPE in the apical to the basal direction. The retina produces large amounts of water, mainly from the considerable metabolic turnover in neurons and photoreceptors.

Intraocular pressure also causes the movement of water from the vitreous body into the retina (Hamann, 2002). The transport of water is very important and is required for close structural interaction of the retina with its supportive tissues in establishment of an adhesive force between RPE and retina (Strauss, 2005).

The RPE also regulates the transport of various ions such as Cl^-, K^+, Na^+ and HCO_3^- to and from the retina. This is essential for the regulation of the pH and the polarization/hyperpolarization of cell membranes (Boulton and Dayhaw-Barker, 2001). Additionally, metabolites and nutrients such as glucose and amino acids are transported from the blood to the photoreceptors via the RPE. Both the apical and the basolateral membranes of the RPE contain a vast amount of glucose transporters (GLUT1 and GLUT3), which allow glucose to be passively transported across both membranes. The asymmetrical distribution and regulation of these specialized transport proteins within the apical and basolateral membranes, which regulate the transport of ions, fluids and metabolites, ensure that the RPE can determine the microenvironment bathing the photoreceptors (Boulton and Dayhaw-Barker, 2001).

1.5.5 Absorption of light and protection against photo-oxidation

The retina is exposed to radiant energy, which is mostly absorbed by the RPE. It is also surrounded by an oxygen-rich environment as it floats on the choriocapillaris. This, together with the high metabolic activity of the RPE, causes the formation of reactive oxygen species (ROS) which cause oxidative damage to cells by harming proteins, DNA and lipids (Boulton and Dayhaw-Barker, 2001). The phagocytosis of the photoreceptor outer segments also produces large amounts of reactive oxygen species (Miceli *et al.*, 1994). To reduce this oxidative damage the RPE has two lines of defence:

1- The absorption and filtering of light by pigments in the RPE, such as melanin, found throughout the RPE and the carotenoids, which are found only in the macula. Melanin, which is found in melanosomes in the RPE cells, is responsible for reducing the levels of light entering the RPE by acting as a neutral filter. The carotenoids, such as lutein and zeaxanthin, however, filter out reactive blue light. Blue light seems to be the most damaging to the RPE cells of adult eyes as it permits the photo-oxidation of lipofuscin components to cell toxic substances (Strauss, 2005).

2- The RPE contains antioxidants which reduce the rate of oxidation reactions by neutralizing ROS. This reduces the damage that is caused by ROS to cellular macromolecules (Boulton and Dayhaw-Barker, 2001). There are two main types of antioxidants found in the RPE, enzymatic and nonenzymatic antioxidants. The enzymatic antioxidants are superoxide dismutase and catalase, both of which are found in high concentrations in the RPE (Miceli *et al.*, 1994). The nonenzymatic antioxidants which accumulate in the RPE include ascorbate, α-tocopherol, carotenoids, glutathione and melanin (Strauss, 2005). Although RPE

cells are able to repair damaged lipids, DNA and proteins (Strauss, 2005), some oxidative damage is still inevitable.

1.5.6 Secretion

The RPE is known to produce and to secrete a variety of growth factors as well as those essential for maintenance of the structural integrity of the retina and choriocapillaris, and survival of the photoreceptors (Cao et al., 1999). Examples of these factors are: fibroblast growth factors (FGF-1, FGF-2, and FGF-5) (Caruelle *et al.*, 1989; Bost *et al.*, 1992, , 1994); transforming growth factor-β (TGF- β) (Kvanta, 1994); insulin-like growth factor-I (Martin et al., 1992); ciliary neurotrophic factor (CNTF) (Cao et al., 1997); platelet-derived growth factor (PDGF) (Campochiaro et al., 1994); VEGF (Adamis *et al.*, 1993); lens epithelium-derived growth factor (LEDGF) (Ahuja *et al.*, 2001); members of the interleukin family (Ishida et al., 2003); and pigment epithelium-derived factor (PEDF) (Dawson *et al.*, 1999; Ogata *et al.*, 2002).

In the healthy eye, PEDF helps to maintain the retinal, as well as the choriocapillaris, structure in two ways. First, it acts as neuroprotective factor against glutamate-induced or hypoxia-induced apoptosis (Cao et al., 2001; Ogata et al., 2001). Second, PEDF was shown to function as an anti-angiogenic factor which inhibits endothelial cell proliferation and stabilizes the endothelium of the choriocapillaris (Dawson *et al.*, 1999; Ogata *et al.*, 2002).

VEGF is a vasoactive factor made and secreted in low concentration by the RPE in a healthy eye (Adamis *et al.*, 1993), where it prevents endothelial cell apoptosis and is essential for an intact endothelium of the choriocapillaris (Burns and Hartz, 1992). VEGF also acts as a permeability factor stabilizing the fenestrations of the endothelium (Roberts and Palade, 1995).

1.6 Phototransduction cascade

The visual pigment opsins stacked in the outer segment membranes belong to the family of seven transmembrane G-protein coupled receptors. These seven transmembrane domains are hydrophobic α-helices that are arranged in the membrane and form a binding pocket in which the chromophore binds (Hargrave, 2001). Three types of opsin are present in humans; rhodopsin, photopsin and melanopsin.

Most opsin pigments contain 11-cis-retinaldehyde (11cRAL) as the light-absorbing chromophore. Absorption of a photon induces the isomeration of 11-cis retinal to all-trans retinol (Hofmann, 1999). Before light sensitivity of the pigment can be restored, the all-trans- retinal must be chemically reisomerized to 11-cis retinal by a metabolic pathway called the visual cycle (Fig. 9). Most steps in this pathway take place within cells of the RPE adjacent to the photoreceptors. The isomeration of all-trans to 11-cis is catalysed by an enzyme activity called isomerohydrolase (IMH) (Rattner *et al.*, 2000).

RPE65 is a retinal pigment epithelial membrane receptor which is abundantly expressed in retinal pigment epithelium expressed in retinal pigment epithelium (Redmond et al., 1998; Znoiko *et al.*, 2002; Gollapalli *et al.*, 2003). Recent studies showed the importance of RPE65 in extracting insoluble atRAL from the membrane, and presents them to IMH (Gollapalli and Rando, 2004; Mata *et al.*, 2004).

Figure 9. Diagram of the visual cycle. Absorption of light by rhodopsin (Rh) changes the conformation of 11-cis retinal to all-trans-retinal and activates rhodopsin (Rh*). All-trans-retinol is then transported to the RPE where it is reisomerized into 11-cis-retinal. Then 11-cis retinal is transported back to the photoreceptor via an interphotoreceptor matrix-binding protein (IRBP). Adapted from Marmor and Wolfensberger 1998.

1.7 RPE development

The RPE is neuroectodermal in origin, it is derived from the outer layer of the optic cup and is continuous with the anterior pigment of the ciliary body (Mann, 1964). RPE cells are generated in a peripheral band which moves outward as cells leave the cell cycle in more central location (Fleming 1996) and complete their last cell division earlier than the overlying layers of the neural retina. Genesis of the RPE has not been extensively investigated in different spacies and only one study showed that RPE genesis in primates begins at E27. Approximately 5% of RPE cells were generated by E33, and 50% by E71. After E85, RPE cytogenesis begins gradually to decrease, and 95% of the cells have been generated by the time of birth (Rapaport *et al.*, 1995).

Melanin production within the eye always occurs first in the RPE, and pigment granules are usually observed between twenty-seven to thirty days of foetal development in humans. Production then ceases within a few weeks, as the cells attain their full complement of granules (Mann, 1964). The resultant granules mature during the first few years of life and in doing so undergo a number of morphological changes (Feeney, 1978). In foetal and postnatal eyes, the entire RPE gradually increases in area due to the increasing size of the eye (Hogan, 1971). This occurs in a disproportionate manner owing to the eye's nonuniform enlargement.

Early in development, the RPE cells undergo a rapid phase of mitosis that is completed prior to the differentiation of the photoreceptors (Mann, 1964). After maturation, the RPE cells are generally considered to be mitotically inactive, although a previous study has noted the presence of two mitotic RPE cells in the adult rat retina (Ts'o and Friedman, 1967). Several studies have shown that the adult mammalian RPE retains the capacity to proliferate under certain conditions, for example in response to injury from intense light exposure (Marshall and Mellerio, 1971; Wallow and Tso, 1973), after cryotherapy (Laqua and Machemer, 1976), or after retinal detachment (Machemer and Laqua, 1975).

In development, the RPE lies adjacent to the retinal ventricular zone (VZ), the outermost layer of the neural retina where progenitor cells undergo repeated cycles of cell division to generate all the neurons and glia of the adult structure. A number of observations suggest that the RPE is required for the normal development of the eye. First, early ablation of the RPE cells leads to disorganization of the neural retina, the arrest of eye growth and ultimately re-absorption of the eye. Ablation of RPE cells at a later time results in disruption of the laminar structure of the neural retina, failure of the vitreous accumulation and adults that are anophthalmic or microphthalmic (Raymond

and Jackson, 1995). Second, studies of albino mammals show that when the RPE lacks pigmentation the neural retina shows developmental defects, including increased cell proliferation and subsequent cell death, a reduction in the rod photoreceptor population and an underdeveloped central retina (Ilia and Jeffery, 1996, , 2000). Thus, the RPE plays a pivotal role in the regulation of cell numbers in the developing neural retina.

1.8 Age-related changes in the retina

Aging has been defined as 'the progressive accumulation of changes with time that are associated with or responsible for the ever-increasing susceptibility to disease and death which accompanies advancing age' (Harman, 1981). Age-related degeneration of the retina is among the most prevalent and feared complications of aging.

Neuronal cell loss is one of the characteristics of aging in humans. Rods appear to be more affected by aging than cones (Curcio *et al.*, 1993). Approximately 15% of all rods are lost between the second and fourth decades and one-third by the ninth decade (Gao and Hollyfield, 1992; Curcio et al., 1993). On the other hand, cone loss usually occurs as a consequence of rod loss, where 6% of cones are lost by forth decay and 23% by ninth decay (Curcio *et al.*, 2000). Aging is also associated with cellular alteration of macular photoreceptors due to exposure to light, including ultraviolet light. This results in damage and accumulation of mitochondrial DNA which induces apoptosis and may play a role in photoreceptor death (Barron et al., 2001).

The number of ganglion cells in the fovea and peripheral retina decreases during aging (Gao and Hollyfield, 1992; Curcio et al., 1993). Inter-neurons between photoreceptor and ganglion cells are also subjected to age-related cell

loss (Alamouti and Funk, 2003). Another feature of aging is changes in astrocytes, which display higher levels of glial fibrillary acidic protein and more cytoplasmic organelles (Prada *et al.*, 1991).

The accumulation of lipofuscin in the RPE is one of the major markers of aging in the retina. Lipofuscin is a by-product of phagocytosis of the photoreceptor outer segments. It progressively builds up in RPE cells during the first decade of life and continues throughout life (Feeney-Burns *et al.*, 1984a; Kliffen *et al.*, 1997; Mata *et al.*, 2000). After phagocytosis, they are degraded by up to forty enzymes (Shamsi and Boulton, 2001) of the comprehensive lysosomal system present within the cells of the RPE. However, despite this extensive lysosomal system, undegradable material still accumulates within the lysosomes to form lipofuscin granules. The age-related accumulation of lipofuscin granules is believed to be damaging to RPE cell function. Studies have shown that lipofuscin is a photoinducible generator of many reactive oxygen species, such as hydrogen peroxide, singlet oxygen and superoxide anion (Sparrow and Boulton, 2005). This causes the inactivation of lysosomes which leads to a build up of nondegradable material and cellular congestion (Shamsi and Boulton, 2001) and ultimately causes cellular dysfunction. It also results in the inhibition of antioxidant enzymes, extragranular lipid peroxidation, cytoplasmic vacuolation and membrane blebbing (Sparrow and Boulton, 2005).

In contrast to lipofuscin, RPE melanin in humans decreases with age (Sarna et al., 2003; Sparrow and Boulton, 2005). RPE produces melanin only during the early stage of its embryonic development. Topographically melanin density shows a slight decrease from the peripheral retina to the posterior pole with an increase in the macular region (Weiter et al., 1986a). This distribution is maintained throughout life, but a significant decline in the total number of granules is observed in all regions after the age of forty years (Feeney-Burns et

al., 1984a). Melanin has an important role as a cellular antioxidant (Sarna *et al.*, 2003) and therefore an age-related decrease in melanin granules results in a decrease in cells' antioxidant potential, as well as an increase in the amount of light entering the RPE.

Another marker of aging is drusen, which is a cellular deposit that accumulates between the retinal pigment epithelium and the choroids. The size numbers and/or degrees of confluence of drusen are associated with aging and are risk factors for the development of age-related macular degeneration (Lewis *et al.*, 1986; Pauleikhoff *et al.*, 1990b; Holz *et al.*, 1994). Although the pathogenesis of drusen has not been fully elucidated, various investigators have proposed that the accumulation of abnormal materials between the outer retina and the choriocapillaris induces RPE and retinal damage by interfering with the exchange of nutrients and waste products by inhibiting bulk fluid flow (Pauleikhoff *et al.*, 1990a).

Some therapeutic strategies for eye diseases, such as macular degeneration or retinitis pigmentosa, point toward replacement of the cellular elements lost due to pathology. However, this requires a better understanding of the topographical variation of the RPE. Further, it is important to define any capacity that it might have to proliferate under normal condition.

In amphibian, retinal neurogenesis dose not cease after the embryonic stage, but continues throughout life. Here, new cells are added continually from the cilliary margin zone to the retina and continue to grow through life (Straznicky and Gaze, 1971; Johns, 1977). Interestingly, retinal detachment/removal in amphibians results in RPE proliferation and its transdifferentiation into the production of a new functional retina (Keefe, 1973; Klein *et al.*, 1990; Reh and Pittack, 1995). This is associated with downregulation of genes normally

expressed by the RPE such as RPE65 and Otx2 (Sakami *et al.*, 2005; Chiba *et al.*, 2006). Recent studies have also shown that many common features exist between the development and the regeneration of the retina in terms of the gene expression of different transcription factors (Kaneko *et al.*, 1999; Kaneko *et al.*, 2001; Goto *et al.*, 2006).

In mammals, recent studies have found quiescent cells located in the pigmented ciliary epithelium, which are capable of proliferating *in vitro* and express neuronal stem cell markers (Ahmad *et al.*, 2000; Tropepe *et al.*, 2001). Further, mammalian RPE cell are also capable of proliferating when the retina is detached (Anderson *et al.*, 1981b; Fisher *et al.*, 1991; Lewis *et al.*, 2002). However, these proliferating cells commonly migrate through retinal breaks associated with the detachment to form pigmented scar tissue within the vitreous (Hiscott *et al.*, 1984; Hiscott *et al.*, 1999). Although it is assumed that RPE cells can not proliferate under normal condition To's & Friedman (1976) noted the presence of two mitotic figures in mature albino rat RPE in fixed preparation. This may suggest that RPE cells have the capacity to proliferate under normal conditions. Hence, mammalian RPE cells may partially mirror amphibian RPE in some aspects however, this hypothesis has not been investigated.

Here I analyse the topographical variation of RPE cell size and the regularity of their distribution across the entire retina in human and rodent, using computational analysis of digital microscopic images (Dryden, Taylor & Faghihi, 1999). I also look at features associated with proliferation such as binucleation, and analyse the distribution of binucleated RPE cells and the association of these cell with drusen, which are age-related lipid-rich deposits found in human. If a cell has the capacity to binucleate, then it may also have the capacity to go though cytoplasmic division as well, which is a key pathway toward tissue repair.

To investigate the capacity of mature RPE cells to enter the cell cycle I immune label rat flat-mounted retina with different cell-cycle markers (Ki67, PCNA, BrdU) in both pigmented and albino animals and analysed the distribution of labelled cells. Further, as mammalian RPE cells proliferation occurs in response to retinal detachment, this operation was employed on rats and the patterns of gene expression in the RPE examined using quantitative real time-PCR.

Chapter 2

Methods and materials

2.1 Materials and methods for human tissue

2.1.1 Tissue preparation

I obtained nineteen human eyes from the Eye Bank at Moorfields Eye Hospital, with Local Research Ethics Committee approval and appropriate consent under the Human Tissue Act 2004 for the use of all human specimens. The eyes (aged 9–93 years) were received 24 to 50 hours post mortem with the corneas removed and fixed with 10% buffered formalin. Using a stereo microscope, the retina and the attached RPE and chorio capillar's were dissected from the sclera. The neural retina was then separated from the RPE-choroid complex and the latter tissue whole-mounted by placing a few radial cuts allowing it to be flattened. The tissue was then mounted on a glass slide with glycerol with the RPE facing upwords.

2.1.2 Sampling methods

As the RPE flat-mount contained approximately 4–6 million RPE cells (Ts'o and Friedman, 1968), it was important to develop a sampling method to cover the maximum number of RPE cells. For that reason, I used three sampling methods in this study to justify the variation occurring across the entire retinal surface and to analyse large numbers of RPE cells. The first sampling method was undertaken on a mature retina (45 years) where a continuous strip spanning the entire radius of a flat-mounted retina was analysed and the size of approximately 3000 RPE cells (2.3.2a) was measured. With this sampling method it was possible to analyse variability in RPE cell size between the central and peripheral regions of the retina. In the second sampling method a comprehensive analysis of RPE cell size and matrix regularity was undertaken for the entire retinal surface. Here two retinae (aged 17 and 58 years) were analysed to verify the variation seen in the first sampling method and in each retina 20,000 RPE cells were analysed (2.3.2b).

Based on the results of the first and second sampling method a new sampling method was developed to analyse the maximum number of eyes. Here three strips spanning the radius of six retinas were analysed and the size and matrix of regularity of 3500 cells were measured in each retina. These strips were picked randomly and they radially trisected the retina in respect to the optic nerve (2.3.3c). Hence the total number of examined RPE cells in this study was approximately ($10x10^4$ RPE cells).

2.1.2a Single RPE strip analysis of human RPE cell size

To investigate any gross variations in RPE cell size across the retina, I examined an RPE flat mount from a 45-year-old donor. The RPE analysed was a single length of RPE which transected the entire radius of the sample. Here trance lucida images were undertaken for a continuous strip of approximately 20 mm length and 150 μm width using light microscopy and drawing tube. Figure 10 shows an example of a trance lucida image of RPE cells representing a sampled area of the strip.

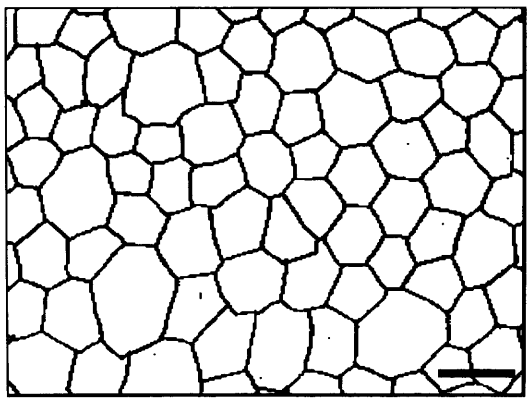

Figure 10. A sample of scanned images of RPE cells from a flat-mount of a 45- year old donor. The image shows the outline of RPE cells which were drawn using light microscopy with an attached drawing tube. Scale bar=20μm.

Each image was then scanned into the computer and analysed for cell size using a programme written with MatLab (Mathworks Inc., Mass, USA; see 2.3.2d). For statistical analysis the retina was divided into two groups – peripheral (0–5mm) and central (5–20mm) – and a T-test was undertaken.

2.1.2b Analysis of RPE cell size and regularity from two donors aged 17 and 58 years

Here a comprehensive topographical analysis of an entire retinal flat-mount was undertaken for two retinae, from subjects aged 17 and 58 years respectively. The retinal surface of the RPE specimens was captured as digital images by using epifluorescence microscopy (Olympus BX50F4, Olympus, Japan, 400 x magnification). Data was captured as 24-bit colour images at 3200 x 2560 px resolution using a Nikon DXM1200 digital camera. A total of 500–600 images were collected along transects from the fovea to the peripheral rim using a motorized microscopic stage (Prior, CS152, Cambridge, UK). In each image cells were analysed within a box measuring 150μm^2 where each box contained approximately 60 cells. The size and matrix of regularity for each cell were measured using MatLab (2.1.3).

2.1.2c Analysis of RPE cell size, matrix of regularity, and binucleation in six human retinae

Six flat-mounted retinae (donor ages of 19, 21, 45, 55, 60 and 79 years) were radially trisected in relation to the optic nerve head (Fig. 11). The three strips of RPE were systematically mapped from the edge of the retina to the centre and then analysed for RPE cell size, regularity and binucleation. In each strip, twenty-five consecutive digital images were captured using light/epifluorescence microscopy (Olympus BX50F4, Olympus, Japan, 400 x magnification). Data was captured as 24-bit colour images at 3200 x 2560 px

resolution using a Nikon DXM1200 digital camera. RPE cell size and matrix of regularity were measured using MatLab (2.1.3). The mean values for the three strips were then calculated for each retina. An ANOVA was conducted to evaluate the difference in RPE cells at each eccentricity. This was followed by Dunnett's multiple comparison tests to identify the statistical significant eccentricity.

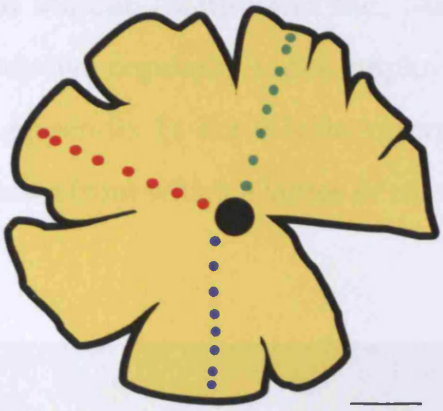

Figure 11. Outline diagram showing the three strips analysed in each retina. Twenty-five consecutive digital images were taken along each strip and analysed for RPE cell size and matrix of regularity. Eight camera lucida drawings were undertaken in each strip to count RPE cells which were binucleated. Here the first two images were taken close to ora serrata at 0.5 and 1 mm eccentricity of it. The other images were taken at an equal eccentricity of 1.5 mm from each other to cover the entire retinal width. Scale bar = 2mm.

The number and location of binucleated cells was explored using the same sampling patterns. Here eight camera lucida drawings were undertaken in each strip, however, the first two images were in close proximity to the ora serrata and to each other. A further six images were then undertaken at 1.5 mm intervals (Fig. 12). The numbers of binucleated cells were counted in the eight images of each strip and calculated as a percentage. The mean values for the

three strips were then calculated for each retina. An ANOVA was conducted to evaluate the difference in RPE cells at each eccentricity. This was followed by Dunnett's multiple comparison tests to identify the statistically significant eccentricity.

2.1.3 MatLab analysis

To measure RPE cell size and regularity the images were analysed using a programme written in MatLab (Mathworks Inc., Mass, USA). This calculated the cell size and the relative regularity index employed, which used a scaleless statistical algorithm (Appendix 1). For this the centre of the cells was recorded as an array of coordinates from which a lattice of triangles was constructed (Fig. 12).

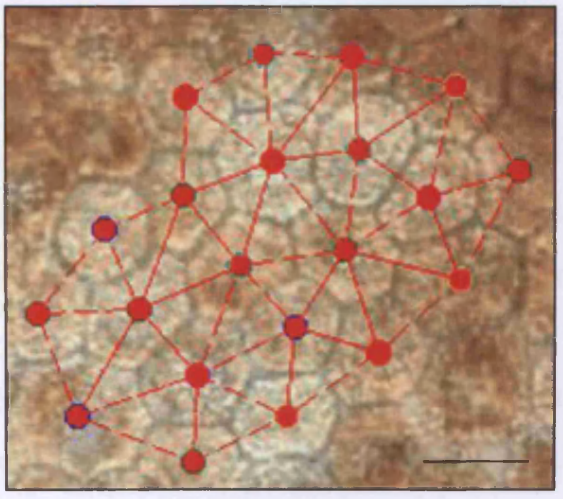

Figure 12. Triangulation pattern applied to the image of retina from a 58-year old donor. The digital image was acquired with light microscopy. The central points of the RPE cells were marked by a mouse click and then the lattice of triangles was constructed. MatLab programme was then used to calculate RPE cell diameter and regularity. Scale bar = 20μm.

This was undertaken within the boxed areas used above. The lengths of the triangles' sides were measured in pixels. This value was used to calculate the

relative irregularity index T, that is a coefficient of variation based on Delaunay triangulations, using the equation given below, where S is the size of the area of triangulation and m is the number of triangles (Dryden, Taylor & Faghihi, 1999).

$$T = \frac{\sum\left(S_i^2 - \bar{S}^2\right)^2}{m\left(\bar{S}^2\right)^2},$$

2.1.4 Neural retinal rim analysis

The human peripheral retina has a cone-rich retinal rim (Wenzel et al., 2001). The aim of this study was to map cone density against changes in peripheral RPE cell morphology. Four eye cups were dissociated and the neural retina was separated from the RPE/choroids layer (2.3.1). Both RPE/choroids and the corresponding neural retina were flat-mounted to be analysed. Consecutive digital images were acquired from RPE strip spinning the first 5 mm of peripheral RPE close to the ora serrata and the corresponding neural retina. These images were reconstructed as strips using Photoshop version CS2.

The neural retinal strip was analysed for the relative distribution of cones. Here images were magnified using Photoshop and the relative location and distribution of cones were marked by a black dot in a different layer then merged with the original neural retinal image and matched to the corresponding RPE region. I did not attempt quantitative analysis of cones since it is beyond the scope of this study.

2.1.5 Central and equatorial RPE cell analysis

The prepared RPE flat-mounted retinae (2.3.1) of twelve eyes aged 9, 21, 33, 37, 45, 53, 61, 70, 75, 78, 82, and 93 years were analysed for the topographical

variations of central and equatorial RPE cells with age. Five digital images were obtained from the macular and equatorial regions for each retina and analysed for cell size and matrix of regularity using MatLab (2.1.3). The macular region was easily identified due to its darker appearance within the RPE layer. However, to ensure that the same region was being looked at in all the tissues, for both central and equatorial areas, the distance from the periphery to the sampled region was measured in each eye. RPE cell density was determined by counting the number of RPE cells in a fixed box measuring 130 x 130μm.

2.1.6 RPE analysis around drusen

The eyes were from donors aged 45, 58, 60 and 73 years and were received and fixed using 4% paraformaldehyde within 24–40 hours post mortem. I carried out the dissection of the eyes using a stereomicroscope aiming to detach and isolate the RPE cell layer from the rest of the eye to produce flat RPE wholemounts. The RPE was then mounted flat in glycerol, cover slipped and left to dry (2.1.1).

I examined the prepared RPE flat mounts using a BX52 Olympus microscope, with an attached drawing tube. Individual drusen were isolated from the equator of the slide-mounted RPE and their coordinates were noted. The cells around drusen were drawn with the aid of the drawing tube at a magnification of X800. The defined image was then scanned, digitized, and recorded in the tagged image file format. The digitized images were then analysed using MatLab (2.1.3). Due to the large size of the images of the drusen and their surrounding RPE they were analysed in individual segments. The graphics system of MatLab presented the transcribed RPE cell boundaries in a window where a grid could then be superimposed to highlight 150μm^2 areas of the image. Proximally increasing the distance from the druse, 150μm^2 segmented

transects could be analysed (Fig. 13) to produce a map of the circumferential influence of the druse upon surrounding RPE cells. The first transect, however, was designed to analyse a 30μm orbital around the entire druse. The programme allowed the druse to be excluded from the analysis. At each 150μm² increment in eccentricity from the druse, four areas were sampled from varied points that were roughly analogous to the cardinal compass points. Within each of the 150μm² quadrants the RPE cell size and matrix of regularity were measured by MatLab.

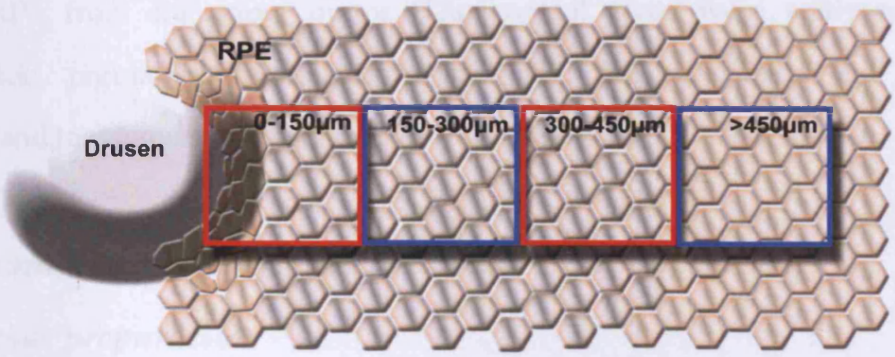

Figure 13. Concept map. Quadrants were analysed within 150μm concentric rings around the druse being analysed. The value for the >450μm ring represents the RPE's control measurements. In the actual investigation the 150μm rings began after 20μm, immediately surrounding the druse (Image created for project by Matthew Schneiders).

The RPE nuclei number was recorded for all the samples within the concentric rings around the drusen. In most instances, the nucleus appeared unambiguously as a circular region devoid of pigment. However, in about 1–5% of the cells, depending on the sample quality, the classification remained in doubt. In such cases, the cell's nucleation was documented as undetermined and excluded from the analysis.

Pigment density of RPE cells was also measured using departmental utility programmes (Image Proplus™) at each eccentricity. The programme allows measurements of pixel density of RPE cell images, which are then converted into arbitrary numbers and compared between different areas.

Control RPE cells

For every 150μm² RPE quadrant analysed, an equivalent area was measured in a drusen-free zone within the same eye at the same longitude from the central region of the eye. This provided a method of comparing the impact of drusen against RPE from the same donor. The control areas were analysed for binucleation, regularity, pigmentation and RPE cell size using the same methods and techniques as the areas within close proximity to the drusen.

2.2 Materials and methods for rat tissue

2.2.1 Tissue preparation

All animal care was in accordance with institutional and Home Office (UK) regulations and the UK Animals (Scientific Procedures) Act 1986. The rats were terminally anaesthetized with carbon dioxide (CO_2) gas and their eyes were immediately enucleated, by microdissection, fixed in 4% paraformaldehyde overnight. In the case of the animals collected at E18, the mother was terminally anaesthetized and the pups removed. The following day, the eyes were dissected using a stereo microscope. The anterior segment of the eye cup was removed, resulting in the release of the major non-retinal components of the eye and the vitreous humour. This exposed the interior of the eye and permitted the neural retina to be drawn away from the RPE-choroid and sclera complex.

2.2.2 DAPI staining for morphological analysis:

As the attached choroids and sclera are too thick to allow transmitted light to be analysed, the tissue had to be stained with 4', 6-Diamidino-2-phenylindole dihydrochloride (DAPI). DAPI was added to the tissue at 1:2500 dilution in PBS for exactly one minute. The eye cups were then turned into whole-mounts by placing 4-5 radial cuts into the cup allowing it to be flattened. The eye cups were then mounted with Victor Shield in order to prevent the tissue from drying and to help maintain the fluorescence. A cover slip was placed on top of the tissue and the slide was sealed and left to dry.

2.2.3 Morphometric analysis of rat RPE cells

To investigate the topographical variation of RPE cells the flat-mounted retinae from a DA rat (age 6 months) were trisected radially into three analytical transects as in human tissue (Fig. 11). Consecutive digital images were taken (Fig. 14) along the three strips of the RPE using motorized microscopic stage and fluorescent microscopy (Olympus BX50F4, Olympus, Japan, 400 x magnification). Along these strips images were analysed within a box measuring 150 x 150 μm and RPE cell size and matrix of regularity were measured using MatLab (2.1.3). The mean values for the three strips were then calculated for each retina. An ANOVA was conducted to evaluate the difference in RPE cells at each eccentricity which was followed by Dunnett's multiple comparison tests. Further in each box the number of cells which were binucleated and mononucleated were counted and calculated as percentages of total the number. The mean values for the three strips were then calculated for each retina. An ANOVA was conducted to evaluate the difference in RPE cell binucleation at each eccentricity. This was followed by Dunnett's multiple comparison test.

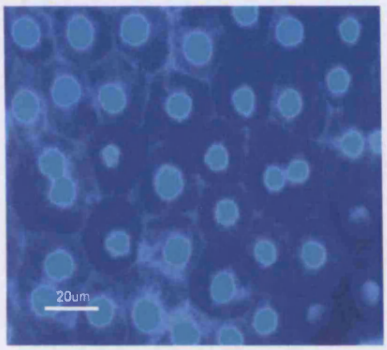

Figure 14. Image of a retinal flat-mount showing DAPI labelling in RPE cells. As the RPE-choroid and sclera complex are too thick to allow transmitted light to be analysed, the tissue had to be stained with DAPI. The tissue was then analysed using fluorescent microscopy to aquire images. Scale=20μm

To explore the effect of age on central and equatorial rodent RPE cells, five rats aged 6 months along with five rats aged 21 months were analysed after they had been stained with DAPI, as above. Here five digital images were obtained from both the equatorial and macular regions and then analysed for RPE cell size and matrix of regularity using MatLab (2.1.3). The RPE cell density was determined by counting the number of cells in a box measuring 130 x 130μm. The results for RPE cell size, regularity and density from the five images were averaged for each area and a T-test was performed between the two age groups.

2.3 Statistics analysis:

Statistical tests were carried out using graphpad Prism (version 3). Analysis of variance ANOVA was used to test the significant variation in RPE cell size, matrix of regularity and binucleation from central to peripheral retina in human. When significant between areas was identified then *post hoc* Dunnett's *t*-test was undertaken. This test compared the tested sampled areas to a control area, which is the area closest to the optic disc. Whereas for rat RPE cell size analysis between central and peripheral retina ANOVA was followed by *post*

hoc new-men keuls, which compare all sampled areas to each other and not to a control area.

2.4 Antibodies used

In this study I examined the RPE in rats and humans using three independent proliferative markers – Ki67, PCNA and BrdU – to assess the latent capacity of this tissue to proliferate. I also used three independent RPE cell markers – RPE65, CRALBP and Otx2 – to confirm the identity of RPE cells (Table 1).

Several studies have shown that these proliferative markers label proliferative cells at different stages in the cell cycle (Brown and Gatter, 2002). Figure 15 show that Ki67 can label proliferative cells through all stages of the cell cycle whereas PCNA and BrdU label cells mainly in the S-phase.

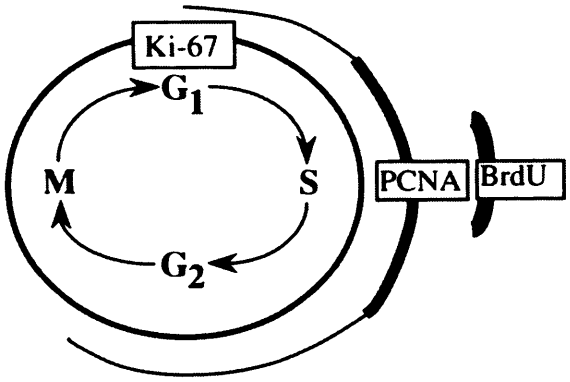

Figure 15. Cell-cycle distribution for immunocytochemical staining of the three proliferative markers Ki67, PCNA and BrdU. The thickness of the line refers to the peak staining. Ki67 labels proliferative cells through all stages of the cell cycle whereas PCNA and BrdU label cells mainly in the S-phase

- ***Ki67***

The primary structure of Ki67 has been established (Schluter *et al.*, 1993). It is a large protein of approximately 395 kDa, encoded for by almost 30,000 base pairs

within the human genome. This protein undergoes phosphorylation and dephosphorylation during mitosis (Schluter et al., 1993).

Several groups have demonstrated that the topographical distribution of the Ki67 antigen is cell-cycle dependent, in the G1 phase the Ki67 antigen is predominantly localized in the perinucleolar region. In the later phases of the cell cycle the antigen is also detected throughout the nuclear interior, being predominantly localized in the nuclear matrix (Braun *et al.*, 1988; Guillaud *et al.*, 1989; Verheijen *et al.*, 1989a). In mitosis, the Ki67 antigen is present on all chromosomes (Gerdes *et al.*, 1983; Gerdes *et al.*, 1984) and appears in a reticulate structure surrounding the metaphase chromosomes (Verheijen et al., 1989a; Verheijen *et al.*, 1989b). Because Ki67 immunostaining rapidly decreases during anaphase and telophase, it has been concluded that the antigen is degraded with a biological half-life of the detectable antigen of less than one hour (Bruno and Darzynkiewicz, 1992).

In contrast to many other cell-cycle associated proteins, Ki67 is consistently absent in quiescent cells and is not detectable during DNA repair (Cabral et al., 1990). Thus, the presence of Ki67 is strictly associated with the cell cycle and confined to the nucleus, suggesting an important role for this structure in the maintenance and/or regulation of the cell division cycle, a point that is confirmed by the finding that removal of Ki67 using antisense nucleotides prevents cell proliferation (Schluter et al., 1993).

- ***PCNA***

Expression of proliferating cell nuclear antigen (PCNA) was originally identified as an antigen expressed in the nuclei of cells during the DNA synthesis phase of the cell cycle (Leonardi *et al.*, 1992). PCNA is clamped to DNA through the processes of DNA replication (Bowman *et al.*, 2004) and it is

important for both DNA synthesis and DNA repair (Essers *et al.*, 2005). PCNA is elevated in the nucleus during the late G1 phase immediately before the onset of DNA synthesis, becoming maximal during the S-phase and declining during the G2 and M phases.

- ***BrdU***

Bromodeoxyuridine or BrdU (5-bromo-2-deoxyuridine) is a synthetic nucleoside which is an analogue of thymidine and used in the detection of proliferating cells (Seki and Arai, 1995; Kuhn *et al.*, 1996). BrdU can incorporate into the newly synthesized DNA of replicating cells during the S phase of the cell cycle, substituting for thymidine. Thus antibody-specific BrdU can be used to detect cells which are actively replicating their DNA. The BrdU technique for *in vivo* labelling of new cells in the brain was first applied to developing animals (Miller and Nowakowski, 1988; Takahashi *et al.*, 1992). The advantage of using BrdU over thymidine is that it could be visualized with immunocytochemical techniques. Furthermore, confocal microscopy can be used to show unequivocal double labelling with BrdU.

- ***RPE65***

RPE65 is a protein predominantly expressed in the retinal pigment epithelium and is a key element in normal RPE function. It plays an important role in the visual cycle, in vitamin A metabolism and ia associated with retinol binding protein and 11-cis-retinol dehydrogenase (Redmond et al., 1998). RPE65 has been reported to associate with the membranes in the RPE, preferentially in the microsomal fraction (Bavik et al., 1991; Hamel et al., 1993). Mutations in the RPE65 gene are associated with autosomal recessive childhood-onset severe retinal dystrophy, Leber's congenital amaurosis (LCA), and some forms of retinitis pigmentosa (Marlhens et al., 1997). The homozygous RPE65 knockout

mouse has shown photoreceptor degeneration and diminished rod response in ERG (Redmond *et al.*, 1998).

- ***CRALBP***

Cellular retinaldehyde-binding protein (CRALBP) is a water soluble protein found only in the retina and pineal (Saari, 1982). It plays an important role in the regeneration of 11-cis-retinal for use in rod visual pigments. Once 11-cis-retinal is photoisomerized in the rod's outer segment, it is converted to all-trans-retinal and further modified into all-trans-retinol. All-trans-retinol then diffuses into the RPE to be converted back to 11-cis-retinol and further oxidized into 11-cis-retinal with the help of CRALBP (Saari and Bredberg, 1990; Saari *et al.*, 1994; Saari *et al.*, 1998). Genetic mutations, resulting in CRALBP's lack of function have been linked to visual disease such as bothnia dystrophy, retinitis punctata albescens and retina pigmentosa. The presence of CRALBP serves as a marker for RPE and Müller glial cells (Saari et al., 2001; Thompson and Gal, 2003).

- ***Otx2***

Otx2 is a homeodomain-containing transcription factor that has an essential role in anterior head formation (Simeone *et al.*, 1992; Simeone *et al.*, 1993). In the vertebrate eye, Otx genes are initially expressed in the entire optic vesicle but their expression soon becomes restricted to the presumptive RPE during optic cup formation, where it is maintained throughout adulthood (Simeone et al., 1993; Bovolenta *et al.*, 1997; Martinez-Morales *et al.*, 2004). Mice deficient in Otx2 show clear defects in the patterning of the RPE, which is replaced by a neural retina-like territory (Martinez-Morales *et al.*, 2001).

Table 1. Antibody used in labelling RPE cells

Antibody	Raised in	Localization	Supplier	Refferance
Ki67	rabbit	nucleus	Novocaster	(Scholzen and Gerdes, 2000)
PCNA	rabbit	nucleus	Abcam	(Jang *et al.*, 2005)
RPE65	mouse	cytoplasmic	Chemicon	(Nicoletti *et al.*, 1995)
Otx2	rabbit	nucleus	Chemicon	(Vernay *et al.*, 2005)
CRALBP	mouse	cytoplasmic	Affinity BioReagents	(Nawrot *et al.*, 2004)

2.5 Tissue staining

- ***Ki67 and PCNA staining***

The rat eye cups containing the RPE were washed four times in phosphate buffer saline (PBS 0.1 M pH 7.4), then blocked with a 5% normal donkey serum in 3% Triton X-100 in PBS for 2 hours. Primary antibody incubation was carried out over night at room temperature at either 1:2000 (Ki67) or 1:500 (PCNA) or 1:1000 (Otx, Chemicon, rabbit polychlonal antibody) dilutions in 3% Triton x-100 in PBS.

Primary analysis was undertaken on tissue stained with Ki67 (Novocaster, Newcastle, UK, rabbit polyclonal antibody). PCNA (abcam, UK, rabbit polyclonal antibody) was used in a confirmatory role, as Ki67 labels cells at all stages of the cell cycle. In most of the albinos and approximately half of the DA rats a second primary monoclonal antibody, RPE65 (Chemicon, Hampshire,

UK, Mouse anti-RPE65, 1:500 dilution) or CRALBP (Affinity BioReagents, Cambrige, UK, Mouse anti-CRALBP, 1:500 dilution) was used to clearly identify RPE cells. Without such staining albino RPE is difficult to image. Following four washes in PBS the eye cup was incubated in the secondary antibody (TRITC donkey anti-mouse, and FITC donkey anti-rabbit, Jackson ImmunoResearch laboratories, West Grove, PA, USA) prepared at 1:200 dilution in 0.3% Triton for 2 hours.

DAPI was added to the tissue after the secondary antibody (1:2500 dilution) in PBS for one minute to label the nuclei of cells. The eye cups were then washed extensively in Tris buffer (0.05 M pH 7.4), mounted flat RPE up with vector shield as a mounting medium, and examined using fluorescent microscopy. The number of rats analysed is shown in Table 1. The same protocol of labelling was used for the RPE sheet taken from human tissue, however, here only Ki67 was used and not RPE65.

Table 2.

Analysis	Pigmented rats		Albino rats		Ki67
	Number	Age	Number	Age	labelling
Pigmented & albino comparison	5	P60	5	P60	+
Affect of age on proliferation	5	P60	5	P60	+
	5	P360	5	P360	+
Developmental analysis	5	E18	5	P10	+
	5	P0	5	P20	+
	5	P5	5	P45	+
	5	P10	5	P60	+
	5	P15			+

	5	P20		+
	5	P25		+
	5	P40		+
	5	P60		+
	5	P150		+

- ***BrdU staining***

Six postnatal 25 day-old DA rats were given an intraperitoneal injection of BrdU (50μg/kg in 0.007 NaOH/PBS) each day for 20 days and then sacrificed one month later after the last dose of BrdU. The animals were terminally anaesthetized with carbon dioxide and the eye cups were fixed in 4% paraformaldehyde for 30 minutes. From each of the six rats one eye was labelled with BrdU and the other one was double-labelled for BrdU and Ki67 or for BrdU and Otx. The eyes which were double-labelled were first incubated overnight with either Ki67 as above or Otx 1:1000 dilutions in 3% Triton x-100 in PBS. The tissue was then incubated in the secondary antibody and fixed in 4% paraformaldehyde for 10 minutes.

Antigen retrieval was the first step in BrdU labelling; this was undertaken by placing the tissue in 6M hydrochloric acid in 1% Triton for 30 minutes. Before incubating in BrdU the tissue was washed extensively with PBS to equilibrate the tissue to a normal pH. The tissue was then blocked with normal donkey serum for 2 hours. BrdU (1:5 dilutions in 3% Triton x-100 in PBS) incubation was carried out overnight at room temperature. Following four washes in PBS, the tissue was incubated in the secondary antibody (TRITC donkey anti-mouse, Jackson ImmunoResearch laboratories, West Grove, PA, USA) prepared at 1:100 dilution in 0.3% Triton for 2 hours. The tissue was then washed once with PBS

and extensively with Tris buffer, mounted flat, RPE up with a vector shield, and examined under a fluorescent microscope.

2.6 BrdU Analysis

The number and distribution of Ki67 and BrdU positive cells were mapped in the RPE flat mounts of both pigmentation phenotypes by marking the position of each cell on a composite map (created using Adobe Photoshop CS version 8) at 400x magnification. RPE65 is a tissue-specific marker normally expressed in all RPE cells and was used to confirm the identity of RPE cells in both pigmented phenotypes. I analysed the distribution of BrdU positive cells in relation to the distribution of Ki67 positive cells. Here the retina was divided into two zones; a proliferative zone, which contains all Ki67 labelled cells, and a non-proliferative zone, which is central to the proliferative zone (Fig. 16).

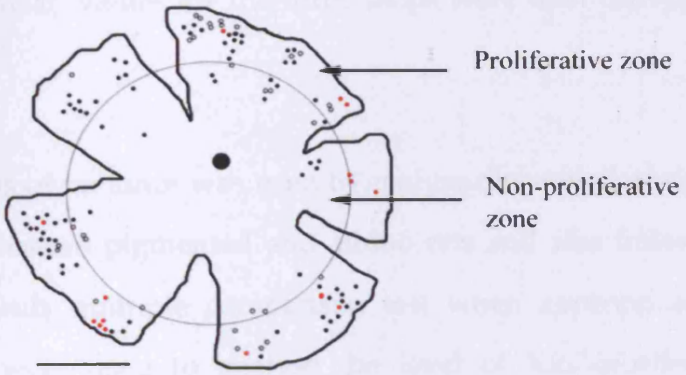

Figure 16. Outline diagram of the retina showing the proliferative and non-proliferative zone. The diagram shows the distribution of positive binucleated (black dots) and mononucleated (black circle) BrdU cells. The red dots represent the relative distribution and density of Ki67-positive RPE cells. The proliferative zone extends from the ora serrata to the nearest Ki67 labelled RPE cell (red dots) from the optic nerve and the non-proliferative zone is the zone central to the proliferative zone. Scale bar = 2mm

The primary aim of using the human tissue was to see if Ki67 cells are detectable in the RPE. Because of the limitation in receiving human donors within 24 hours post mortem, no attempt was made to conduct a complete analysis of Ki67 distribution on human RPE cells.

Many mature rodent RPE cells are binucleated (Stroeva & Mitashov, 1983). To determine the relative distributions of these cells, three strips of RPE were analysed from five pigmented and five albino rats age 60 days. The flat-mounted retinae were radially trisected in relation to the optic nerve head (2.3.2). In each transect, three digital images (150 x 150μm) were acquired from the central, equatorial and peripheral areas. The number of binucleated and mononucleated RPE cells were noted in each image and calculated as a percentage of the total number of RPE cells in that image. Cells with more than two nuclei were rarely encountered and were not recorded for the purpose of this study. The mean values for the three strips were then calculated for each retina.

One-way analysis of variance was used to analyse the statistical significance of Ki67 labelling between pigmented and albino rats and was followed by post-hoc Newman-Keuls multiple comparison test when appropriate. The same statistical tests were used to analyse the level of Ki67-labelled cells over development in both pigmentaion phenotypes.

2.7 L-DOPA affect on the cell cycle

L-DOPA regulates retinal neurogenesis by restricting levels of neural cell proliferation in the developing retina (Tibber *et al.*, 2006). To determine the effect of exogenous application of L-DOPA on the proliferative capacity of the RPE, four pigmented and four albino (P60) rats received a single intraperitoneal

injection of L-DOPA, at a concentration of 15μg/g of body weight. The animals were then sacrificed in the morning, 18 hours post injection. The eye cups were then processed with Ki67 antibody as in (4.3.3). The number of Ki67-positive cells were counted across the whole retina and compared to age-matched retinae from both pigmented and albino rats that had not received an L-DOPA injection.

2.8 The adaptive state of the retina

To determine whether the light/dark adaptation of the animals influenced the latent capacity of RPE cells to enter the cell cycle, I used animals in the different adaptive states. Twenty postnatal 60-day-old pigmented rats were divided into four groups: the first group was light-adapted for 27 hours; the second and third groups were dark-adapted for 17 and 40 hours, consecutively; and the last group was subjected to a normal light/dark cycle. All adaptation times were planned so that the animals could be sacrificed at 10 a.m. to control for any effect of endogenous circadian rhythms. All retinae were processed for Ki67 (4.3.3) and the number of Ki67-positive cells were counted.

2.9 Retinal detachment

Forty DA rats were used for retinal detachment. They were all six-weeks-old (P45) females with an average weight of 180 grams. These animals were anaesthetized by a 0.2ml intraperitoneal injection of Ropun (Xylezine, 2 mg/kg) and Ketaset (Ketamine, 25 mg/kg). The pupils were dilated using Tropicamide and a lubricant gel was applied to each eye. A cover slip was placed over the gel allowing the retina to be viewed directly through a binocular operating microscope with a coaxial light source. Retinal detachment was achieved by injecting 2μl of phosphate-buffered saline (PBS) between the neural retina and RPE surface using a 34 gauge needle. The injection was in a superior position

for most of the study but, to assess the effect of larger retinal detachments, a superior and inferior injection of 2 µl (PBS) was undertaken. The rats were then revived by intraperitoneal injection of Antiseden (0.05ml).

The rats were killed in a carbon dioxide gas chamber at 1, 2, 4, 7, 12, 18, 22, 24 and 36 hours after retinal detachment. The detachments were made in 4 sessions and the animals were assigned randomly for each time point of the analysis to control for any variation in the size of detachment. The eye cups were fixed overnight with 4% paraformaldehyde. The anterior segment was dissected out with the vitreous leaving the eye cup with the neural retina and RPE exposed. An image of the whole cup was obtained from 5 animals from different sessions to measure approximately the width of the detachment, which was on average 1.5 ± 0.2 mm (Fig. 17). The neural retina was then removed and the eye cups were processesed for Ki67 staining as described in chapter 3.

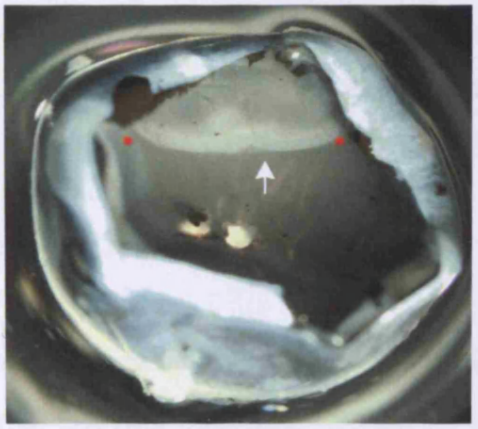

Figure 17. Image of an eye cup with a superior retinal detachment as indicated by the arrow. The width of the detachment (between the two red dots) was measured for 5 eyes from different sessions to assess the reproducibility of detachment area as a control for the size of retinal detachment.

2.10 Retinal detachment analysis

The eye cups were whole mounted by making five radial cuts, dividing the retina into five approximately equal size quadrants. Each quadrant was subdivided into small square boxes using a (430μm x 430μm) sized grid (Fig. 18) and the number of Ki67 labelled cells in each box were counted. The relative number and distribution of Ki67 positive were then plotted on an out line diagram of each retina.

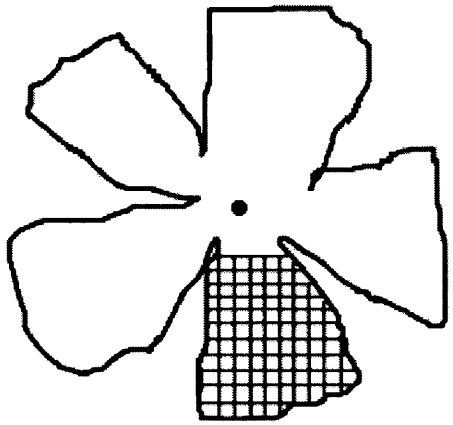

Figure 18. Diagram of flat mounted RPE, illustrating the method of analysis post retinal detachment. The RPE was divided into Central, Equatorial and Peripheral regions using the distance between the optic disc and the iris. On flat mounting the RPE was divided into five quadrants. A 430μm x 430μm grid was used to record the position of Ki67 cells within a quadrant.

To analyse the contribution of RPE cells to cells entering the cell cycle to the monolayer RPE sheet, five DA rats were analysed for RPE cell density, size and regularity apart from and close to retinal detachment. Six areas measuring 150 X 150 μm were analysed in each retina, of which three areas were associated with retinal detachment and three were away from it. The number of RPE cells was counted in each of the 150 X150 μm boxes and the result from the three boxes was averaged for each animal.

Finally the relationship between the size of retinal detachment and the number of proliferative cells was analysed. Here five animals were subjected to superior and inferior retinal detachment in both eyes. These eyes were then stained with Ki67 and the number and distribution of positive cell were mapped as above.

2.11 Gene expression methods

Sixty DA rats were used here to analyse the expression level of different progenitor and stem cell gene markers. The rats were divided into 3 groups, each group consisting of 20 rats of which 10 were used as control and 10 had retinal detachment. They were killed 18, 24 or 48 hours after retinal detachment using a CO^2 gas chamber. The eyes were preserved immediately after enoculation in RNAlater solution (Ambion Inc. Austin, TX) for 30 minutes. The RNA extraction and first strand cDNA synthesis was undertaken at the same time for each group.

2.11.1 Total RNA extraction

RNA was extracted from tissue preserved in RNAlater solution. The anterior segment, vitreous, and retina were removed leaving the eye cup with the RPE exposed. The RPE was brushed away from the choroids and a total RNA was extracted from approximately 50mg of tissue using a RNAaqueous-Micro kit according to the manufacturer's instructions (Ambion Inc. Austin, TX). The RNA was suspended in 20 μl of molecular grade Rnase-free water and the concentration of RNA extracted was measured by spectrophotometry.

2.11.2 Estimating concentration and purity of RNA

The concentration of RNA was measured using an Eppendorf Biophotometer. The machine was first calibrated by measuring the absorbance of pure molecular grade water. The RNA sample was diluted 3 μl in 50 μl of molecular

grade water, mixed thoroughly, and pipetted into a cuvette, and the absorbance at 260nm and 280nm measured, the concentration and purity were calculated by the Biophotometer.

$$\frac{\text{OD of sample at 260nm X Total Volume(µl) X Conversion Factor (40mg/ml)}}{\text{Sample volume (µl)}} = [\text{RNA µg/ml}]$$

The absorbance spectra of nucleic acids has a specific shape, they absorb relatively little light at 280m. The purity of the RNA or DNA can be assessed by the ratio OD_{260}:OD_{280}. Pure RNA ~1.9-2.0 (Sambrook and Russell, 2000).

2.11.3 *First strand cDNA syntheses*

Prior to cDNA synthesis, the RNA samples were treated with Dnase to remove genomic DNA contamination. A DNase I kit (Sigma-Aldrich Inc.) was used; 1 µl of RNA was mixed with 2 µl of Dnase I and with the supplied buffer in a volume of 10 µl. This was incubated at 37 °C for 30 minutes after which 1 µl of stop reagent was added, and incubated at 70 °C for 10 minutes then chilled on ice. The first strand cDNA synthesis was carried out with the MMLV- reverse transcriprase kit following the manufacturer's guidelines (Ambion Inc.). Reverse transcription was carried out with random decamers to transcribe any RNA, 2 µl of primer was added to the treated RNA, and this was incubated for 2 minutes at 80 °C and was then chilled on ice. A reverse transcriptase master mix was made containing 2 µl RT buffer, 4µl dNTPs, 1µl Rnase inhibitor, and 1 µl reverse transcriptase, 10 µl of this was added to the RNA and primer mix. The reverse transcription was carried out for 1 hour at 42 °C with a final incubation at 92 °C for 10 minutes to terminate the reaction.

2.11.4 Primer design

Most primers used (Table 3) were designed using Primer 3 (http://frodo.wi.mit.edu/) with the following specifications (based on the AB technical bulletin and Bustin, 2000):

1- 20–30 bp long
2- G/C content between 20 and 70 %
3- Melting temperatures of between 58 and 60 °C
4- The difference between primer pair melting temperatures to be only 1–2 °C
5- Produce a 100–400bp product with Tm below 92–95 °C
6- If possible to have only 1–2 G/Cs in the last five nucleotides of the 3′ end (reducing non-specific priming)
7- If possible the product should also span an intron to prevent amplification of genomic DNA.

A BLAST search (http://www.ncbi.nlm.nih.gov/BLAST/) was carried out on the primers to check they were specific only to the target sequence. All primers were synthesized by Sigma Genosys (The Woodlands, TX).

Table 3 Primers used for quantitative real-time PCR[1]

Target transcript	**Accession number**	**Primer 5′ to 3′**	**Recording temp. (°C)**	**Product Size (bp)**
Hprl	NM 012583	Forward-TGACACTGGTAAAACAATGCA Reverse-GGTCCTTTTCACCAGCAAGCT	76.5	93
Mertk	NM 022943	Forward- AAGCAGCCTGAGAGCGTGAATG Reverse-TGGGGAAGGGATGACTTTGATG	80.3	227
Tbp	NM 001004198	Forward-TGGGCTTCCCAGCTAAGTTC Reverse-	79.3	138

		GGAAATAATTCTGGCTCATAGCTACTG		
Thy1	NM 10666	Forward-GTCGCTCTCCTGCTCTCAGTCTTG Reverse-TCATCCTTGGTGAAGTTGGC	82.5	283
Rhodopsin	NM 053688	Forward-ATCGGCAGAAGGGGCAAAGTAG Reverse-GCAACGCAGACTTCTCATCTTCAAG	82	174
melanopsin	NM 138860	Forward- GCTCTTCGGGGAGACAGGTT Reverse- AAAGAAAGGCGGCAGACTCC	82.7	213
Nestin	NM 012987	Forward-CCCTGGAGCAGGAGAAGCAA Reverse-GCTTCAGCTTGGGGTCCAGA	80.5	200
Otx2	XM 224009	Forward-ACCGCCTTACGCAGTCAATG Reverse-CACTCTCTGAACTCACTTCCCGAG	81.5	355
Pax6	NM 013001	Forward-AGTTCTTCGCAACCTGGCTA Reverse- TTGAGCCTCATCCGAGTCTT	80	228
Dcx	NM 053379	Forward- TCGTAGTTTTGATGCATTGC Reverse- GCTTTCCCCTTCTTCCAGTT	77	141
Sox2	XM 574919	Forward-GTGAACCAGCGCATGGACAG Reverse-TCTGCGAGCTGGTCATGGAG	84.5	188
Ki67	NM 002417	Forward-TGCTCCAGGTGAAAAGAAAAGTCC Reverse-TTCAGGTCTTAGATGACCCCAAA	78.3	198
PCNA	NM 022381	Forward-CGTCTCACGTCTCCTTAGTGCAG Reverse- GGACATGCTGGTGAGGTTCAC	80.5	103
RPE65	NM 053562	Forward- ATGGTGCCACTGCTCATCCA Reverse- TGGCTTGAACCGATCACTGC	76.5	177
Six3	NM 023990	Forward-AGCAAGAAACGAGAACTGGCG Reverse-GAGGTTACCGAGAGGATAGAAGTGC	88	274

Six6	XM 001077640	Forward- TCCCAACCCCAGCAAAAAGC Reverse- AACAGGTCAGATGTCGCACTCG	86	271

2.11.5 Polymerase chain reaction

Polymerase chain reaction (PCR) was carried out to amplify fragments of DNA and to test the primers. PCRs were generally carried out in total reaction volumes of 50 or 25µl. PCR master mixes generally consisted of 200–500µM of each dNTP, 200–500nM of each forward and reverse primer, and 0.01–0.05 units of BioTaq DNA polymerase (Bioline Ltd), 1–5µl of template (cDNA, genomic DNA or diluted PCR products) was generally added to the aliquoted master mix. One 'no template control' in which molecular biology grade water was substituted for a sample was run in parallel to samples to check reagents for contamination. Thermal cycling was carried out on an Eppendorf Mastercycler gradient. The cycling conditions consisted of 3 minutes at 94 °C initial denaturation, followed by 35–40 cycles of 15 seconds at 94 °C denaturation, 30 seconds at optimum primer annealing temperature (usually between 50 and 68 °C), and 30 seconds at 72 °C for primer extension, all followed by 5 minutes at 72 °C for final primer extension.

2.11.6 Gel electrophoresis

PCR products and other DNA products were separated and visualized by agarose gel electrophoresis. Gels were prepared of 1.0–2.0% (w / v) agarose in 1xTAE (Tis/Acetic Acid/EDTA buffer 50x, BIO-RAD). The agarose was dissolved in the TAE by heating. After this had cooled to approximately 50 °C, ethidium bromide (0.5 µg/ ml) was added. The gel was poured into a sealed gel tray and a comb inserted to make loading wells. The gel was allowed to cool and solidify on the bench top. Gels of 1.0% were used to resolve DNA

fragments, or to separate products prior to purification. Depending on well size, 10–20 µl of PCR product would be loaded into the gel. Prior to loading, 1µl orange loading dye (Promega, Madison, USA) was mixed with the samples. A 100bp or 1kb ladder (New England Biolabs Inc.) was also loaded on the gel for reference. The gel was then submersed in 1X TAE in a gel tank and electrophoresed to the desired separation at 60–90 V. The gel was then removed and DNA viewed on a UV transilluminator in a gel documentation system. A digital photo was taken of the gel and saved as a tif file (Fig. 19).

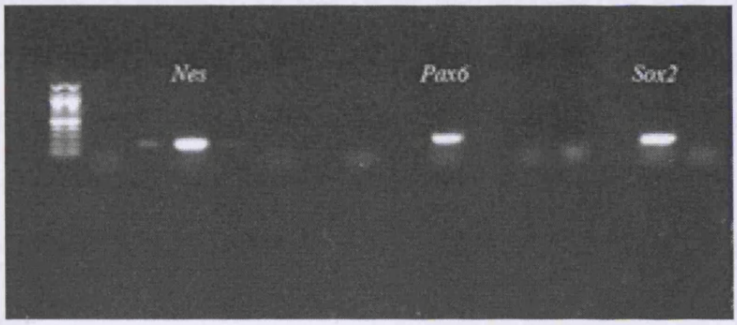

Figure 19 Agrose gel electrophoresis. Ten microns of PCR product of Nestin, Pax6 and Sox2 was loaded in to each well. A 'no template control' sample was run in parallel to samples to check reagents for contamination.

2.11.7 *DNA gel extraction*

The gel was viewed on a UV transilluminator; products of interest were excised using a sterile scalpel blade. If the band was bright then it was excised and purified using the (Qiagen Ltd. Crawley, UK) following the manufacturer's guidelines for gel extraction. The DNA was finally eluted in buffer EB (10mM Tris-CL, pH8.5) supplied in the kit.

2.11.8 *Sample sequencing*

Sequencing was carried out on ABI automated sequencers using the Big DYE terminator Kit from Applied Biosystems (Foster City, CA). Two mixes were

prepared, first was the product-primer mix, consist of 11.5 µl of PCR product with 0.5 µl of a primer known to bind to the PCR product in a total volume of 12 µl. The second was a sequencing mix which consists of 4 µl Big Dye, 2 µl BD buffer, 8µl of water and 6µl of the first mix. Thermal cycling was carried out on a Techne Progene thermocycler. The cycling conditions consisted of 3 minutes at 95 °C initial denaturation, followed by 35 cycles of 10 seconds at 96 °C denaturation, 10 seconds at optimum primer annealing temperature of 50 °C followed by 4 minutes at 60 °C for primer extension. The reaction was then held at 10 °C overnight. A mixture of 0.5 µl of (0.5 M) EDTA, 2 µl of (3M, pH5) NaOAc and 50 µl Benzene free (96%) EtOH was then added to the sequencing reaction to precipitate and incubated at room temperature for 15 minutes. The mixture was then centrifuged at 13,000*g* for 30 minutes at 4 °C and the supernatant was removed, then 70 µl EtOH was added to the pellet and centrifuged at 13,000*g* for 15 minutes. The alcohol was removed and the pallet was left to dry, then 12 µl Hi Di Formamide was added to the pallet just before loading to the sequencers. The result was viewed using Chromas 2.

2.11.9 Quantitative Real–time PCR

Description of the assay

Quantitative real-time PCR (QRT-PCR) using fluorescent DNA binding dyes allows visualization of PCR product accumulation throughout the PCR. A sample containing higher concentrations of target sequence will accumulate PCR product at earlier cycles than a sample with a low concentration. The resulting amplification plots can be used to calculate either the absolute copy number of target sequences in the sample, or measure the proportional change in expression of the target gene relative to the control condition. In the studies presented here, real-time quantitative PCR was used to assess relative changes in gene expression.

Real-time PCR was conducted using power Sybr® I green dye (Biosystem). This dye specifically binds to double-strand DNA, following each cycle of PCR as DNA content increases, the fluorescence intensity increases proportionally. The QRT-PCRs were carried out on an ABI PRISM™ 7700 Sequence Detection system (Applied Biosystems). This system comprises a built-in thermocycler with 96 well positions, an argon ion continuous wave laser, and a spectrograph with a charge-coupled device (CCD) camera. During the PCR laser light is distributed among the 96 wells by fibre optics, the resulting fluorescent emission from the samples is returned via the fibre optics to the spectrograph and CCD camera, and fluorescence between 500 and 660nm is detected. A computer running Sequence Detector software (SDS), version 2.2 (Applied Biosystems), controls the system and converts the raw fluorescent data output into an analysable form.

Primers were tested in a PCR using the Power Sybr® Green PCR Master Mix (Applied Biosystems), the same reagent to be used in the final quantitative real-time PCR run. This master mix contains ready-mixed Sybr Green I dye, AmpliTaq Gold® DNA polymerase (this enzyme is hot-start activated, helping to minimize non-specific product formation), optimized buffer and PCR components and a passive reference dye (ROX), all that needs to be added for a successful PCR are forward and reverse primers and the target sequence.

Each standard test PCR was set up in a total volume of 50µl, this contained 25µl of Sybr® Green PCR Master Mix, forward and reverse primers each at a final concentration of 500nM and 1µl cDNA. A no-template control containing molecular grade water in place of the cDNA was also included. The thermocycling conditions were slightly different from a standard PCR, they were carried out on a Techne Progene thermocycler, using the following parameters: 95 °C for 10 minutes to activate the DNA polymerase, then 40

cycles of 95 °C for 15 seconds, and 60 °C for 60 seconds for both primer annealing and product extension.

The 25µl sample was pipetted into a 96-well plate and loaded into the ABI PRISM™ 7700 Sequence Detection System. The temperature was ramped from 60 to 95 °C over 20 minutes and the fluorescence recorded at each 0.1 °C change in temperature. The fluorescence data was then exported into Dissociation Curve (version 1.0) software (Applied Biosystems) for analysis. An example of a melting curve for products of HPR primers is shown in Figure 51. The melting temperatures of products in samples can be visualized by plotting the rate of change of fluorescence, the first negative derivative (–d(Fluorescence)/d(Temperature) versus temperature) (Fig. 20). This shows the melting temperature of the product as a peak and will also indicate the presence of primer dimers or other undesired amplified products. This is also a useful diagnostic tool to discover the temperature at which the fluorescence should be recorded during the real-time PCR run. The recording should be made at a temperature just below that of the product melting temperature, but above that of any primer dimers formed, as such the fluorescence recorded can be attributed to the desired PCR product alone.

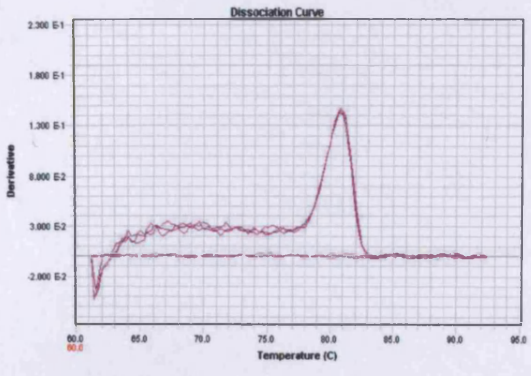

Figure 20. The melting peak plots for HPR. The fluorescence should be recorded at 78.5 °C and the primer dimers will be melted at this temperature.

Quantitative real-time PCR-assay setup

Each QRT-PCR was carried out in a reaction volume of 25µl loaded into a 96-well plate. The reactions contained 300 nM of each primer as well as the ocular cDNA template. To help reduce intra-assay variability, large master mixes were made that contained both primers and Power Sybr® Green PCR Master Mix diluted in water, these mixes were made in excess to allow for residual losses during pipetting and on plastic ware. The quantification for each cDNA sample was done in triplicate, enabling a measurement of intra-assay variance. The large master mix was aliquoted into 85µl aliquots (in excess of the 75µl required for the triplicates) to which 1µl of cDNA was added and mixed thoroughly. A triplicate no-template control was also set up on every plate to check for contamination. After thorough mixing, triplicates of 25µl were pipetted from each aliquot into a 96-well plate, optical caps were placed on the wells and the plate was loaded into the sequence detection instrument.

Thermocycling and data collection

The sequence detection system was controlled by the SDS 2.2 software. The cycling conditions for the PCR consisted of an initial *Taq* activation step of 95 °C for 10 minutes, followed by 40 cycles of 95 °C denaturation for 15 seconds, followed by a 60 °C annealing/extension step for 1 minute. A final data collection step of 20 seconds was added to each cycle, with fluorescence measured at 2 °C below the melting temperature of the desired product as determined by melting curve analysis. This ensured that any primer dimers did not contribute to measured fluorescence. During data collection periods the system records fluorescence (across a broad spectrum from 500 to 660nm) every 7 seconds, approximately 3 fluorescent readings would be taken and automatically averaged for each cycle.

2.11.10 Data analysis

Two initial corrections were made automatically to the raw fluorescence data by the SDS software. Firstly the data was corrected to a passive internal reference dye (ROX). Each PCR reaction in addition to the Sybr® Green contains ROX, this fluoresces at a longer wavelength than Sybr® Green and is used as a control for the amount of reagent in each PCR (controlling for pipetting errors and any evaporation within the tubes). The fluorescence recorded for Sybr® Green is corrected with respect to the reference dye to give a relative fluorescence (R_n) value at each cycle. Secondly R_n values are further modified by subtraction of background fluorescence levels. The background fluorescence level is calculated as the mean fluorescence during the first 3–15 cycles of PCR before products can be seen to accumulate (this is user defined and may be limited with high expression targets). These final R_n values were then exported to a text file.

The text file was imported into Excel (Microsoft, Redmond, WA) and further analysed using an automated workbook entitled 'Data analysis for real-time PCR (DART-PCR)', described and created by (Semo *et al.*, 2003). This analysis is quite complex and is described in detail in the publication; the following is a simple overview of the analysis undertaken for each relative quantitative PCR. DART-PCR is designed to analyse the data from direct comparisons between sample groups (samples in which the same target gene is being amplified with the same primers), if more than one comparison was set up on a single plate then the data would be analysed separately. The workbook was designed to calculate the theoretical starting fluorescence (R_0), which is proportional to the amount of starting template. This is calculated using the formula:

$$R_0 = R_{Ct}(1+E)^{-Ct}$$

Where Ct is the threshold cycle, R_{Ct} is the fluorescence at this cycle and E is the efficiency of the PCR amplification reaction (as with biochemical reactions rated 0 (no reaction) to 1 (maximum reaction)).

In an ideal PCR reaction E has a value of 1 in which there would be an exact doubling of product with each additional cycle, the fluorescence would follow an exponential increase with each cycle. In reality the efficiency of amplification in a PCR is not exactly 1, and in later cycles reagents become limiting, or the accumulation of PCR product in itself becomes inhibitory to the reaction (Kainz, 2000). On a log R_n scale the real-time PCR amplification plot can be described as having three distinct stages, firstly the background noise stage, during which exponential increase in the product is not visible, secondly the effective linear phase during which the efficiency of amplification is at its highest level and then thirdly the plateau phase during which the efficiency is decaying.

The R_n values for the triplicates were averaged and the efficiency was calculated by linear regression for each around the midpoint of fluorescence using DART-PCR. The workbook also assessed whether the efficiency was comparable both within and between sample groups using analysis of variance (ANOVA). If outliers within groups were detected then they were removed from the analysis. If the efficiency was comparable within and between sample groups then the average overall efficiency was used in the calculation of R_0. Whilst it is theoretically possible to make individual efficiency corrections, this will introduce systematic errors, since efficiency correction is exponentially applied (Semo et al., 2003). In the majority of quantitative real-time PCR assays I analysed for this study, no significant differences of efficiencies between sample groups were found, suggesting variations are due to measurement techniques. In one instance when this was seen, it was due to high background noise levels (leaving only a few points in the effective linear phase for efficiency

calculation), and high intra–assay variability. This assay was repeated and with lower assay noise no significant differences were found.

The level of fluorescence at which the Ct was recorded was set at the calculated midpoint of fluorescence on a log scale (the solid black line in Fig. 21) in the linear phase. The R_0 values for each sample were then exported to a new worksheet; the data was then normalized. The relative expression, and fold change between normalized sample groups were then calculated.

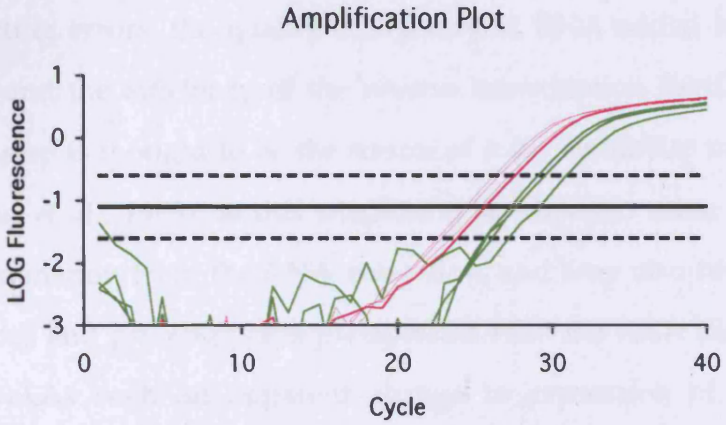

Figure 21. Amplification plot of fluorescence data from a QRT-PCR run for HPR. The solid line indicates the threshold fluorescence at which cycles values were obtained. The dashed lines define the linear phase from which the efficiency was calculated for each sample.

In the example shown the average efficiency is 0.977, this is comparable between the two groups and within the groups so this could be used as an estimate of the efficiency of amplification in all plots. The threshold log fluorescence was set at the midpoint –1.097 (calculated automatically by the workbook). This is marked as the solid black line in the graph and appears to be both above the background noise and within the linear phase before the plateau. The cycle number at this fluorescence was recorded. At this point a

clear difference between groups (pink and green) can be seen, the pink group samples have lower Ct values at this fluorescence (hence would be expected to contain more initial transcript). The R_0 values are calculated by the spreadsheet, there is a increase of six times in expression in the pink group of samples, but this value must be normalized before final comparisons are made.

2.11.11 Normalization of data

A parameter that must be controlled for in real-time PCR is the amount of cDNA loaded into each reaction. There are multiple factors that can affect this, such as pipetting errors, the quality and purity of RNA added to the reverse transcription and the efficiency of the reverse transcription itself. The reverse transcription step is thought to be the source of most variability in quantitative PCR (Freeman *et al.*, 1999) as this reaction is sensitive to salts, alcohols and phenol contamination from the RNA extraction, and may also be inhibited by polysaccharides and proteoglycans precipitated with the RNA (Sambrook and Russell, 2000). As such an apparent change in expression of a gene in a treatment could be due to differing amounts of cDNA added to the real-time PCR. It is important then that one assays the expression of at least 3 internal housekeeping genes for each of the samples as an RNA loading/reverse transcription control. Housekeeping genes were chosen as those with most stable expression across the treatments being compared. Here 5 genes were examined for stability of expression and then a normalization factor, which is the geometric mean of the multiple internal control, was calculated for the most stable genes using Genorm (Vandesompele *et al.*, 2002). The three housekeeping genes used here were HPR, MERTK and TATA binding protein (TBP). To normalize, the R_0 values of the test genes were divided by the normalization factor. Again the plates were set up so that groups being directly compared

(control and treatments) were on the same plate, such that any differences in gene expression would not be due to inter-assay variability.

2.11.11 Statistical analysis

Statistical tests were carried out using Microsoft office Excel 2003. T-test was used to analysis the significant changes in expression level. Here, the level of expression in control samples was tested against retinal detachment samples. However the data was represent in the corresponding figures as fold change.

Chapter 3

RPE cell topography in human and rats

3.1 Introduction to topographical variation in human RPE cells

In the foetus, the eye diameter doubles every 2.5 to 3 weeks between the third week and the second month, and it doubles again between the third week and the fifth month of gestation. The eye growth then slows down during subsequent development (Robb, 1982). During postnatal life, the human eye grows most rapidly within the first year and continues to grow at a relatively high rate until the third year (Streeten, 1969). From the second to the thirtieth year, growth is relatively slow and is almost absent beyond thirty years (Harman *et al.*, 1997). On the other hand, the primary increase in cell density in the RPE occurs between the fourth and sixth month of gestation. Here, RPE cell proliferation occurs at a rate faster than the rate of enlargement of the surface area covered by them. However, cell density then decreases between the sixth month of gestation and the second year of life, despite an increase in the total number of cells (Ts'o and Friedman, 1968; Rapaport *et al.*, 1995) because at approximately the sixth month of gestation the relationship between eye growth and RPE cell proliferation reverses. Here the surface area of the eye grows at a faster rate than RPE cell proliferation as a result an apparent decrease in RPE cell density and a variation in cell size develops (Ts'o and Friedman, 1968). Post-natally the RPE appears to change only by increasing its area throughout maturation (Mann, 1964), the slow increase in surface area of the eye will be accompanied with expansion in the RPE monolayer to cover the underlying surface area. However as soon as the eye growth ceases, the RPE cells become uniform in their shape, size, and pigmentation (Streeten, 1969).

RPE cell loss is a characteristic feature of aging (Panda-Jonas *et al.*, 1996) and also of retinal disease such as macular degeneration or retinitis pigmentosa (Adler et al., 1999). As these cells are mitotically inactive postnatally, many studies have been carried out to determine the changes in human RPE cell

density with increasing age. However, the results have been inconsistent. In most studies the retina was analysed as three regions; central (macular), equatorial and peripheral. In general, most studies agree that central RPE cell density is higher than in the peripheral region (Robb, 1985; Gao and Hollyfield, 1992; Panda-Jonas et al., 1996; Harman et al., 1997). Del Priore (2002) suggested that this decrease in peripheral RPE cell density is due to migration of peripheral cells to replace apoptotic central RPE cells (Del Priore *et al.*, 2002). Panda-Jonas and colleagues (1996) concluded that the decrease in RPE cell density is approximately 0.3% per year with increasing age with a general decrease in cell density from the central to peripheral regions (Panda-Jonas *et al.*, 1996).

On the other hand, studies of macular and equatorial RPE density showed contradictory results. Watzke and colleagues (1992) showed that macular RPE cells were more densely packed and more hexagonal than those of equatorial regions, this hexagonality is lost with age (Watzke *et al.*, 1993). Gao and Hollyfield (1992) found an age-related decrease in equatorial RPE cells, which occurred between the second and ninth decade, however, this decrease did not affect the macular regions. In contrast, Harman and colleagues (1997) found a significant increase in central RPE cell density with age which did not affect the equatorial region (Harman *et al.*, 1997). An additional facet that marks many earlier studies is that they largely avoided the far peripheral retina. It is probable that this is because the majority of retinal diseases that affect vision afflict the central retinal regions and that the periphery is harder to analyse because it can be damaged during tissue processing.

Aims of this study

- Analyse the topographical variation of RPE cell size and matrix of regularity across the entire retina in humans, using computational analysis of digital microscopic images (Dryden, Taylor & Faghihi, 1999), and compare with previous studies.
- Identify binucleated RPE cells and their distribution as this feature is associated with cells entering the cell cycle.
- Analyse the effect of ageing on RPE cell.
- Compare the topographical variation of basic RPE cell features between human and rodent, as only one study has attempted to compare basic features of the RPE across different species (Ts'o and Friedman, 1967).

2.5 Results

When viewed in hydrated flat-mounted retina preparation, the central and equatorial RPE cells appeared as a tightly packed homogenous, hexagonal and phenotypically similar population of cells (Fig. 22C). However, peripheral RPE cells showed a nonhomogeneous distribution and exhibited a striking variability in pigment content distribution and histological features (Figs. 22A, B).

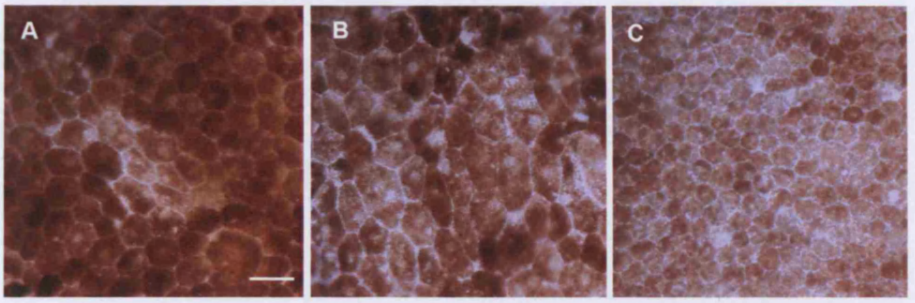

Figure 22. Image of far peripheral and equatorial RPE cells undertaken using light microscopy. (A) and (B) are examples of two populations of RPE cells which differ in histological features and were both within the first 2 mm of the peripheral retina, close to the ora serrata. Adjacent to the retinal edge cells were small, hyperpigmented (A) and central to these cells was a second population which was larger in size , highly distorted and with variable levels of pigmentation (B). (C) Shows equatorial RPE cells which are homogenous and hexagonal in shape, with a normal level of pigmentation. Scale bar = 20 μm.

2.5.1 Central to periphral variation in human RPE cell size

To determine regional variation from the centre to the periphery of the retina, one retina from a 45-year-old donor was analysed. Here trance lucida images of the RPE were analysed as a single length which transected the entire radius of the flat-mounted retina. The length of the strip analysed was approximately 20 mm and the width 150 μm (Fig. 23).

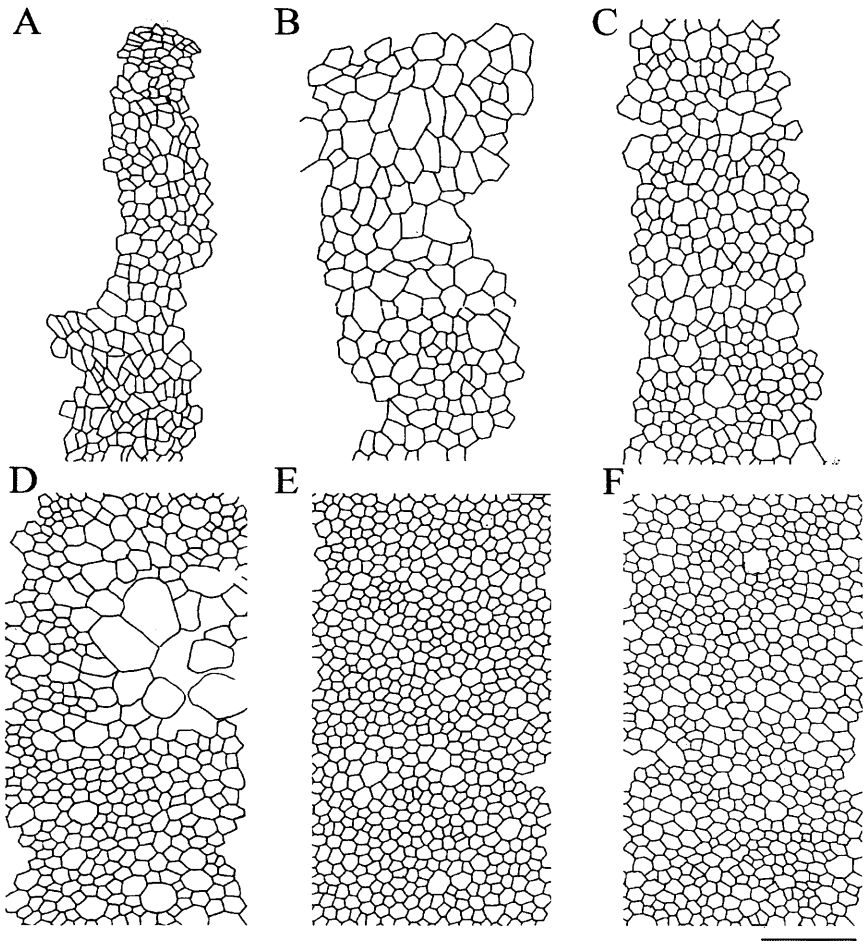

Figure 23. Images of RPE cells drawn using light microscopy with an attached drawing tube. (A), (B) and (C) Consecutive images of RPE cells for the first 5 mm of the far periphery. These images show the variation in RPE size and shape within the first 5 mm of the far periphery. (D) represents an area of equatorial RPE at a distance of 8–9 mm from the far periphery which is distorted due to the accumulation of drusen beneath the cells. (E) and (F) are examples of normal equatorial and central RPE cells, respectively. Scale bar = 100 μm.

The first peripheral 5 mm (5000μm) of the strip contained three populations of RPE, according to the size of the cell (Stroeva and Panova, 1976). The first population had an average cell diameter of 12.5 μm and occupied the first 0.5 mm of the strip. The second population of cells had an average cell diameter of 17.5 μm and occupied the area between 0.5–2.5mm of the strip. The increase

observed within this region was statistically significant (P<0.0001 between centre and periphery of the retina). The third group represents the first homogeneous cells seen in the periphery of the retina, these cells had an average diameter of 14.3 μm (Fig. 24).

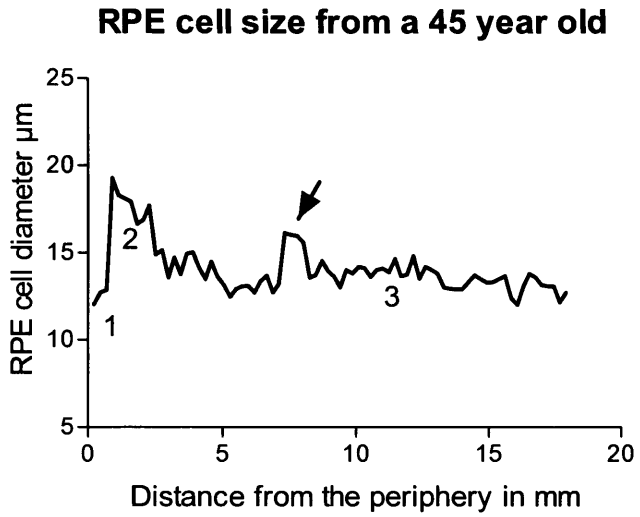

Figure 24. Analysis of a radial strip from peripheral to central retina. This illustrates the presence of three RPE cells populations: (1) small peripheral RPE cells adjacent to ora serrata with average diameter of 12.5 μm, these cells occupy the first 0.5 mm of the peripheral retinal rim; (2) large cells with an average cell diameter of 17.5 μm and occupying the area within 0.5-2.5mm of peripheral retina and then gradually normalize in size. The increase in RPE cells observed in this region was statistically significant P<0.0001. (3) The third population represents the entire central and equatorial RPE cells with an average cell diameter 14.3 μm. The arrows point to a second peak in RPE cell size, this increase is related to the presence of drusen in that region which is discussed in Chapter 4.

The next 14 mm (14,000 μm) of the strip represented equatorial (7 mm) and central (7 mm) RPE cells; these cells were homogeneous with an average cell diameter of 13μm. At approximately 8–9 mm from the periphery, which is part

of the equatorial retina, another peak in RPE cell size was observed. This peak was associated with drusen which will be discussed in detail in Chapter 3.

2.5.2 Regional variation RPE cell size and regularity of the entire retinal surface

In this study, I sampled the two flat-mounted retinae systematically to cover the entire retinal surface. The first retina was from a young donor aged 17 years. Here the analysis of RPE cell size showed a relatively small variation across the central and equatorial regions, however their distribution was highly regular. On the other hand, analysis of the far periphery of the retina showed a distinctive population of cells, which were larger in size and highly irregular. This cell population formed a band running around the entire retinal edge (Fig. 25). The second retina was from an older donor aged 58 years. Here, the same pattern of increase in RPE cell size and irregularity was observed in the far periphery however, there was also an increase in RPE cell size and irregularity across the equatorial region. This increase is associated with the accumulation of drusen and aging which will be discussed in Chapter 3.

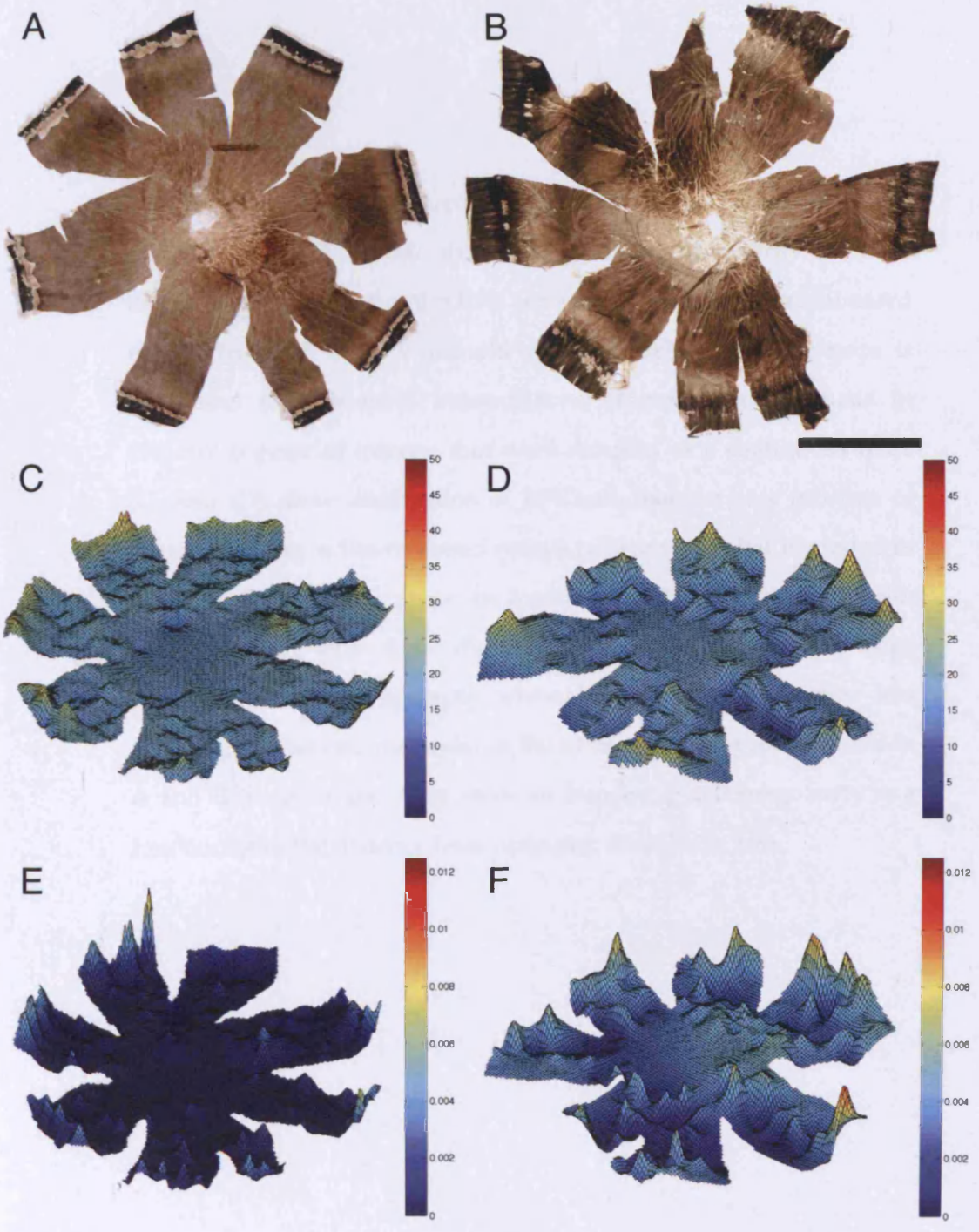
A
B
C
50
45
40
35
30
25
20
15
10
5
0
D
50
45
40
35
30
25
20
15
10
5
0
E
0.012
0.01
0.008
0.006
0.004
0.002
0
F
0.012
0.01
0.008
0.006
0.004
0.002
0

Figure 25. Pseudo-coloured topographic maps illustrating the distribution of RPE cell diameters and the irregularity of their distribution across the entire RPE surface as measured in flat-mounted retinae from 17- and 58-year old subjects. Each of the four maps is generated from bi-cubic interpolations of measurements made in 150μm2 regions of interest that were sampled as a continuous map. (C) and (D) show distribution of RPE cell diameter as a function of spatial location in flat-mounted retinae, where colour bar is graded in microns. Both retinae show an increase in RPE cell diameter with radial distance from optic disc. (E) and (F) are topographic maps depicting RPE cell regularity where larger numbers describe less regular patterns (see methods) in the same tissue preparation used in A and B, respectively. They show an increase in cell irregularity as a function of radial distance from optic disc. Scale bar = 2cm.

2.5.3 Comparison of human and rat RPE

Having established that the far periphery differed in RPE cell size and regularity, three strips that were separated like the spoke of the wheel were analysed, for size regularity and binucleation, from six retinae aged 19, 28, 45, 55, 60 and 79 years. As the strips were separated by similar angles, but placed randomly in relation to the eye orientation, it is very unlikely that there were regional differences in the features examined. Further, there was little variation in the features examined between retinae, hence the data have been pooled together and averaged for all ages.

In Figure 25 three distinct populations of cells were identified within the first 5 mm of the peripheral retina. The first group, found within the first 0.5 mm of the retinal edge, were similar in size to those in the central region, being approximately 12 μm, largely mononucleated, but relatively irregular in their distribution. Central to this was a second population with a statistically significant increase in cell size of approximately 17.5 μm (ANOVA =0.0005). Dunnett's multiple comparison test showed that this significance was mainly associated with cells within 0.5–2.5 mm of the retinal edge ($P < 0.001$). The increase in size was also associated with an increase in matrix of irregularity (ANOVA = 0.0001, Dunnett's multiple comparison test $P < 0.001$). Furthermore, 10% of these cells contained more than one nucleus. Between 4 and 5mm from the retinal edge the size of RPE cells and regularity of distribution gradually normalized and remained consistent towards the macular region. In addition almost all RPE within this normalized area were mononucleated (Fig. 26). Cells within this region represent the third group of peripheral RPE cells. While data derived from the far periphery were more variable than central region, this variability was no greater or less in individual segments. In all of the human

eyes the region displaying the features seen in the far periphery were equally marked around the retinal rim.

The morphological patterns found in rats were significantly different from those described for humans (Fig 27). The general impression of the rat RPE was of a tissue that displayed greater homogeneity than that present in humans. This was obvious in the three variables examined (Fig. 28). Rat RPE was very consistent in terms of cell size, being approximately 27μm at all eccentricities, which is larger than any found in the central or peripheral regions of the human retina. There was no tendency for an increase in cell size towards the periphery ($P = 0.14$; Fig. 28A). Likewise, there was no decline in the regularity of the cellular mosaic toward the retinal edge ($P = 0.58$; Fig. 28B).

Rat RPE showed also a distinct difference from that of human RPE in terms of the cell populations that were binucleated. In humans this feature was rare in the posterior pole and occurred in relation to extreme eccentricity, where 10% of cells within this region were binucleated. However in rats almost 80% of central RPE cells were binucleated (Fig. 28C) and a few cells at such locations could have as many as five nuclei. With increased eccentricity the proportion of cells that were binucleated declined in a roughly linear manner, such that at the retinal margin only about 10% contained more than one nucleus. This indicated that binucleation is a feature of the central RPE in rats as opposed to humans where it is a feature of the peripheral RPE. Furthermore, binucleation did not significantly change the size of rat RPE cells because cell size did not change between the central and peripheral regions of the retina, whereas in humans peripheral binucleated cells were larger than central mononucleated ones.

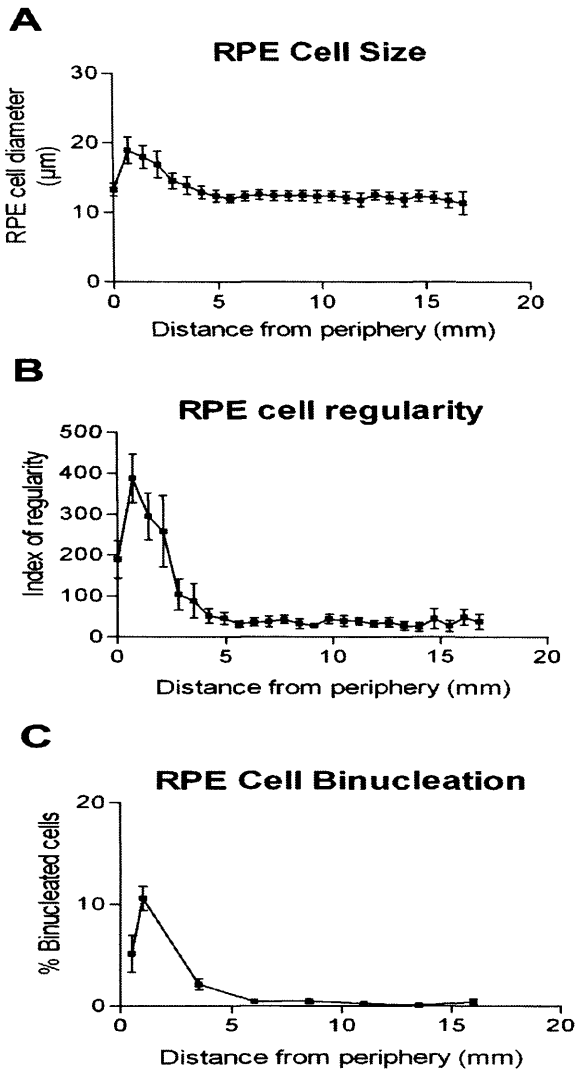

Figure 26. The graphs displaying the mean variation in RPE cell diameter, regularity and binucleation from peripheral to central retina in human. The data in each graph were pooled from the 6 retinae aged between 19-79 years. (A) Graph of RPE cell diameter showing an increase in RPE cell diameter at peripheral retina ANOVA = 0.0005. Dunnett's multiple comparison test further shows that points 0.5–2.5mm in the periphery are significant $P < 0.001$, while the rest are not significant. (B) Showing an increase in the index of RPE cell irregularity in peripheral retina ANOVA = 0.0001. Dunnett's test further shows that points 0–2.5mm in the periphery are significant, $P < 0.001$, while the rest are not significant. (C) The graph shows an increase in the average percentage of binucleated cells in the peripheral two populations of cells, ANOVA = 0.0001. Dunnett's test further shows that points 0.5–2.5mm in the periphery are significant, $P < 0.001$, while the rest are not significant.

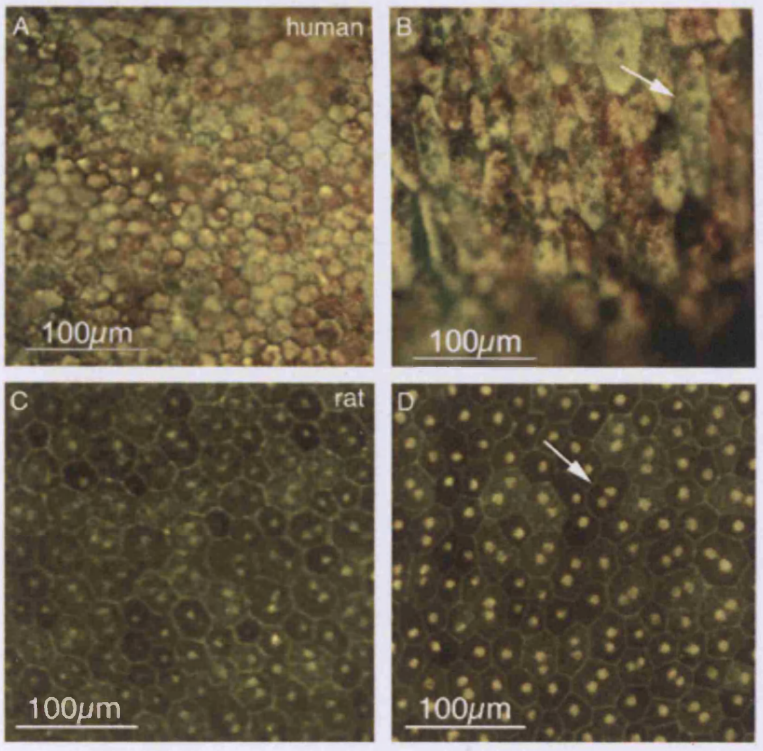

Figure 27 Example of images of the central and peripheral RPE cells in human and rat. (A) Micrograph taken from the macular region of 58-year old, and (B) sampled from the periphery, close to the ora serrata, of the same retina. (C) RPE lattice sampled from the central retina in rat, and (D) from the periphery of the same retina stained with ZO1. Human RPE has a markedly less regular appearance in the periphery compared to the centre. This regional difference was not seen in rats. The arrows in B and D shows binucleated cells.

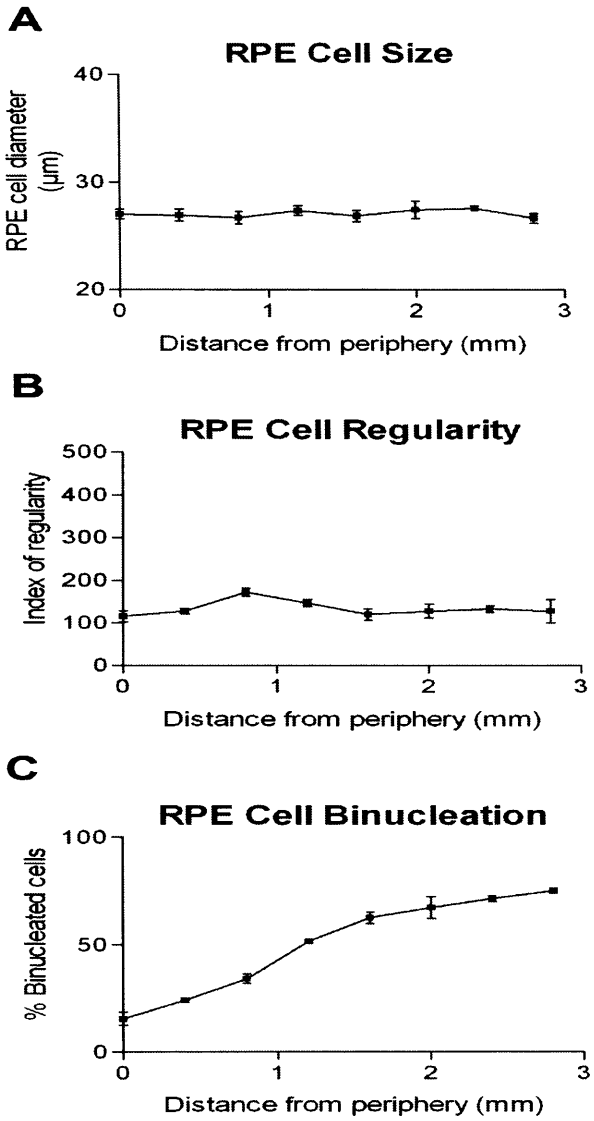

Figure 28. The graphs displaying the mean variation in RPE cell diameter, regularity and binucleation, from peripheral to central retina from 5 rats aged 180 days. (A) shows homogeneity in central to peripheral RPE cell size P=0.7. (B) shows no variation in RPE cell regularity between central and peripheral retina, P=0.05. (C) The graph shows an increase in the averaged percentage of binucleated cells in central retina which gradually decreases toward peripheral retina (ANOVA = 0.0001, Newman-Keuls < 0.05 central and peripheral).

2.5.4 Age-related changes in the central and equatorial RPE

In humans the central and equatorial RPE cells are homogeneous and they represent the vast majority of RPE cells. The aim of this study was to assess the stability of cell homogeneity with age. I analysed the size, regularity and density of the RPE cells in macular and equatorial regions of the retina from 12 eyes aged between 9 and 93 years. In general, the sizes of RPE cells in the macular region were smaller than the equatorial ones. As a result the density of RPE cells in the macula was higher than in the equatorial region. For example, at nine years of age, the mean cell density in the macula is 117.83 cells/130μm^2, whereas in the equatorial regions, the mean cell density is 87.4 cells/130 μm^2.

Figure 29 shows a gradual and statistically significant (Anova - P=0.003, correlation coefficient - r^2 =0.61) decrease in RPE cell density with aging in the macular region (Fig. 29A). This was accompanied with an increase in RPE cell size (ANOVA, P=0.001, r^2=0.66) and regularity (ANOVA, P=0.04, r^2=0.35). On the other hand analysis of the equatorial region did not show any statistically significant variation in RPE cell density with aging and as a result there was no change in RPE cell size and regularity (Fig. 29).

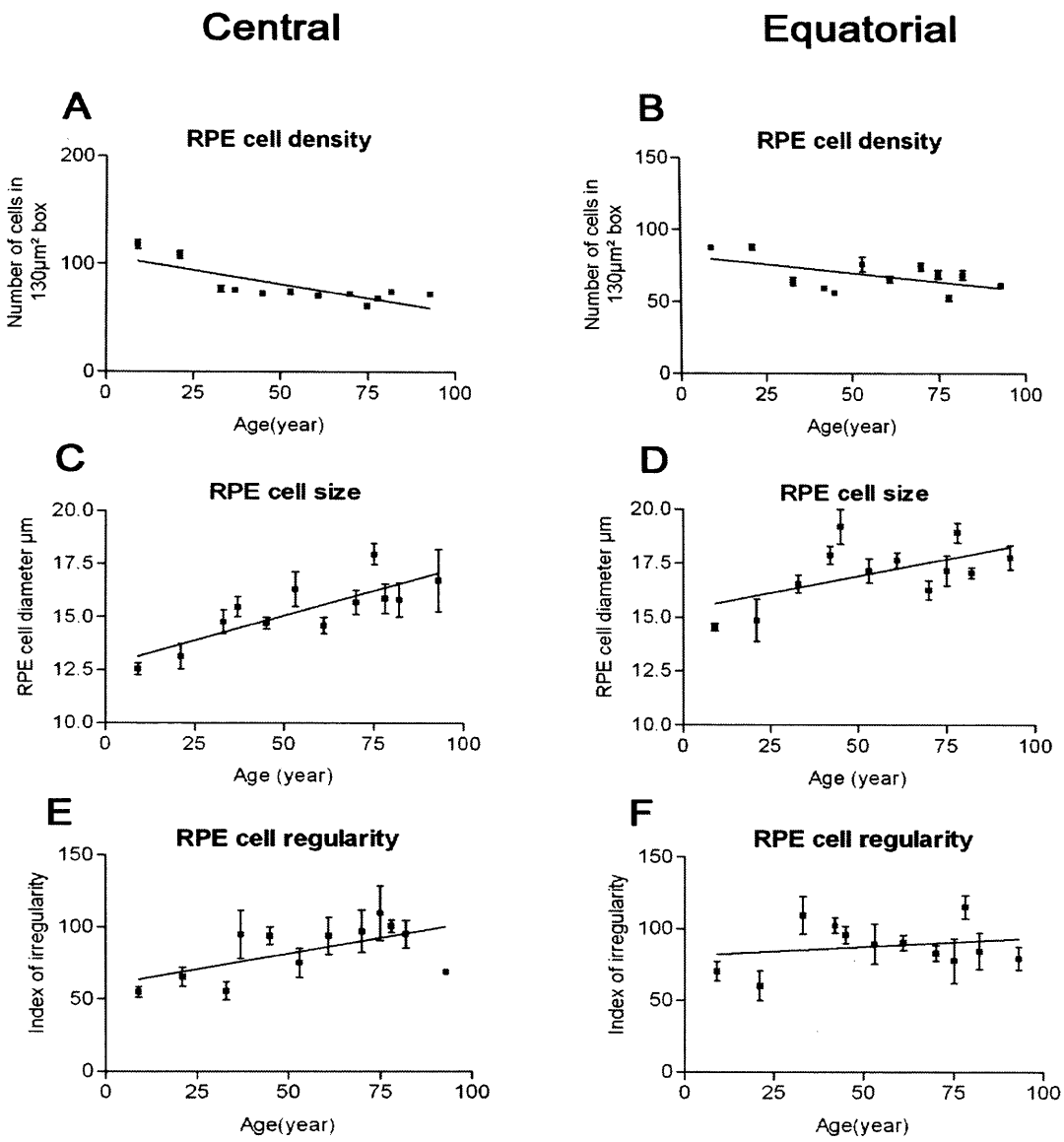

Figure 29. These graphs illustrate the effect of aging in humans on central RPE cell density, size and irregularity in both central and equatorial retinal regions. Twelve retinal flat-mounts were analysed. Graph A shows that with increasing age the average cell density decreases in humans (ANOVA - P=0.003, correlation coefficient - r^2 =0.61), which is accompanied with an increase in average cell size P=0.001, r^2=0.66 (C) and increase in matrix of irregularity, P=0.04, r^2=0.35 (E). However analysis of equatorial RPE cells showed no significant change in cell density (B), size (D) or matrix of regularity (F).

The differences found in the organization of the RPE between humans and rats were also reflected in how this tissue aged. Because of the relatively shorter lifespan of the rat only two time points were examined, 180 and 600 days old. It is rare for a DA rat to live beyond 700 days and at 600 days the animals are obviously aged, showing a greying of coat colour, increased body weight and becoming relatively sedentary. In spite of these gross age-related changes, there were no significant age-related changes in the RPE of old animals similar to those found in human tissue. The density of RPE cells did not decline, their cell size remained unchanged and their organizational pattern was not disrupted (Fig. 30).

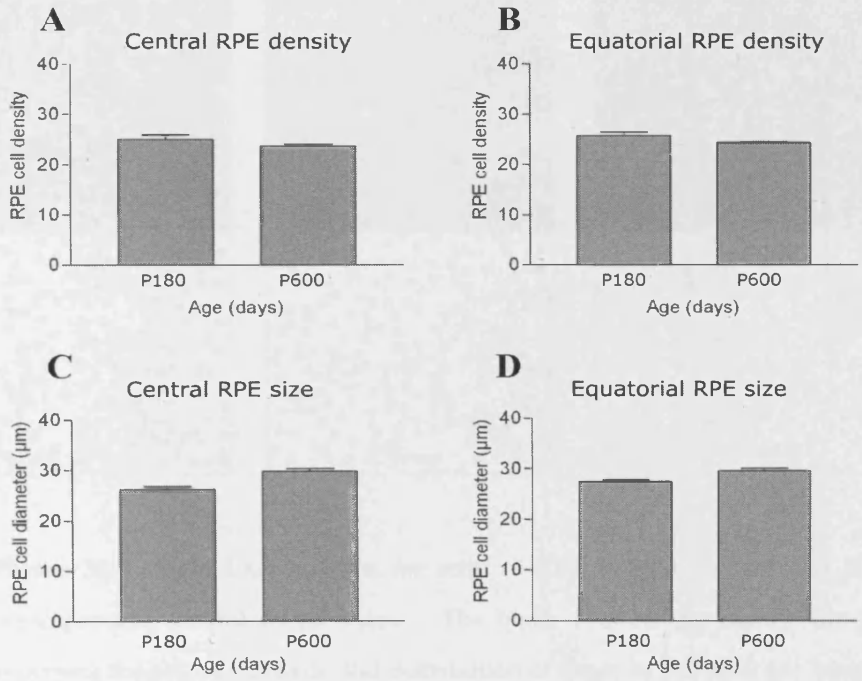

Figure 30. The graphs illustrate the effect of aging in rat RPE cells: (A) No change in central RPE cell density P = 0.2000, or cell size P=0.0500; (B) No significant decrease in equatorial RPE cell density P = 0.0749, with age or cell size P = 0.0500.

2.5.5 Cone-rich retinal rim analysis

As the retina was found to have a cone-rich retinal rim, which was approximately 1mm in width (Williams, 1991), it was of interest to find the correlation between the large, irregular, binucleated cells and the cone-rich retinal rim. Here both the flat-mounted RPE and their corresponding flat-mounted neural retina were analysed. Figure 23 shows three images taken from peripheral retina of the RPE cells with the corresponding relative distribution of cones in the neural retina. Here the cone-rich retinal rim coincides with the two distinctive groups found in the peripheral retina and their density decreases towards the central retina (Fig. 31C). I did not attempt to quantify the cone density as it is beyond the scope of this study.

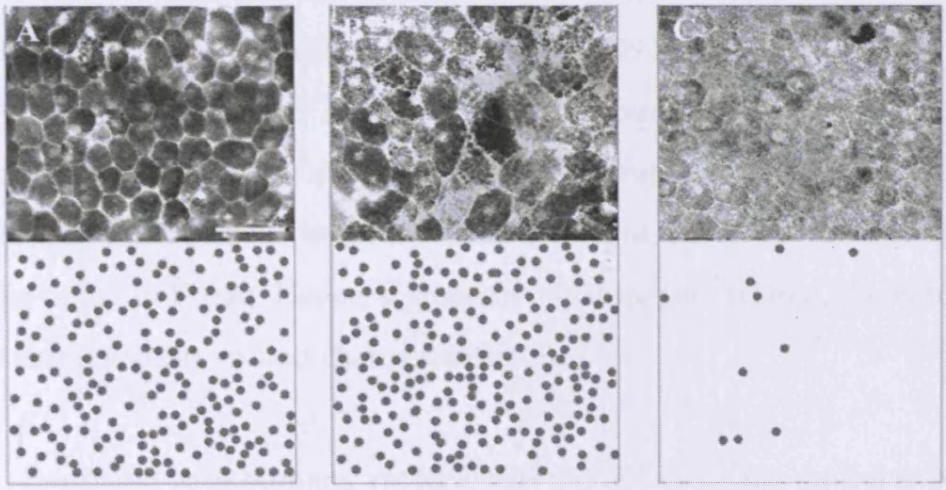

Figure 31. Sample images from the strip of RPE cells at the top and the corresponding neural retina below. The black dots on the bottom image represent the relative density and distribution of cones in this area. (A) Image of the small, mononucleated, relatively irregular RPE cells within the first 0.5 mm of peripheral retina on top, with the corresponding high cone density neural retina at the bottom. The black dot represents the relative distribution and density of the cones. (B) Image of the large, binucleated, highly irregular cells within the first 0.5–1.5 mm of the peripheral edge with their corresponding high cone density of the neural retina. (C) Shows normal RPE cells with the corresponding normal distribution of cones. Scale bar = 25 μm.

2.6 Discussion

Topographical analyses of human RPE cells highlighted a distinctive population of cells in the far peripheral retina that were histologically different from cells of the posterior pole. These cells were larger in size and their matrix of regularity was disrupted by approximately ten times. Furthermore, 10% of these cells contained more than one nucleus, which is not a common feature of human RPE.

The abnormally large, irregularly-packed peripheral RPE cells form a distinctive annulus, which is approximately 4–5 mm wide and coincides with a particular part of the neural retina that is rich in cones (Williams, 1991). However, it is important to note that the cone-rich rim is almost certainly generated prenatally during the later stages of retinal cell addition (La Vail *et al.*, 1991). But the distortions to the far peripheral RPE appear to arise much later, around the second decade of life (Streeten, 1969; Harman et al., 1997). Further, the rat lacks any distortion in the far peripheral RPE, but does have an increase in cone density at the retinal margin (Vugler et al., In Press). Hence, if these two features are related, the nature of the relationship is complex and changes with time.

When compared with humans, rat RPE cells did not show any central to peripheral variation in cell size or regularity. In fact, with the exception of binucleation, it is not possible to distinguish rat RPE cells from the central region of the retina from those from the peripheral retina. In rats, central RPE had the highest percentage of binucleated cells (80%) in contrast to peripheral cells, of which only (10%) were binucleated. Stoeva and Panova (1983) showed that binucleation is a postnatal event in rats, where central RPE contains only about 5% binucleation by the first day of life. This proportion increases gradually and reaches about 50% by the fifth day and 80% by the ninth postnatal day. However, at the periphery, the 50% level of binucleation was found by the ninth postnatal day and did not change later

(Stroeva and Panova, 1983). Interestingly, the binucleation did not significantly change the size of rat RPE cells, whereas in humans there was an increase in size of binucleated cells. Taken together these data argue that the underlying mechanism driving binucleation in rat central retina may be different from that in the human peripheral retina. Although the reason and mechanism for the nuclear division is unknown in both species, a recent study showed that the absence of *p27 kip1* gene in mice, which is a negative cell-cycle regulator, results in enhanced RPE nuclear division, without an increase in cellular division (Defoe *et al.*, 2007).

Analysis of topographical variation with age showed a marked decrease in RPE cell density in the central region of approximately 40% over the time period examined. Over this period there was also an increase in the size of RPE cells of almost 40% from approximately 12μm to approximately 17μm. Hence, cell numbers decline with age and the remaining cells appear to increase in size to cover the loss. At the same time there are marked changes in the regularity of the RPE cell matrix. This regularity declines by approximately 40% over the same period. Rats were clearly different in this respect and although aged animals showed aging in terms of their body morphology and coat colour they showed little signs of RPE cell loss from the central retina or distortions to the cell matrix. This indicates that the RPE in the two animal types also age differently.

In the mature mammal, RPE cells are lost with age which results in a 0.3% decrease in RPE cell density per year (Panda-Jonas *et al.*, 1996). This loss is due to the increase in oxidative stress which is related to the increase in lipofuscin, A2E and loss of melanin with age reviewed in (Cai et al., 2000; Sparrow and Boulton, 2005). As postnatal RPE cells are mitotically inactive many studies were conducted analysing the aging of these cells, however the results were inconsistent. There have been a number of studies on the aging of human RPE where whole-mounted

preparations have been used. The results are rather confusing and literature can be cited to support a wide range of arguments. For example, Gao and Hollyfield (1992) find evidence for RPE cell loss throughout life roughly matching declines in photoreceptor numbers. Likewise, Panda-Jonas and colleagues (1996) show a gradual decline in RPE cell numbers in the central retina with age at a rate not dissimilar to that presented here. However, a comprehensive study undertaken by Harman and colleagues (1997) found evidence for an actual increase in cell density centrally. In spite of these differences, the weight of evidence supports the notion that, in the central region of the retina, RPE cells are lost with age, which is clearly supported by the results of this study.

The increase in RPE cell loss in the central region is due to a higher level of photoreceptor outer segment phagocytosis in this region compared with other retinal regions, which results in higher levels of lipofuscin accumulation (Feeney-Burns *et al.*, 1984b; Weiter *et al.*, 1986b; Sparrow and Boulton, 2005). Hence, the central retina encounters high levels of oxidative stress factor which leads to a higher rate of cell loss with age. This region is also subjected to a 35% decline in RPE melanin granules, which are considered as protective organelles, with advancing age (Boulton and Dayhaw-Barker, 2001). Furthermore, apoptosis is more common in the macular region (Del Priore *et al.*, 2002) and a recent study found a higher level of expression of genes associated with apoptosis in the macular region than in the peripheral retina (Ishibashi *et al.*, 2004).

While there is no evidence of cell proliferation, Ts'o and Friedman (1968) noted the presence of two mitotic RPE cells in rats, but no attempt was made to locate the distribution of these cells. Here the histological features of peripheral RPE cells may possibly suggest that these cells are entering the cell cycle, but why is it only observed in the peripheral retina? Previously it has been suggested that RPE cells

migrate from the the periphery to the centre to replace apoptotic cells in the central retina and maintain RPE cell density within this area (Del Priore *et al.*, 2002). It is possible that stretching of peripheral RPE cells to cover the peripheral surface may act as a stimulus for cells to enter the cell cycle (Curtis and Seehar, 1978; Folkman and Moscona, 1978) and this could explain the regional variation. Further, the difference between proliferative capacity in the peripheral and central regions has been suggested where an *in vivo* study on humans showed that RPE cells from peripheral areas entered the proliferative phase earlier than cells from the macular region (Flood *et al.*, 1984). In addition, in an analysis of 50 of the most highly expressed retinal genes, eleven showed differential expression between central and peripheral human RPE. Of these, two were cell-cycle genes that were down-regulated in the central retina and not in the periphery (Ishibashi *et al.*, 2004).

Many regional functional differences in the RPE have also been demonstrated. For example, posterior pole RPE cells have lower Na^+ /K^+ -ATPase pump density (Burke *et al.*, 1991), and lower activity of cytochrome oxidase (McKay and Burke, 1994). The posterior RPE also has lower activities of some lysosomal enzymes such as acid phosphatase, β-glucuronidase, and *N*-acetyl-β-glucuronidase (Cabral *et al.*, 1990). It is likely that there are many other as yet unidentified differences between peripheral and posterior RPE cells. Taken together these data indicate not only that central and peripheral RPE cells are different morphologically, but they also differ functionally and have different proliferative capacity. In addition to differences in the RPE from different topographical regions of the eye, RPE cells within regions also vary, showing differences among individual cells in granule content (Burke and Skumatz, 1998). Also the expression of many specific proteins can differ from cell to cell in the RPE (Burke *et al.*, 1996; Burke *et al.*, 2000).

Chapter 4

The lateral affect of drusen on human RPE

4.1 Introduction to drusen

Drusen are age-related extra-cellular lipoproteinaceous accumulations that deposit in the space between the RPE and the inner collagenous layer of BM (Fig. 32). They are named after the German word for node or geode, and were first described by Donders in 1854, who observed the presence in a 70-year-old retina of a reflective sphere surrounded by rings of hyperpigmentation, which he called 'drusen' (Donders, 1854). Muller (1856) confirmed Donders' description of the frequent presence of hyperpigmentation around the rims of drusen, and suggested that they were likely to be displaced RPE cells caused by the protrusion of drusen. Müller proposed that drusen result from aberrant secretion of basement membrane components by the aged RPE (Muller, 1856). Friedman and colleagues (1963) hypothesised that drusen originate from blood constituents and are closely associated with the collecting choroidal venules (Friedman et al., 1963). A recent study showed that these deposits are strongly associated with the lateral walls of the choriocapillaris, which is an area commonly known as the intercapillary pillars of the choriocapillaris (Lengyel *et al.*, 2004).

Drusen are classified into two main subgroups, hard and soft drusen (Marmor and Wolfensberger, 1998). Hard drusen are usually less than 64 μm in diameter, hemispherical structures with well-defined borders and a uniform structure and composition throughout. Soft drusen are typically larger in diameter, more irregular and heterogeneous in structure and composition (Lewis et al., 1986; Sarks et al., 1994; Spraul and Grossniklaus, 1997). Although a molecular difference in composition is not yet apparent between the two classes of drusen, studies have shown that hard drusen are mainly distributed around the equatorial retina and are present in almost 100% of individuals above the age of 43 years. Soft drusen, usually observed as a large concentration of confluent drusen, are mainly

distributed around the macular area and are representative of the development of AMD (Sarraf *et al.*, 1999).

Figure 32. Light micrograph depicting the appearance and location of a hard druse. Note the attenuation of photoreceptor outer segments (OS); druse (asterix); choroid (CH); inner segments (IS); outer nuclear layer (ONL); inner nuclear layer (INL); and ganglion cell layer (GCL). Adapted from Hageman 2001.

Although the presence of drusen per se is not an absolute predictor for the development of AMD, drusen are generally regarded as strong risk factors for the disease (Bressler *et al.*, 1990; Pauleikhoff et al., 1990b; Vinding, 1990; Bressler *et al.*, 1994). AMD is the leading cause of irreversible blindness in many countries. In the early stages of AMD, soft drusen are present clinically as yellow lesions on the retina, which may be associated with a decrease in visual acuity. However, late stages of AMD are associated with large and prominent changes in vision due to the development of either dry or wet types of AMD (Bressler *et al.*, 2005).

AMD can be divided into two types; dry and wet. Dry AMD is the more common form of the disease and accounts for up to as much as 90% of AMD. This type is characterized by a discrete area of hypopigmentation, central atrophy and high concentrations of soft drusen in the macula, and causes severe loss of central vision. Wet AMD is less common but more severe than dry AMD due to the development of choroidal neovascularization (Bressler et al., 1990). This is where the choroidal blood vessels migrate below the RPE and may leak under the retina. The bleeding may eventually cause macular scarring and complete blindness (Abdelsalam *et al.*, 1999).

Recent studies appear to be suggesting an immune-mediated contribution to the events of drusen development (Hageman *et al.*, 2001). The most compelling support for this theory is that many of the proteins identified within drusen have been functionally associated with or related to the process of inflammation or its aftermath. For example, both compliment activating molecules (Barron et al., 2001; Hageman et al., 2005; Haines et al., 2005; Klein et al., 2005) and vitronectin, a known component of the extracellular matrix of BM, have been identified within drusen (Hageman *et al.*, 1999). However the lipid composition of drusen is consistent with their derivation from RPE and photoreceptor breakdown (Holz et al., 1994). Many of the molecules identified in drusen are also common to the pathological deposits associated with other diseases, including Alzheimer's disease, atherosclerosis, elastosis, amyloidosis, and glomerulonephritis (Mullins *et al.*, 2000), thus raising the possibility that common pathogenic pathways may be involved in their formation.

The development of drusen causes lateral stretching of the RPE monolayer and physical displacement of RPE from its immediate vascular supply, the choriocapillaris (Fig. 33). This distortion affects the overlying photoreceptor cell

function by interrupting supportive RPE maintenance of the rods and cones and by shifting their alignment (Pauleikhoff et al., 1990a; Bird, 1992).

Figure 33. In the healthy eye, cones are neatly lined up to maximize their exposure to light. During age-related macular degeneration, the cones become disoriented. In addition, drusen accumulate in the underlying retinal pigment epithelium (RPE), and the membrane below the RPE thickens. Adapted from Marmor and Wolfensberger 1998.

The precise involvement of the RPE in drusen biogenesis has not been characterized rigorously and it is unclear if drusen are a cause or a consequence of RPE dysfunction. In addition, although it is generally accepted that RPE density decreases with age, little information is available concerning the density of the RPE in association with AMD and drusen grades. A number of studies have addressed the origin and composition of drusen (Haimovici *et al.*, 2001; Mullins *et al.*, 2001; Li *et al.*, 2007), however there is little information on the influence that drusen have on overlying and surrounding RPE cells.

Aim of this study

- Analyse the lateral effect of drusen on RPE cell histological features such as cell size, matrix of regularity, pigment density and binucleation, using the same method as in the previous chapter.

4.2 Results

The RPE cell layer appeared homogeneous in the central retina. In the equatorial region the presence of drusen was characterized by an absence of RPE cell layer, which was roughly circular with clear distortion of the RPE surrounding the drusen. Figure 34A is a typical image of healthy retinal RPE tissue; it displays the continuous regular hexagonal arrangement of RPE cells. The cells were all similar in size, shape and pigmentation. Figure 34B displays one of the drusen observed during this investigation. The surrounding RPE were distorted both quantitatively and qualitatively. The RPE on top of a druse appears stretched and fractured and pushed upwards. There was a general hyperpigmentation immediately adjacent to the druse.

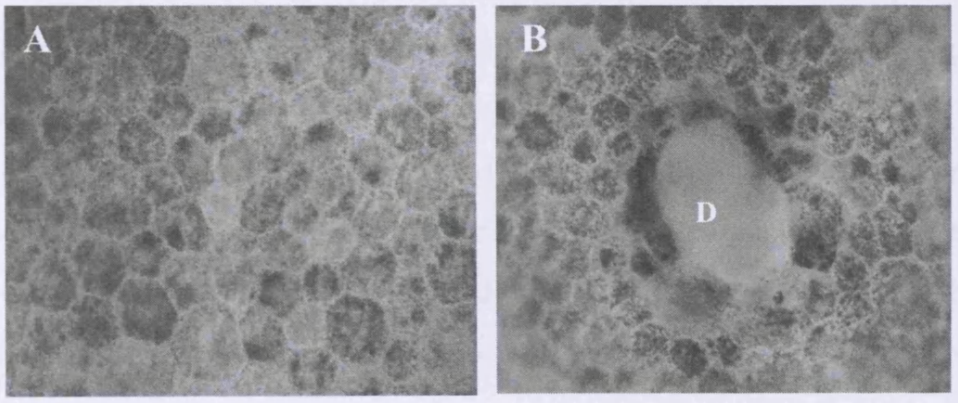

Figure 34. Images of the RPE from a 45-year old retina using an Olympus PX50 microscope with a Nikon digital camera DXM1200 attachment. (A) displays an area where there are no drusen within at least 470μm. The cells have a regular shape, pigmentation, diameter and nucleation. (B) is an image of a druse (D) and the surrounding RPE monolayer. There is apparent hyperpigmentation in some of the surrounding RPE and the RPE is considerably more irregular in shape. The marginal loss of focus indicates that the RPE in close proximity is at a different elevation to the surrounding RPE surface. Scale bar = 20μm

Another apparent difference between the control RPE samples and the RPE samples taken in the vicinity of drusen was the number of nuclei that were observed. The control cells and the majority of the RPE cells in the equatorial region were all mononucleated. However, there was an additional presence of binucleated cells within close proximity of drusen.

The results from this study show that the presence of drusen significantly alters the morphology and character of proximal RPE cells. The RPE cells were found to be smaller in regions adjacent to the drusen, however there was a significant increase in cell size within the 31–180μm band surrounding the drusen, $P = 0.0089$ (Fig. 35A). RPE cells closer to drusen appeared to have a cell shape of greater irregularity than those of the control samples (Fig. 35B). The mean presence of binucleated cells also increased within the ring of hypertrophic cells (Fig. 35C). RPE cells in direct contact with drusen were hyperpigmented, this could be due to the decrease in RPE area which increased packing in melanin granules. However, analyses of pigment density around drusen revealed no significant increase in pigment density (Fig. 35D). The effect of drusen on RPE cells was seen only in local proximity to drusen, there was no significant difference in cell irregularity, cell size and RPE cell binucleation between the control samples and all the samples that were beyond 330μm from the drusen.

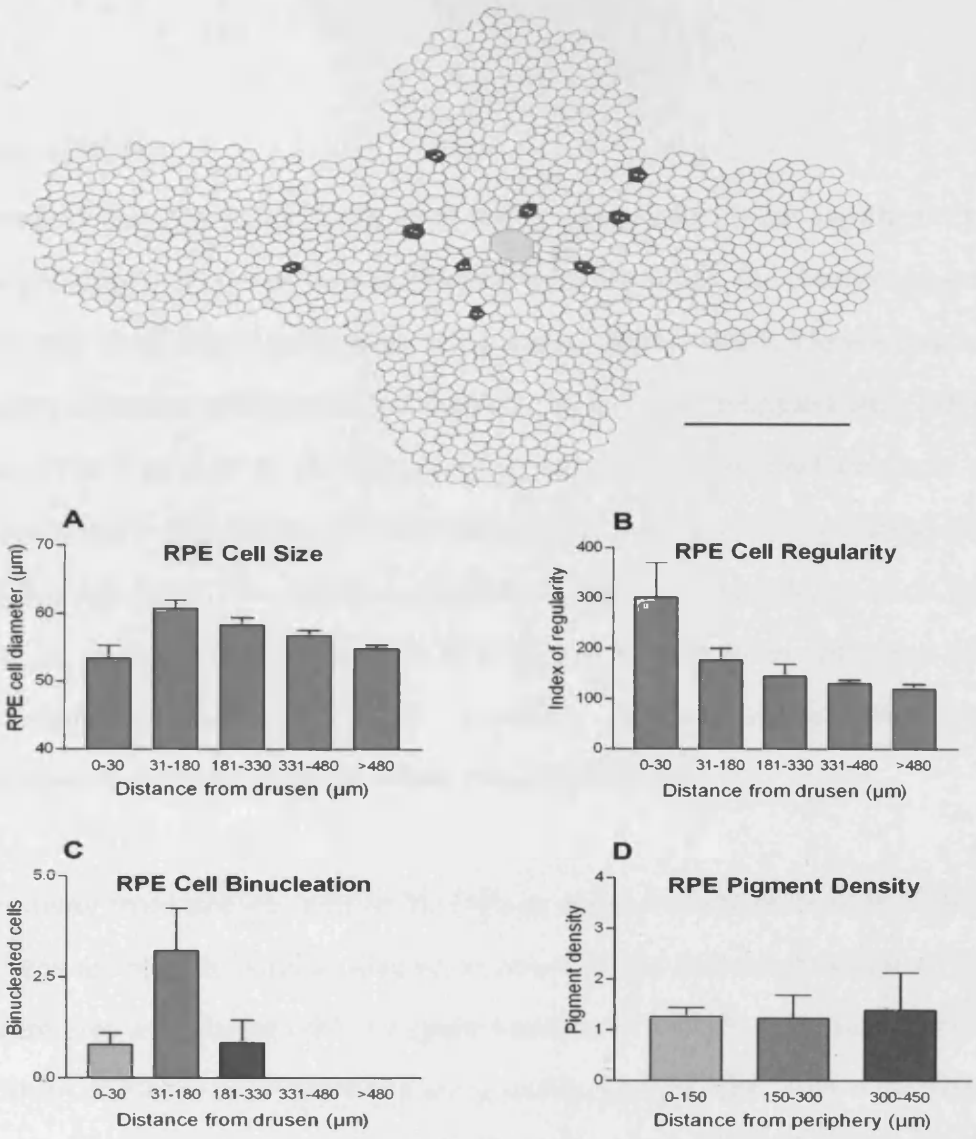

Figure 35. A depiction of the RPE surrounding a drusen (solid yellow central area) and the surrounding binucleated RPE cell from RPE sample of the 73-year-old donor. The graphs illustrate the changes seen in RPE cell histology around the drusen: (A) line chart to display the change in the mean RPE cell diameter, the RPE cells which are located within 30 microns of drusen are significantly smaller than the next group of cells ($P < 0.001$). On the other hand cells which are all 31–180 microns from the drusen are significantly larger that normal RPE cells which are at a distance of >480 from drusen (B). This graph shows that RPE cells which are close to drusen are highly irregular compared to control RPE cells, $P = 0.0297$. The greater the irregularity value (Y axis) the more irregular the cell. (C) displays the mean number of binucleated RPE cells which are significantly higher at a distance of 31–180 microns from drusen; D). shows no significant change in pigment density around drusen. Scale bar = 150 µm.

4.3 Discussion

The results from this study show that the presence of a druse significantly alters the morphology of the RPE cells surrounding it. However, the changes observed in the RPE cells were dependent on their proximity from drusen. Here a ring of small and highly irregular cells have been found to lie in an area immediately adjacent to a druse. This was due to the direct druse-induced mechanical pressure exerted upon the inner 0–30μm ring of RPE cells and can account for their small diameter and high irregularity. The relative decrease in cell diameter results in an apparent increase in melanin and lipofuscin RPE pigments which would cause a higher optical density and provide a possible explanation for the observed hyperpigmentation within the 0–30μm ring of RPE cells.

Further away from drusen, within 31–180μm, there was an increase in RPE cell size which was associated with a relative increase in the matrix of irregularity. These cells were also associated with a higher number of binucleated cells. Between 300 and 450μm the size and matrix of irregularity and of RPE cells normalized and almost all cells were mononucleated. The presence of binucleated cells in close proximity to drusen may indicate that these cells are entering the cell cycle. But the question here is what stimulates these cells to enter the cell cycle?

The RPE is a non-dividing system, however the adult mammalian RPE retains the capacity to proliferate under certain conditions, for example in response to injury (Miller *et al.*, 1986), after cryotherapy (Laqua and Machemer, 1976), or after retinal detachment (Anderson *et al.*, 1981a). When the RPE monolayer is disrupted by laser or mechanical debridement there is an upregulation of the platelet-derived growth factors (PDGF) and PDGF-receptors which contribute to the proliferation

and migration of RPE cells (Campochiaro *et al.*, 1989; Marmor and Wolfensberger, 1998).

Focal mechanical injuries to the retina have also been shown to upregulate the level of basic fibroblast growth factor bFGF, which is a known potent stimulator of RPE cell proliferation (Leschey *et al.*, 1990; Bennett and Schultz, 1993; Iseli *et al.*, 2002). Here protrusion of drusen through RPE cells results in mechanical debridement of the cells and may possibly result in upregulation of PDGF and bFGF. This could be one of the mechanisns involved in RPE cell proliferation around drusen, which is represented here as an increase in number of binucleated cells around drusen.

Retinal detachment is also associated with an increase in PDGF (Marmor and Wolfensberger, 1998) and RPE cell proliferation (Anderson et al., 1981a). Here protrusion of drusen through the RPE monolayer may also result in relative retinal detachment. This could be another mechanism contributing to the increase in the number of binucleated cells observed around drusen.

A recent study showed that the distribution of pigmented epithelial-derived factors (PEDF) was different between aged human choroids and those of AMD patients (Bhutto *et al.*, 2006). In AMD the distribution of PEDF was mainly observed in disciform scars and drusen and was significantly lower in the RPE cells. PDGF and bFGF are another two factors that are involved in AMD pathogenesis and are known to influence angiogenesis (Bennett and Schultz, 1993), which result in neovascularization. If these two factors have a distribution similar to PEDF in AMD, we would expect them to have a gradient around drusen which would decrease as we move further away from drusen. As a result the further the RPE cell is from drusen the lesser the chance of it being stimulated to enter the cell

cycle and that could also explain the proliferation observed around drusen. However further studies need to be undertaken to find out if these proliferating cells are going through complete cellular division and if not why are they inhibited.

Chapter 5

RPE cell proliferation in pigmented and albino rats

5.1 Introduction

Most vertebrates, including humans, are born hyperopic with their eyes too small relative to the refractive power of the lens and cornea (Curtin, 1985). When the eyes first receive clear images, rates of ocular growth are increased so that the eye size is matched to refractive power (Wallman, 1993), which is determined by the growth of the sclera.

In fish, amphibians and teleosts, retinal neurogenesis does not cease after the embryonic stage, but continues throughout life. The principal site of post-embryonic neurogenesis is the ciliary margin zone (CMZ), which is a ring of cells situated in the periphery of the retina. New cells are added continually from this area to the retina and continue to grow through life (Straznicky and Gaze, 1971; Johns, 1977). In amphibians these cells also participate in the regeneration process after retinal injury (Keefe, 1973).

In birds and mammals, postnatal ocular growth is not believed to involve the addition of new neurons. Instead, a passive stretching of the retina takes place to accommodate eye growth (Teakle *et al.*, 1993). However, recent studies have shown that in early postnatal chicks there is a proliferating marginal zone containing cells that share similarities with embryonic retinal progenitors and retinal stem cells of fish and amphibians (Fischer and Reh, 2000; Kubota et al., 2002). Further, the non-pigmented epithelium of the ciliary body, which is adjacent to the ciliary margin between the retina and the iris, contains quiescent stem cells. These cells do not normally proliferate but when stimulated with growth factors they undergo proliferation and are able to produce neurons (Fischer and Reh, 2003).

Although it is assumed that there is no proliferation in the neural retina of adult mammals, Ts'o & Friedman (1967) noted the presence of two mitotic figures in mature albino rat. Furthermore, recent mammalian eye studies found quiescent cells located in the pigmented ciliary body. These cells are capable of proliferating when stimulated with growth factors and they express the neuroectodermal marker nestin, which is a stem-cell marker (Ahmad *et al.*, 2000; Abdouh and Bernier, 2006). Another *in vitro* study showed that these cells are also capable of proliferating without the addition of growth factors (Tropepe *et al.*, 2001).

While it is commonly assumed that the neural retina and RPE are senescent in the adult, the observation of Ts'o and Friedman (1967) raise the question of whether mitosis might be taking place in the mature form, but, at such a low level as to be only detectable when large samples are considered. Further, the tendency to examine tissue in section rather than in whole-mount reduces the probability of identifying cell populations with a low density. Consequently, I have readdressed this issue by examining RPE whole-mounts stained with three independent markers of cell proliferation; Ki67, PCNA and BrdU.

Aim of this study

- Immune label rat flat-mounted retina with different cell-cycle marker (Ki67, PCNA) to identify RPE cells that entered the cell-cycle in pigmented and albinos animals.
- Analyse the number and distribution of RPE cells which are in cell cycle in both pigmentation phenotype.
- Immune label the flat-mounted retina with BrdU to identify and quantify RPE cells, which have undergone cellular division in pigmented animal.
- Analyse the affect of L-DOPA and light adaptation on RPE cells entering the cell cycle.

5.2 Results

5.2.1 Peripheral RPE cells entering the cell cycle

RPE cells positively identified with CRALBP and RPE65 were apparent in the pigmented and albino rat retinae that were examined (Fig 36, 37, 38). These cells had a clear hexagonal morphology and in the pigmented animals all were packed with melanin granules and had a size consistent with them being RPE cells in a single hexagonal matrix in a single plane (Fig. 37J).

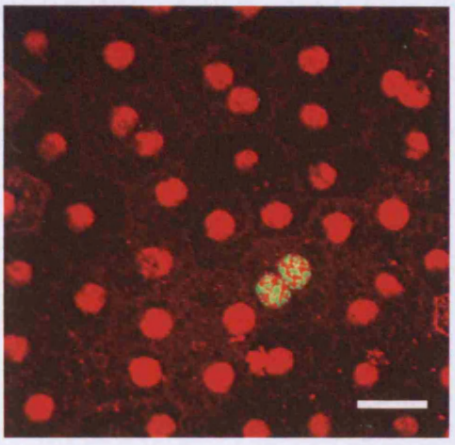

Figure 36. Image of flat-mounted retina of a P60 pigmented rat double-labelled with Ki67 (green) and CRALBP (red) using confocal microscopy. Scale bar = 20 μm.

Some of the cells positively labelled for RPE cell markers were also clearly labelled with the proliferative marker Ki67 (Figs. 37A and D); similar cells were also labelled with the other proliferative marker used, PCNA (Figs. 37K and L). However, fewer cells were labelled with the latter marker than the former, due to the fact that Ki67 labels cells in all phases of the cell cycle except G0, while PCNA labels cells in the S-phase alone. Because Ki67 labels a larger proportion of cells, subsequent analysis focused on this proliferative marker alone. Labelling with RPE65 and CRALBP defined RPE cells in both pigmented and albino rats, however

the density of labelling RPE65 was variable in some RPE cells which are also positive for Ki67 (Figs. 37D–F).

In both pigmentation phenotypes (P60), Ki67 positive cells were mainly found in the peripheral and equatorial retina (Fig. 39A and B). Almost none were seen centrally, close to the optic nerve head. Negative controls for Ki67 failed to show any label in the RPE. The number of Ki67 positive cells found in the RPE of pigmented animals was relatively small, being of the order of 20–30 in each retina. In contrast, in albino retinae this number was markedly larger, being in the order of 200–300 (Figs. 39C and D). Thus the number of cells in the cell cycle in albino retinae was approximately ten times greater than that found in pigmented animals (Fig. 40C).

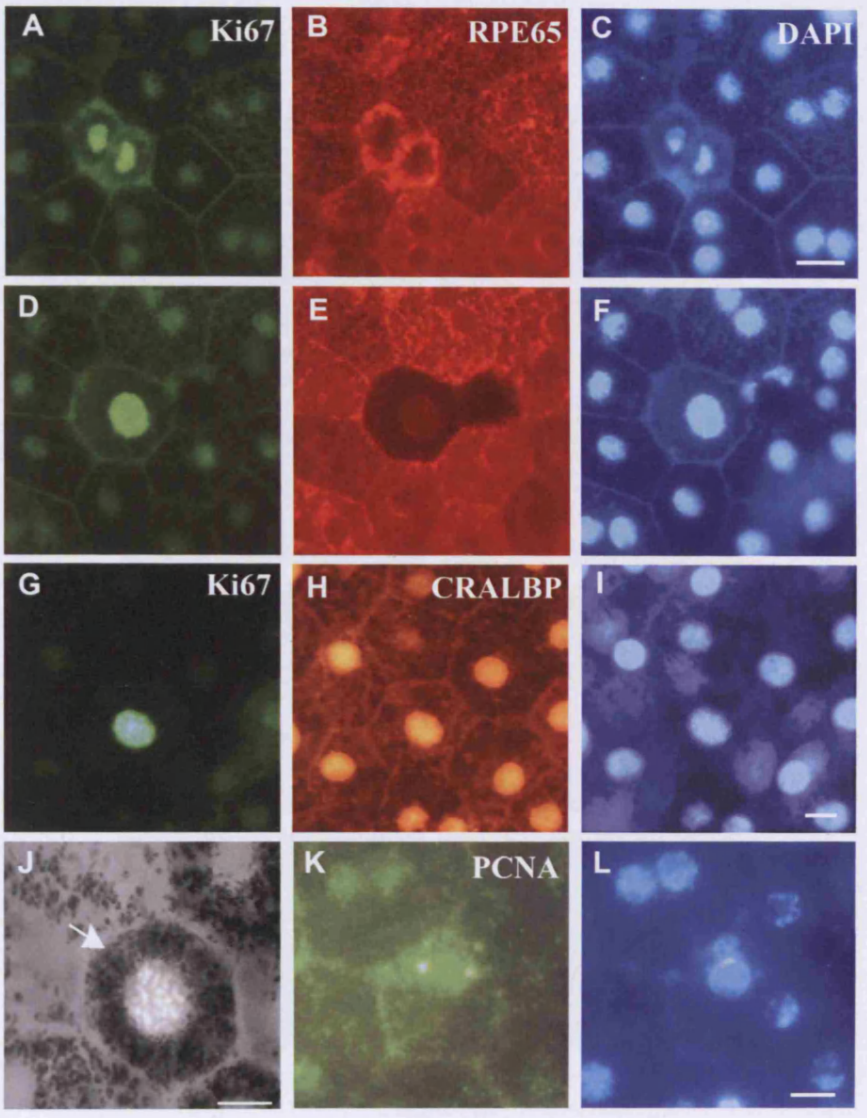

Figure 37. Labelling patterns in whole-mounted eye pigmented cups looking down at the RPE surface. (A) is an RPE cell positive for Ki67 in the apparent anaphase. (B) shows the same cell labelled with RPE65, and (C) the same cell stained with DAPI revealing the nuclei of the cells. (D), (E) and (F) are similar preparations; however, in this case the RPE cell positive for Ki67 has down-regulated RPE 65 to a level just above that found in negative controls. (G) is again a Ki67 positive cell, but in (H) it has been labelled with a second RPE-specific marker CRALBP, again confirming that it is an RPE cell. (I) is the DAPI image. (J) is a Ki67-positive cell where the melanin granules can be clearly identified around the labelled nucleus, confirming its identity as an RPE cell. (K) is an RPE cell positively labelled with the cell cycle marker PCNA and L is the DAPI image of the same cell. Scale bar = 10μm.

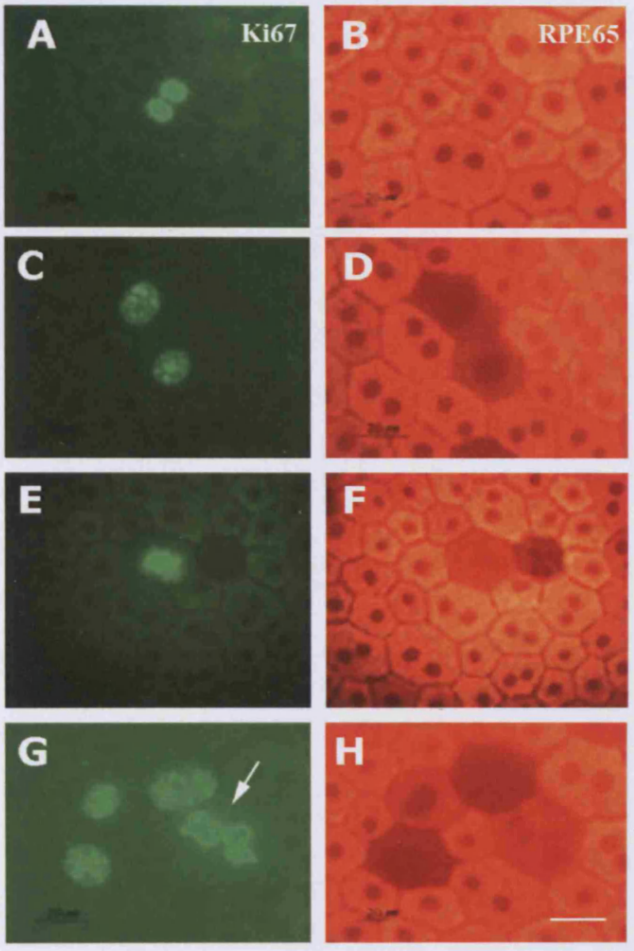

Figure 38. Images of a flat-mounted retina from a P60 albino rat. (A) & (B) show binucleated Ki67-positive RPE cells with the corresponding RPE65 labelling. (C) & (E) show two positive Ki67 cells which appear to have the same origin with their corresponding RPE65 labelling in (D) & (F) respectively. (G) & (H) show four positive Ki67 cells; the arrow points at an RPE which is anaphase of the cell cycle. Scale =20μm.

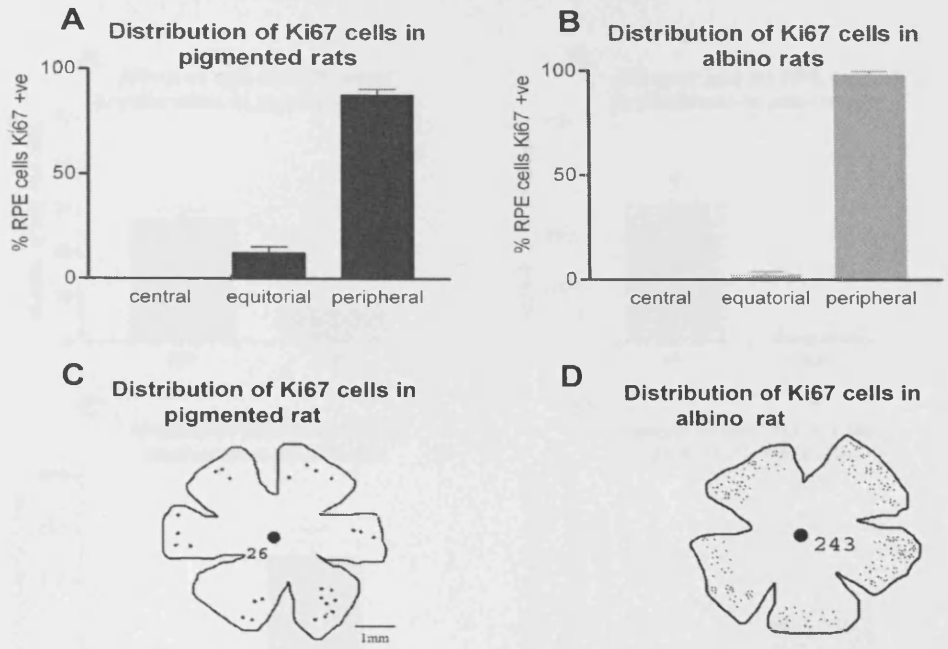

Figure 39. The distribution and relative number of Ki67 cells in pigmented and albino retinae. In both pigmentation phenotypes the distribution of Ki67-positive cells was strongly biased towards the retinal periphery, with a few spreading into equatorial regions (A and B) ANOVA, P< 0.0001. Equatorial versus peripheral, Newman Keuls P< 0.001. (C) and (D) are outline diagrams of retinae showing the distribution and density of Ki67 cells in both pigmented and albino rats. On average, the total number of positive Ki67 cells in pigmented rats was 25 ± 5 cells/retina whereas in albino rats it was 250 ±50 cells/retina (N=5).

Figure 39 shows that aging reduces the number of proliferative cells in both pigmented and albino rats. At 360 days, only 8–10 Ki67-positive cells were found in DA rats, which was significantly less than what is found at 2 months (P<0.0001) and only around 15 in albino ones, which again was a statistically significant age-related reduction (P<0.0001). In spite of this decline, the numbers found in albino animals still remained significantly higher than in the age-matched pigmented animals (P<0.01).

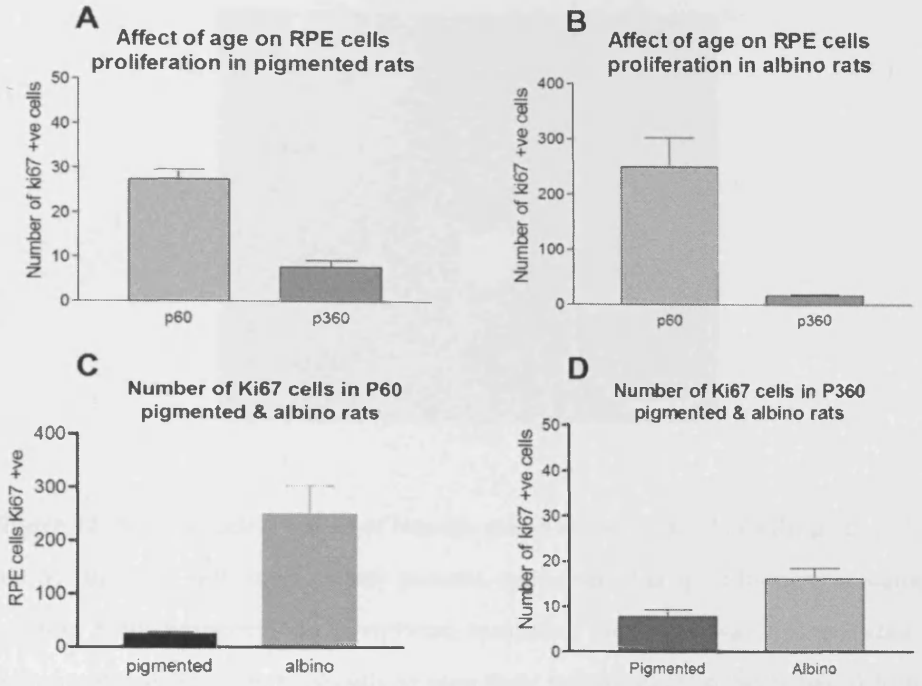

Figure 40. Graphs A and B show the effect of age on RPE cell proliferation in both pigmented and nonpigmented animals. Both graphs show a statistically significant decrease in levels of proliferation with age (pigmented P = 0.0001; albino P = 0.0007). Graph C shows approximately a ten-times increase in Ki67-positive cells found in the albino rats compared with the pigmented ones, with a statistical significance of Newman-Keuls ($P < 0.01$). Graph D shows a reduction in proliferation with age in both pigmented and non-pigmented animals, but the proliferation is still more significant in albino rats (P= 0.0076; N=5).

The presence of Ki67-positive cells was also confirmed in human tissue (Fig. 41), however, given that only a small sheet of human RPE was examined, it was not possible to determine their number or distribution, only to confirm their presence.

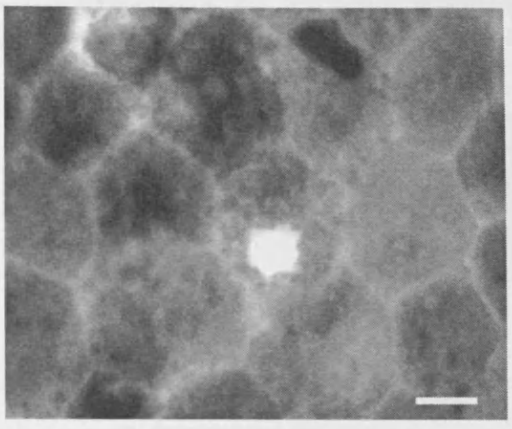

Figure 41. A grey scaled image of human retina showing Ki67 labelling of an RPE cell. While these cells were clearly present, only a small strip of tissue was stained running from equatorial to peripheral locations. Hence, it was not possible to estimate the number of these cells or map their retinal location. Scale bar =10μm.

The RPE is generated as a monolayer prenatally, but by the second week of life in rats a large cell population undergoes nuclear division, which does not appear to translate into full cell division, leaving a cellular population that is largely bi-nucleated (Stroeva and Mitashov, 1983). Figure 42 shows the distribution of bi-nucleated cells in P60 pigmented and albino rat retinae that have been divided into central, equatorial and peripheral retinal regions. In both pigmentation phenotypes approximately 75% of central RPE cells were binucleated and few contained more than two nuclei. The percentage of binucleated cells decreases slightly in the equatorial region of pigmented animals to approximately 65%. However a significant decrease in the number of binucleated cells was observed in peripheral retinae of both pigmentation phenotypes, where only 10–20% of cells contained more than one nucleus.

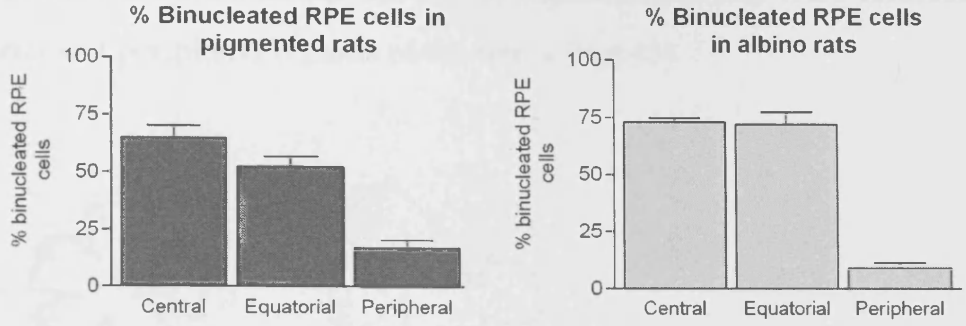

Figure 42. In adult rodent retinae many of the RPE cells are binucleated. The proportion of these have been determined in both pigmented (A) and albino (B) retinae. In both pigmentation phenotypes the majority of the binucleated cells are located towards the central retina, although many are also found in equatorial regions. In this respect the distribution of these cells is the reverse pattern of that found for Ki67-positive cells revealed in Figure 4. The differences in (A) and (B) are statistically significant (ANOVA, $P<0.001$). In both cases the small differences between central and equatorial regions were not significant. However, differences between central and peripheral regions were statistically significant (Newman-Keuls, $P<0.01$), as were those between equatorial and peripheral areas (Newman-Keuls, $P<0.01$; $N=5$).

As the retina develops with a centre to periphery gradient (Mann, 1964), such that late cell division occurs in the peripheral retina, it is natural to ask whether the relatively peripheral patterns of Ki67 labelling found in the mature RPE are not simply a reflection of those patterns present during late development, or whether they represent a distinct and separate event.

RPE flat mounts from pigmented animals at progressive stages from E18 through the postnatal period and into maturity were immune stained with Ki67. Unfortunately, it was not possible to generate retinal whole-mounts of sufficient quality prior to E18 consistently without inducing some damage to the periphery that resulted in loss of labelled cells. At all stages of development, few if any Ki67-

positive cells were identified in the central region, rather they were confined to the equatorial and peripheral regions of the retina (Fig. 43).

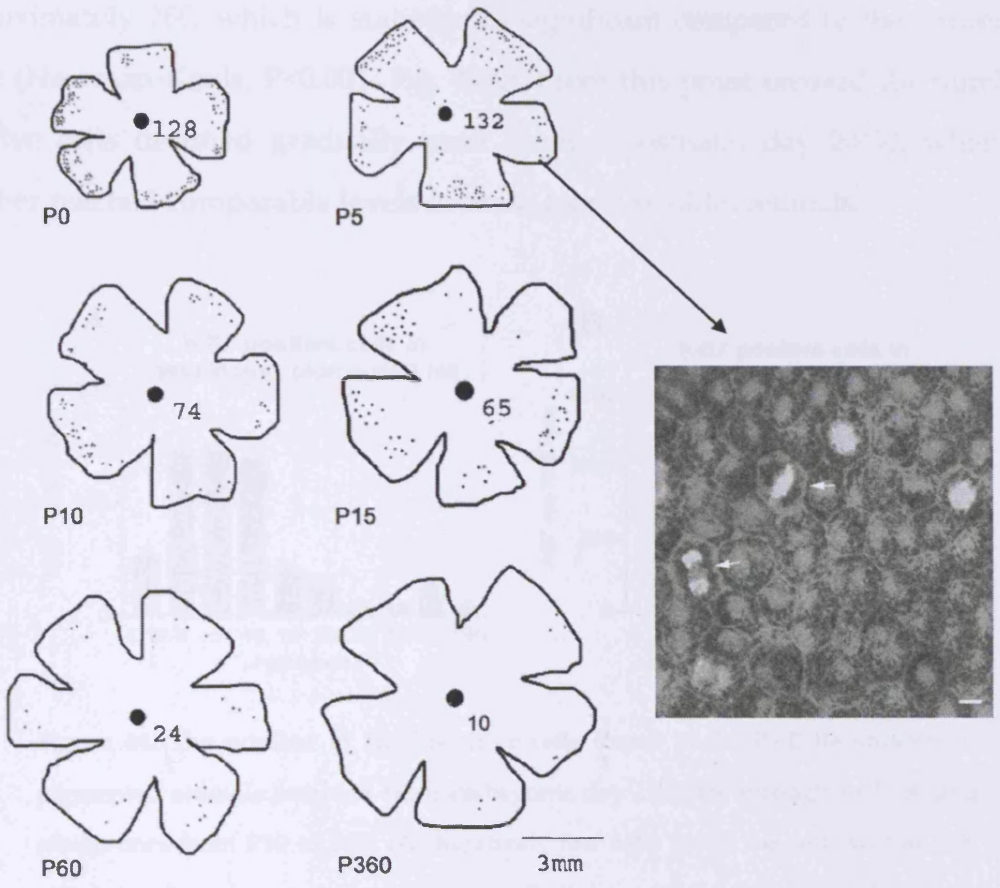

Figure 43. (A) Outline diagrams of the relative location and distribution of Ki67-positive RPE cells (black dots) in developing retina of P0-P360 pigmented rats. At all ages labelled Ki67 cells are mainly distributed in the peripheral and equatorial retinae and their numbers decrease with age. (B) Ki67-positive cells at different stages of the cell cycle (arrow pointing to anaphase and metaphase) from postnatal day 5 pigmented rats. Scale bar =10μm.

At E18 approximately 50 Ki67-positive cells could be identified in the RPE whole-mounts of pigmented animals. However, three days on from the day of birth, there was a large increase in the number of positive cells found, from around 50 to approximately 260, which is statistically significant compared to the earlier time point (Newman-Keuls, P<0.001; Fig. 44A). From this point onward the number of positive cells declined gradually until around postnatal day 20/30, when their number reached comparable levels to those found in older animals.

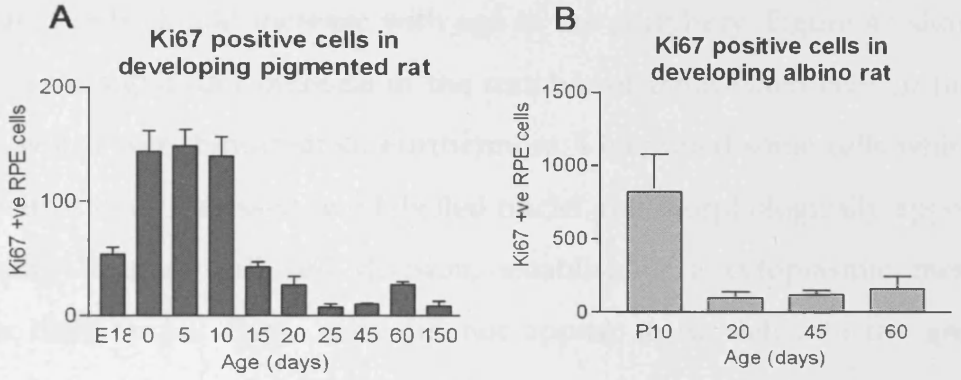

Figure 44. The number of Ki67-positive cells found in the RPE flat-mounts of pigmented animals sampled from embryonic day 18 (E18) through to P150 and albino ones from P10 to P60. (A) Relatively few cells are in the cell cycle at E18, which is when the normal patterns of cell division in the developing tissue are coming to an end. However, there is a marked increase (ANOVA, P<0.0001) in the number of these cells on the day of birth (0) which is statistically significant compared with the earlier time point (Newman-Keuls, P<0.001). From that point their number gradually declines with age. (B) shows similar patterns of cell division in the developing albino rats with a marked decline at approximately P15-20 (N = 5).

The analysis in albino rats did not cover as extensive a time period as in the pigmented animals. The patterns of Ki67 labelling through postnatal development were nevertheless similar to pigmented rats, although the absolute number of positive cells found was markedly elevated (Fig. 44B). These data are consistent

with the notion that the increase in cell labelling found in the RPE around the time of birth may represent a distinct and separate event from earlier patterns that established this cellular population.

To find out if the Ki67-positive cells in the periphery were dividing or undergoing only nuclear division to become binucleated, a comparative analysis of the number of binucleated cells in P20 and P60 pigmented animals was undertaken. If the nuclei of RPE cells are dividing but not the cytoplasm, then the number of binucleated cells should increase with age in the periphery. Figure 45 shows that there was no significant increase in the number of binucleated cells in the older animals which were binucleated. Furthermore, I identified some cells which were Ki67 positive that possessed two labelled nuclei and morphologically appeared to be passing through full cell division, establishing a cytoplasmic membrane between their nuclei. These cells did not appear to fit well into the geometric configuration of the regular RPE (Fig. 46).

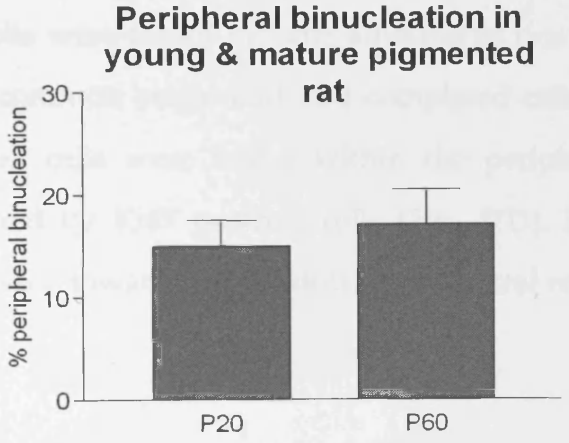

Figure 45. The graph shows the percentage of RPE cells that are binucleated in the peripheral retina in both young (P20) and adult (P60) pigmented rats. There is no significant change in the number of binucleated cells seen in the periphery in young rats compared to an adult in pigmented animals. (P= 0.7302; N=5).

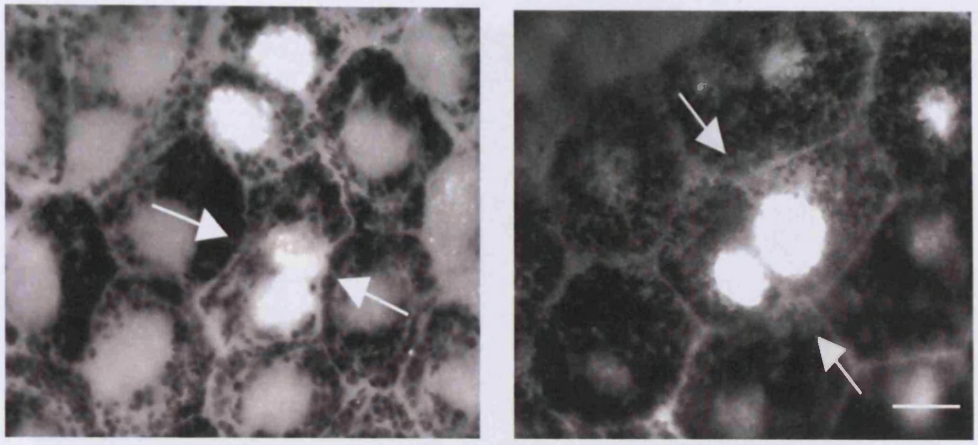

Figure 46. In the peripheral retina a small number of cells could be identified that appeared to be passing through full cell division. In the two cases shown, two Ki67+ nuclei can be identified that appear to be forming a plasma membrane between them. Further, the two together appear irregular in the RPE cell matrix (Scale bar = 10 μm).

To confirm cellular division six DA rats were injected with BrdU for 20 days and then immune labelled with BrdU. Figure 46 (A, B) shows binucleated RPE cells positively labelled for BrdU and Otx2 which is an RPE cell marker. Almost all mononucleated cells were found in pairs adjacent to one another, indicating that these cells had a common origin and had completed cellular division (Fig. 47C). Here BrdU-labelled cells were found within the peripheral proliferative zone, which was occupied by Ki67 positive cells (Fig. 47D). However, 16% of BrdU positive cells migrated toward the equatorial and central retina (Fig 48).

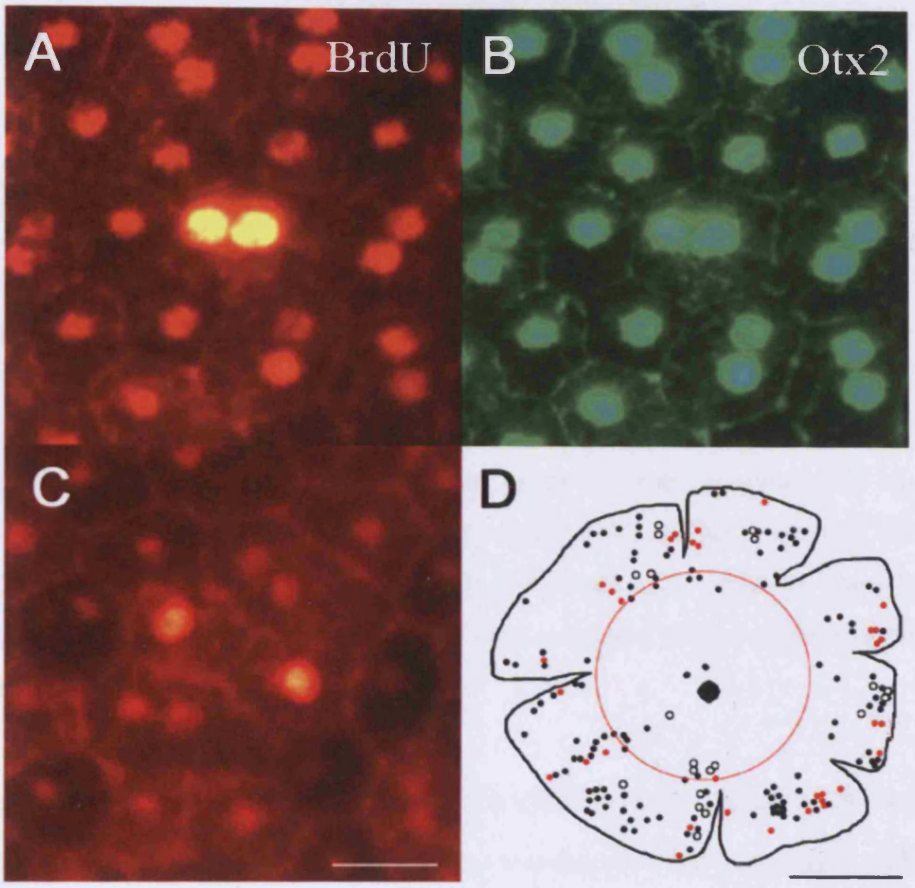

Figure 47. BrdU labelling in mature RPE cells. (A) & (B) show a double-labelled cell with BrdU on a red channel and Otx on a green channel which is an RPE-specific cell marker. (C) shows two adjacent mononucleated cells which have common origins indicating complete cellular divisions. Scale bar = 20μm. Line drawing (D) represents a flat-mounted retina double-labelled for Ki67 and BrdU. The diagram shows the distribution of positive binucleated (black dots) and mononucleated (black circle) and BrdU cells. The mononucleated cells were almost always found in pairs in close proximity. The red dots represent the relative distribution and density of Ki67-positive RPE cells which show similar distribution to BrdU positive cells. (Scale bar= 2.5 mm).

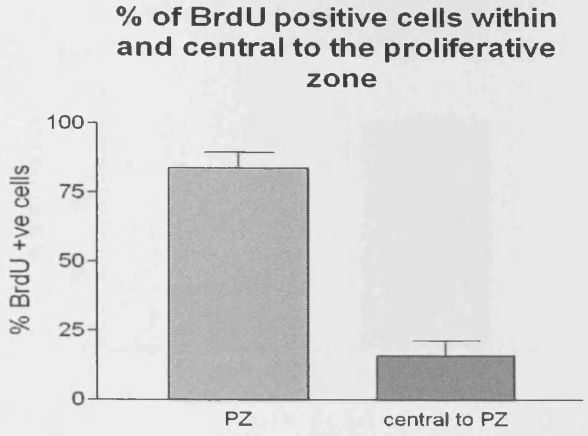

Figure 48. The graph illustrates the percentage of BrdU positive cells that migrated centrally beyond the peripheral proliferative zone. An average of 16% of BrdU-labelled cells migrated from the peripheral zone, which is normally occupied by Ki67 positive cells, toward equatorial and central regions of the retina. (N=3)

To identify what proportion of cells undergo full cellular division as opposed to only nuclear division, the number of mononucleated BrdU positive cells which were in close proximity (indicating similar origin) were counted and compared to the number of binucleated BrdU positive cells. As the animals were sacrificed 20 days after the last BrdU injection, we were expecting all labelled cells to be mononucleated indicating that they have undergone cellular division as opposed to nuclear division. However, the total number of positive BrdU cells was 150 cells, of which 75% were binucleated and 25% mononucleated (Fig. 49). This indicates that only 25% of RPE cells were capable of completing cellular division and the rest had undergone nuclear division.

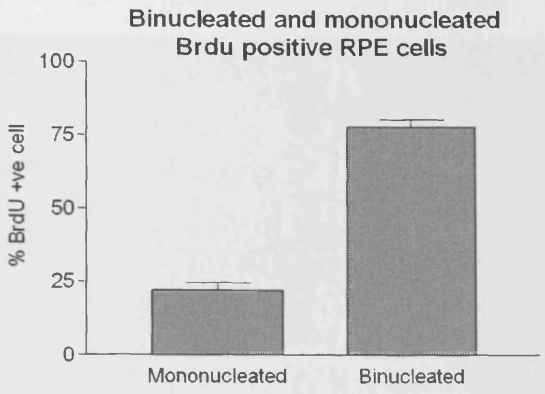

Figure 49. The graph compares the percentage of mononucleated positive RPE cells to binucleated positive BrdU cells in pigmented rats. On average the total number of labelled Brdu cells is 150 + 20 cells/ retina. Of these cells, 25% are mononucleated, these undergo cellular division, and the remaining 75% of binucleated cells are probably cells withheld within the cell cycle ($P<0.0001$).

5.2.2 RPE65 and Ki67 colocalization

The level of RPE65 protein expression is higher in pigmented rats than in albino rats (Iseli *et al.*, 2002). This difference was observed in two pigmented phenotypes as a difference in the density of RPE65 labelling. In albino rats the density of RPE65 labelling varied across the retina. Some RPE cells showed negative or low density labelling of RPE65, whereas other cells showed normal labelling of RPE65. The distribution of these cells was random across the retina. In pigmented animals the entire retina was positive for RPE65 and the control showed a black image (Fig. 50C). However, the density of labelling varied from the central to peripheral regions of the retina. In the central retina the density of RPE65 labelling was higher than in the periphery, showing clearly the hexagonal structure of each cell with the central two nuclei. The peripheral region showed a lower level of intensity of labelling compared to the control and both the structure and the nucleus were not very clear (Fig. 50).

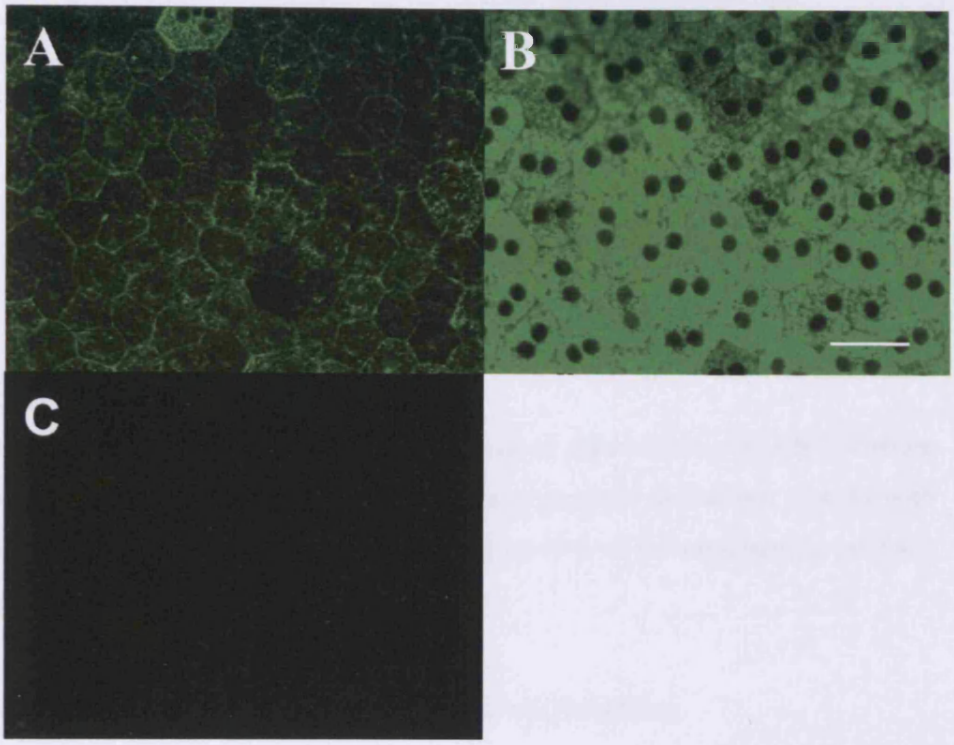

Figure 50. The difference in RPE65 density labelling between the peripheral and central retina in a P60 pigmented animal. (A) Image of the low density labelling of RPE65 in the peripheral retina, here the distribution of RPE65 is mainly observed in the cell membrane. (B) Image of the normal intensity of RPE65 labelling in the central retina, which shows a clear distribution of the labelling in the entire RPE cell. (C) shows control image without the RPE65 antibody. Scale bar=20μm.

The other important observation was the relationship between Ki67-labelled cells and the density of RPE65 labelling. In pigmented animals there was approximately 75% colocalization between Ki67-positive cells and low density labelling with RPE65 (Fig. 51). This relationship could be simply related to the peripheral distribution of Ki67-labelled cells. However, this relationship was also observed in albino animals where approximately 70% of Ki67-labelled cells were negative for RPE65. This may suggest that there is a relationship between the expression of RPE65 and RPE cell proliferation.

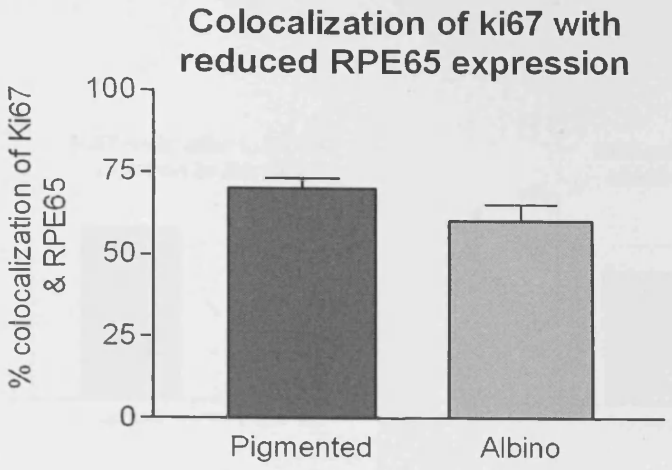

Figure 51. The graph shows the percentage of colocalization of Ki67 labelling with RPE65 low density labelling in both pigmented and albino rats. In both groups the percentage of localization was 60–70% of the total number of Ki67-positive cells (N=5).

5.2.3 Effect of L-DOPA on RPE cell proliferation

Insufficient levels of L-DOPA in albino animals are considered responsible for abnormal development of the underlying neural retina (as reviewed by Jeffery (1997). In addition, albinos have abnormal patterns of cell production in the developing retinae, as the number of mitotic figures is elevated compared with age-matched retinae from pigmented animals. The addition of L-DOPA normalizes this abnormality (Ilia and Jeffery, 1999; Tibber et al., 2006). Furthermore, exogenous dopamine significantly prolongs mitosis in retinae from albino, but not pigmented animals (Kralj-Hans *et al.*, 2006). Here we explore the effect of L-DOPA on RPE cell proliferation in both pigmentation phenotypes from postnatal day 60. An intra-peritoneal injection of L-DOPA was given to both albino and pigmented animals and then the retinae were analysed for the number of Ki67-labelled cells 18 hours post injection. Figure 46 shows that giving an injection of L-DOPA decreases the number of Ki67-positive cells in pigmented rats (P= 0.0043) but had no effect on albinos (Fig. 52).

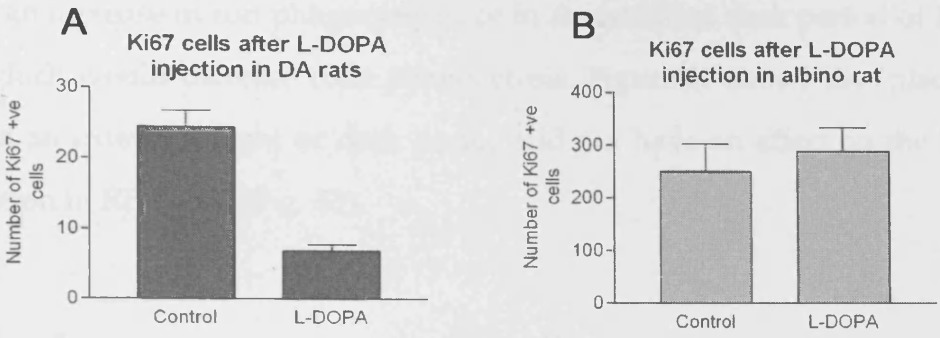

Figure 52. The effect of an 18-hour L-DOPA injection on the level of proliferation in pigmented and non-pigmented animals. Graph A shows a decrease in the number of Ki67-134 positive cells in P60 pigmented animals due to an L-DOPA injection P=0.0043, whereas graph B shows no effect of L-DOPA on the level of proliferation in P60 non-pigmented animals.

5.2.4 The light-adaptive state of the retina

Intraocular luminan levels are much greater in albino eyes. It was thus of interest to find out if it is the case that the greater light levels experienced by albinos due to the absence of light-absorbing melanin in some way contributes to different patterns of RPE cell proliferation. Furthermore the light/dark cycle of the day has a fundamental role in many processes that take place in the retina. One important example is photoreceptor outer segment (POS) phagocytosis (Saari *et al.*, 1994), where outer segment phagocytosis of rods takes place shortly after the beginning of the light period and outer segment phagocytosis of cones takes place in the dark (Young and Bok, 1969). This process may represent one method of communication between the neural retina and the RPE, which could be manipulated by prolonged dark or light adaptation (LaVail, 1980, , 1983).

To find out whether increased phagocytosis of either rods or cones has any affect on RPE cell proliferation, I manipulated the light-dark cycle. Here pigmented animals were placed in either an extended light period of 27 hours, which would

result in an increase in rod phagocytosis, or in an extended dark period of 17 or 40 hours, which would increase cone phagocytosis. Figure 37 shows that placing the animal in an extended light or dark period did not have an effect on the level of proliferation in RPE cells (Fig. 53).

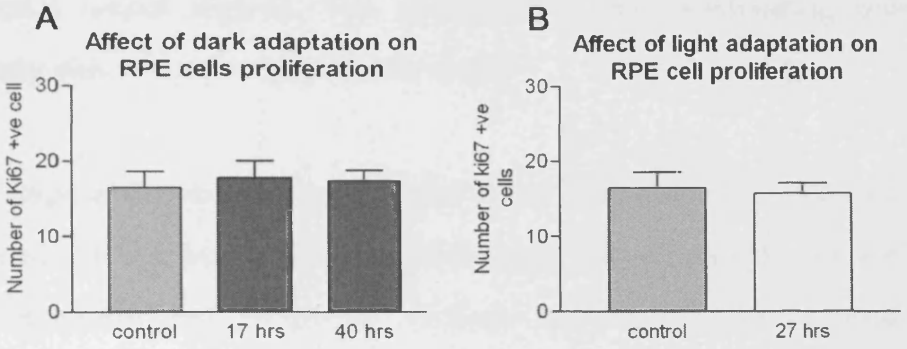

Figure 53. The effect of light and dark adaptation on RPE cell proliferation in P60 pigmented animals. (A) DA rats were dark adapted for 17 and 40 hours; the graph shows no effect of dark adaptation on the number of Ki67 positive cells. (B) DA rats were light adapted for 27 hours; here also the graph shows no effect of light adaptation on the number of Ki67-positive cells (N=5).

4.6 Discussion

I have shown, using three independent markers for proliferation (Ki67, PCNA, BrdU) and three independent functional markers of RPE cells (RPE65, CRALBP, Otx), that a proportion of mature RPE cells has the capacity to enter into the cell cycle and complete cellular division in the peripheral retina and to a lesser extent in equatorial retinal regions. The number of these proliferating cells is very significantly elevated when pigment is absent.

At every stage of development examined, the distribution of binucleated cells was largely confined to central and equatorial regions alone, and that of Ki67 positive cells to equatorial and peripheral regions. Hence, we find no evidence that geographic patterns for the two populations are dynamic; Ki67-positive cells remain confined largely to the periphery and binucleated cells are mainly located centrally, irrespective of the postnatal age.

A question that arises from this study is what proportion of cells identified here are going through full cell division compared with nuclear division alone? The weight of evidence suggests that at least some of these cells are going through full cell division, based on the stability of the binucleated population in the periphery, and the morphological identification of dividing cells. Furthermore, of those cells labelled with BrdU approximately 25% were capable of completing cellular division and approximately 16% appeared to be migrating toward central retina. RPE cell migration, from central to peripheral retina to replace apoptotic central RPE cells, has been suggested by Del Priore *et al* 2002. However, we can not rule out the possibility that a very slow rate of RPE cell proliferation is taking place in central retina, which could have been picked up by repeated injections of BrdU.

Both pigmented and albino rats were used, as albino photoreceptor numbers are significantly reduced (Jeffery *et al.*, 1994a; Jeffery *et al.*, 1997; Grant *et al.*, 2001) and this reduced contact between the two tissues may mimic in a small way the changes found when the retina is detached which results in RPE cell proliferation (Anderson et al., 1981a). Also, during development albino retinae are abnormally proliferative due to the absence of L-DOPA, a key cell-cycle regulator and an upstream element in melanin synthesis (Ilia and Jeffery, 1999; Tibber et al., 2006).

When the level of proliferation between pigmented and hypopigmented animals was compared there was an increase of ten times in the number of Ki67 positive cells in the latter group, which may indicate a possible role for either L-DOPA or the number of photoreceptors on RPE cell proliferation. Further, in both pigmented phenotypes approximately 70% of cells which were positive for Ki67 expressed low levels of RPE65. As the level of RPE65 is lower in albino animals compared to pigmented ones (Iseli *et al.*, 2002), this could be another factor influencing the level of proliferation in albino rats.

In the light of these results I examined two factors for a possible role in RPE cell proliferation. The first factor is the effect of L-DOPA, a key cell-cycle regulator (Ilia and Jeffery, 1999; Tibber et al., 2006), on both pigmentation phenotypes. The second is the effect of the level of illumination on proliferation, as intraocular luminan levels are much greater in albino eyes. Could it be the case that the greater light levels experienced by albinos, due to the absence of light-absorbing melanin, in some way contributes to different patterns of RPE cell proliferation? A possible route for this might be their own ability to detect light levels via intrinsic expressions of melanopsin (Peirson *et al.*, 2004; Peirson and Foster, 2006). In addition, the light/dark cycle affects many physiological processes in the retina such as the concentration of retinal dopamine (Wirz-Justice *et al.*, 1984) and

photoreceptor outer segment disk shedding (LaVail, 1976, , 1980). Hence, I increased illumination levels in pigmented phenotypes to see if there is a significant variation.

Increasing the levels of endogenous L-DOPA had a significant increase on the number of proliferative RPE cells in pigmented animals but not albinos. Since neural cells play a role in converting L-DOPA in dopamine cells (Kubrusly *et al.*, 2003), the reduction in the effect of L-DOPA in albinos may be due to a reduction in neural cell density (Jeffery and Kinsella, 1992; Jeffery *et al.*, 1994b). On the other hand changing the level of illumination had no effect on a number of proliferative RPE cells.

Why has cell division in the mature RPE not been identified before and why might it occur? Rodent RPE is rarely viewed in whole-mount because it is very difficult to remove as a coherent tissue without significant damage. For this reason it is commonly viewed in section, where this important, but relatively sparse, cell population would be hard to identify. Examination of normal adult cat retinae, labelled with tritiated thymidine to mark dividing cells, failed to produce positive labels in the RPE (Anderson *et al.*, 1981b). Ts'o & Friedman (1967) noted two mitotic nuclei in mature albino retinae, but these could have been dividing nuclei as opposed to dividing cells, and were not noted in other retinae used in their study. An additional reason why these cells have not been identified is simply that no investigation hitherto has used cell-cycle markers such as Ki67 or BrdU on whole-mounted mature RPE. In spite of this, a proliferative zone in the neural retina and the RPE at the retinal margin has been noted at an early stage in the hatched chick (Fischer and Reh, 2000; Fischer, 2005) and here the level of proliferation was of sufficient magnitude to be obvious in section, but it is unclear for how long this was sustained.

Another important question that arises from this study is: Why is it only the peripheral retina that has the capacity to proliferate and can these proliferative cells act as progenitor cells? Previous *in vitro* experiments on adult bovine RPE cells have shown that RPE cells from the periphery have higher proliferative capacity than do RPE cells derived from the posterior pole (Burke and Soref, 1988). This was also observed in cultured human RPE where cells from peripheral areas entered the proliferative phase earlier than cells from the macular region (Flood *et al.*, 1984). In addition, in gene analysis studies, two cell-cycle genes were found to be upregulated in the peripheral retina and not in the central retina (Ishibashi et al., 2004). However, the most revealing *in vivo* experiment, comparing the proliferative capacity of RPE cells in the central and peripheral regions of the retina, was done by Kiilgaard and colleagues (2007). They showed that in porcines, experimental surgical injury of the RPE below the central retina was followed within 48 hours by a peripheral, but not central, proliferation of RPE cells (Kiilgaard *et al.*, 2007). In addition, a recent study showed that postnatal chickens have a zone of proliferating cells at the peripheral margin of the retina, similar to that of fish and amphibians (Straznicky and Gaze, 1971; Johns, 1977; Fischer and Reh, 2000). The above studies clearly show that RPE proliferative capacity is controlled by regional distribution, however the reason for this is unknown.

In rat retinae I found no histological difference between central and peripheral RPE cells, as discussed in chapter 2. In this study, however, I did observe an interesting difference between the central and the peripheral retina. In pigmented animals, the density level of RPE65 labelling was lower in the peripheral cells than in the central retinal cells, which may indicate a down-regulation of RPE65 in the periphery. However in albinos, more cells were observed to have a low RPE65 density and they were randomly distributed. This could be due to lower expression of RPE65 in albino animals (Iseli *et al.*, 2002). Furthermore, in both

pigmentation phenotypes 70% of cells which were labelled for Ki67 were also down-regulating RPE65. This may indicate a relationship between down-regulation of RPE65 and the capacity of RPE cells to proliferate. It is of interest here that amphibians' mature RPE cells also express the tissue-specific marker RPE65. However, following retinal removal, RPE cells down-regulate RPE65 while proliferating and transdifferentiating, and it is only up-regulated when retinal production is complete and transdifferentiation ceases (Chiba *et al.*, 2006).

During the development of the eye, a group of founder cells in the optic vesicle gives rise to multipotent progenitor cells that generate all the neurons and glia of the mature retina (Wetts and Fraser, 1988). In most vertebrates, a small group of retinal stem cells persists at the margin of the retina, near the junction with the ciliary epithelium. In fish and amphibians, the retinal stem cells continue to produce progenitors throughout life, adding new retina to the periphery of the existing retina as the eye grows (Raymond and Jackson, 1995). While in amphibians and fish new neurons are added in the retinal periphery throughout the life of the animal, retinal histogenesis in mammals occurs only during development and is completed in the rodent at postnatal days 11–12 (Young, 1985). In addition, a recent study showed that postnatal chickens have a zone of proliferating cells at the peripheral margin of the retina, similar to that of fish and amphibians (Straznicky and Gaze, 1971; Johns, 1977; Fischer and Reh, 2000).

If the peripheral RPE is undergoing gradual cell addition, then it is probable that this is a process that replenishes the tissue when it is subjected to normal age-related cell loss. However, a confounding factor in attempting to understand what these cells are doing is that we have no idea of how long their cell cycle is. No data exists for RPE cell-cycle length during development. The retinal cell-cycle lengths vary with time from around 10/14h early in development to more than 30h when

the last retinal neurons are added around postnatal day 4 (Young, 1985). Because of this it is possible that the cell cycle in the mature animals studied here could be taking weeks.

Here I demonstrate that mature RPE has a proliferative capacity that is rare in the mammalian CNS. A recent *in vitro* study showed that adult human RPE cells, even from elderly persons, are capable of transdifferentiating into neurons, although the ratio of mature neurons was greater in the young than in the old cell line (Amemiya *et al.*, 2004). This capacity is enhanced if the retina is removed (Anderson et al., 1981b). Some amphibians have the ability to take this a stage further and are able to regenerate a new retina from transdifferentiation of the proliferating RPE population (Chiba et al., 2006). Mammals seem to have retained an element of this process in their ability to proliferate, but appear to lack the regulatory elements necessary to control RPE proliferation appropriately and induce transdifferentiation. However, if entry into the cell cycle and division of these cells could be regulated, it would have very significant implications for disease processes where the RPE is either lost or damaged, such as age-related macular degeneration, and the important question would be what determines the proliferation of these cells?

Chapter 6

Changes in RPE cell gene expression after retinal detachment

6.1 Introduction

6.1.1 Retinal detachment

Retinal detachment is the separation of the neural retina from the retinal pigment epithelium (Fig. 54) and clinically it could occur for a number of reasons. First, due to a tear in the retina that allows fluid to pass from the vitreous space into the subretinal space, which is called rhegmatogenous retinal detachment. Second, due to the accumulation of fluid under the retina with out a tear due to inflammation or vascular abnormalities, this is called exodative retinal detachment. Third, tractional detachment, which occurs when fibrovasclar tissue pulls the sensory retina from the RPE.

Figure 54. 3-D Schematic image of the retina showing retinal detachment. The neural retina has dissociated from the back of the eye in the inferior quadrant. Retinal detachment may occur as a result of retinal tear. A break in the retina allows vitreous fluid to leak behind the retina causing it to separate from the RPE. Adopted from Steven Fisher (www.shands.org/health/ surgeries/100132.html).

In human retinal detachment starts a cascade of events resulting in cellular changes in the retina. Several studies have been undertaken to analyse the neuronal changes associated with retinal detachment in an attempt to understand the pathogenesis associated with this. Figure 55 shows a summary of the changes associated with retinal detachment. These changes included loss of structural integrity and apoptotic death of photoreceptor cells, neurite outgrowth from second-order neurons, proliferation of non-neuronal cell types, and extensive hypertrophy of Müller cells (reviewed by Sethi *et al.*, 2005).

Figure 55. A schematic diagram of normal retina on the left and the remodelling that occurs due to retinal detachment on the right. 1. The outer segments of rod (R) and cone (C) photoreceptors are greatly shortened and separated from the apical surface of (RPE). 2. The synaptic terminals of many rods are withdrawn from the outer plexiform layer (OPL) and the dendrites of rod bipolar cells (RB) grow into the outer nuclear layer (ONL). 3. The axon terminals of the B-type horizontal cell (HB) terminate next to withdrawn rod spherules or grow wildly into the outer retina, and often into the subretinal space. 4. A subpopulation of ganglion cells (G) extend short spiky processes from the base of their cell body after detachment, but can also grow thickened processes into the outer retina. 5. Astrocytes (A) proliferate and often appear in epiretinal membranes. Adapted from (Fisher et al., 2005)

An important consequence of retinal detachment is the cellular proliferation of the RPE cells (Fisher *et al.*, 1991), which can continue for some time after retinal reattachment (Lewis et al., 2002). However, this proliferative capacity varies between different species. For example, in cat, rabbit and human , the RPE cells proliferate within a day or two after detachment (Anderson et al., 1981a), whereas in California ground squirrel, the RPE remains senescent (Linberg et al., 2002). In humans, proliferative RPE cells migrate and participate in the formation of epiretinal membranes and contribute to the pathogenesis of many retinal diseases that lead to vision loss, such as proliferative vitreoretinopathy (Hiscott *et al.*, 1999).

RPE cell proliferation in retinal detachment is an intriguing process, however, the signalling and molecular mechanisms underlying it are not yet known. In many vertebrates, cell divisions are driven by extracellular signals known as mitogens. These alter the expression or activity of cyclic dependent kinases (CDKs), which are regulatory proteins. The ability of CDKs to trigger cell cycle events is dependent on an associated cyclin subunit, whose oscillating concentrations underlie CDKs activity (Morgan, 1997). The mammalian cell division cycle is mitogen-dependent. The progression of the cycle though the first gap phase (G1) and initiation of DNA synthesis (S) is regulated by several cyclin and cyclin-dependent kinases (Fig 56). The balance between CDK activation and inactivation determines whether cells proceed through G_1 into S phase, and from gap phase (G_2) to metaphase (M). The involvement of different mitogens, such as different growth factors in the stimulation of RPE cell proliferation, has been thoroughly investigated (Grant *et al.*, 1990; Leschey *et al.*, 1991; Kishi *et al.*, 1994; Spraul *et al.*, 2000).

In amphibians, complete removal of the original retina results in regeneration of a new functional retina, even in adults (Reyer, 1977; Reh and Pittack, 1995). The

regenerated retina originates primarily from the RPE cells (Keefe, 1973; Klein et al., 1990). Following retinal removal, the RPE cells begin to proliferate and quickly form two layers of cells instead of their normal single layer. These cells then begin to lose their pigmentation and genes normally expressed by RPE cells, such as RPE65, are down-regulated (Chiba *et al.*, 2006).

Figure 56. The different phases of the cell cycle. In the first phase (G1) the cell grows. When it has reached a certain size it enters the phase of DNA-synthesis (S) where the chromosomes are duplicated. During the next phase (G2) the cell prepares itself for division. During mitosis (M) the chromosomes are separated and segregated to the daughter cells, which thereby receive exactly the same chromosome set up. The cells are then back in G1 and the cell cycle is completed. The progression of the cell cycle is dependent on cyclin and cycline dependent kinase. The progression of the cell cycle from G1 to S phase and from G2 to M phase in dependent on cyclin and cycline dependent kinase (CDK). Adapted from Leland H. Hartwell work.
(http://nobelprize.org/nobel_prizes/medicine/laureates/2001/press.html)

In amphibians, complete removal of the original retina results in regeneration of a new functional retina, even in adults (Reyer, 1977; Reh and Pittack, 1995). The regenerated retina originates primarily from the RPE cells (Keefe, 1973; Klein et al., 1990). Following retinal removal, the RPE cells begin to proliferate and quickly form two layers of cells instead of their normal single layer. These cells then begin to lose their pigmentation and genes normally expressed by RPE cells, such as RPE65, are down-regulated (Chiba *et al.*, 2006).

The regenerative capacity of RPE cells was also demonstrated in early embryonic chick retina by the work of Coulombre (1965). Here surgical removal of the retina in chick embryos results in the formation of a new retina *in vivo* from RPE cells, but in an inverted orientation (Coulombre and Coulombre, 1965). In late embryonic chicks, RPE-based retinal regeneration does not occur spontaneously but can be induced by FGF (Park and Hollenberg, 1989, , 1991) and requires cell-cell interaction (Pittack *et al.*, 1991). The factors that limit the competence of RPE cells in late embryonic and post-hatched chicks are not yet known. However, a recent study has shown that activin played an important role in blocking regeneration of RPE cells (Sakami *et al.*, 2007). In mammals, RPE proliferation due to retinal detachment has been reported (Stevenson *et al.*, 1988), however, RPE differentiation has not yet been reported.

Several studies have been undertaken to identify the different factors that regulate RPE proliferation and redifferentiation *in vitro* and *in vivo*. The involvement of individual growth factors in the stimulation of RPE cell proliferation has been thoroughly investigated in different spacies, for example, fibroblast growth factor (Fgf), which is a mitogenic factor for a wide variety of cells derived from the mesoderm and neuroectoderm including the retina (Burgess and Maciag, 1989). FGFs are produced at a low level in RPE cells (Caruelle et al., 1989; Bost et al., 1994)

and may inhibit apoptoss, as in retinal dystrophy, cell apoptosis is prevented by a single subretinal injection of exogenous Fgf1 (Faktorovich *et al.*, 1990).

The transdifferentiation of RPE cells is an intriguing process and although bFgf has been suggested as a mitogenic factor involved in RPE transdifferentiation, the molecular mechanisms remain unclear. Recent studies have suggested that many common features exist between the gene expression of several transcription factors necessary for ocular development (Callaerts *et al.*, 1997) and regeneration of the retina in, such as Pax-6 and Notch (Kaneko *et al.*, 1999; Kaneko *et al.*, 2001).

Aims of this study

- Identify the time period required for RPE cells to enter the cell cycle after retinal detachment.
- Analyse the distribution of the RPE cells entering the cell cycle due to retinal detachment.
- Analyse the association between the size of retinal detachment and the number of cells entering the cell cycle.
- Assess the contribution of the cell entering the cell cycle to the RPE monolayer (4.3.2).
- Analyse the expression level of different proliferative cells such as Ki67 and PCNA.
- Analyse the expression level of different stem cell marker genes after retinal detachment such as:

1. ***Nestin*** is an intermediate filament protein expressed in mitotically active CNS and PNS progenitor cells during early stages of development (Hockfield and McKay, 1985; Cattaneo and McKay, 1990; Lendahl *et al.*, 1990). During cell division the cytoplasmic and nuclear compartments

require reorganization and partitioning into daughter cells. These processes are achieved by the help of microtubule, intermediate filament and actin microfilaments (Fuchs and Cleveland, 1998; Goldman et al., 1999). Upon differentiation, nestin becomes downregulated and replaced by tissue-specific intermediate filament protein (Zimmerman *et al.*, 1994; Lothian and Lendahl, 1997), but reappears transiently after injury to the CNS (Lendahl, 1997; Namiki and Tator, 1999). Nestin is also found expressed in the ciliary body and iris pigment epithelium of the adult mammalian eye *in vitro,* which suggests that these two cell types may be used as models to investigate the biology of retinal stem cells (Ahmad *et al.*, 2000; Asami *et al.*, 2007).

2. ***Pax6*** belongs to a subfamily of genes which contain both a homeobox and a second DNA-binding motif known as the paired box. Paired domain-containing gene products are transcription factors and are thus capable of executing a genetic programme (Chalepakis *et al.*, 1991). In humans, heterozygous loss of function mutation typically produce aniridia, a congenital panocular malformation associated with severe visual impairment, however *PAX6* gene was also implicated in human anophthalmia (Glaser et al., 1994). Studies of the distribution of *Pax6* expression during development in mouse indicate that it is expressed in defined regions of the forebrain, optic cup, hindbrain, and spinal cord, as well as in the lens placode and nasal epithelium (Gruss and Walther, 1992). Heterozygous mutations in the mouse *Pax6* gene result in absence of the iris, as well as abnormalities of the lens, cornea and retina. Homozygous defect is lethal and results in failure of ocular development (Grindley *et al.*, 1995).

3. ***Otx genes,*** *Otx1 and Otx2,* are a homeodomain-containing transcription factor that plays an essential role in anterior head formation (Simeone *et al.*, 2002). In the vertebrate eye, *Otx* genes are initially expressed in the entire optic vesicle but their expression soon becomes restricted to the presumptive RPE during optic cup formation, where it is maintained throughout adulthood (Bovolenta et al., 1997; Simeone et al., 2002; Martinez-Morales et al., 2004). In human, *OTX2* mutation may result in microphthalmia through failure of retinal differentiatiom reviewed in (Verma and Fitzpatrick, 2007). Mice deficient in *Otx2* show clear defects in the patterning of the RPE, which is replaced by a neural retina-like territory (Martinez-Morales et al., 2001). *Otx2* is involved in RPE differentiation and is down-regulated in differentiation of RPE cells of the regenerating newt retina (Sakami et al., 2005).

4. *Doublecortin* (***Dcx***) is a microtubule-associated protein required for neuronal migration. DCX was previously shown to be expressed predominantly in the brain, and at high levels only during development, based on Northern analysis of human tissues (Gleeson *et al.*, 1998). Based on Western analysis, DCX was highly expressed at 22 weeks gestation and at lower levels during the early childhood developmental time points of 2 years and 4 years of age, and very little was detected in adult brain (Gleeson *et al.*, 1999). In addition to the developmental role, expression of DCX remains high within certain areas of the adult mammalian brain (Couillard-Despres *et al.*, 2005). These areas, mainly the dentate gyrus and the lateral ventricle wall within the olfactory bulb, retain the capacity to generate new neurons into adulthood. DCX it transiently expressed in proliferating progenitor cells and newly generated neuroblasts (Brown and Gatter, 2002). A strong evidence for neuronal stem or progenitor properties

exists for the cilary body derived cells and it was found that these cells also expressed DCX (Engelhardt et al., 2004).

5. ***Sox*** proteins comprise a family of transcription factors having DNA-binding HMG domains (Pevny and Lovell-Badge, 1997). SOX1, SOX2, and SOX3 are initially expressed in the anterior neural plate and invaginating optic vesicle. However, during the formation of the optic cup, SOX1 and SOX3 are down-regulated, while SOX2 is maintained and restricted to neural retinal cells (Kamachi *et al.*, 1999). To date, the importance of SOX 2 in the nervous system hes been highlighted by misexpression and dominant interfering studies in mouse cell lines, *Xenopus*, and chick embryos, which suggests that SOX2 maintains neural progenitor identity (Mizuseki *et al.*, 1998).

6. ***Six3 & Six6.*** Six members of the *Six* gene family have been identified in mice (Six1-6) (Boucher *et al.*, 1995; Heath *et al.*, 1997) and humans (Six1-6) and these code for transcription factors characterized by the presence of a homeodomain and a *Six* domain (Kobayashi *et al.*, 1998). Of these, only Six3 and Six6 are expressed during the early stages of eye development (Oliver *et al.*, 1995; Jean *et al.*, 1999; Lopez-Rios *et al.*, 1999). Six3 has a role in cell proliferation, an overexpression which results in the expansion of the rostral forebrain, while inactivation of Six3 results in the loss of forebrain structures including the retina (Loosli *et al.*, 1998; Lagutin *et al.*, 2001). In the Six6 mutant there is premature cell cycle exit implicating a direct role of Six6 in regulating the cell cycle (Iseli *et al.*, 2002). Overexpression of Six6 in *Xenopus* has been shown to induce ectopic retinal tissue and expand the optic vesicle and the rostral neuroepithelium (Zuber *et al.*, 1999; Abdouh and Bernier, 2006).

6.2 Result

6.2.1 Retinal detachment

Retinal detachment was undertaken on DA rats and the animals were sacrificed 18, 24 or 48 hours after retinal detachment. In general, areas with retinal detachment had a large number of cells which were positive for Ki67 indicating that they had entered the cell cycle. In addition a small number of Ki67-positive cells were found in peripheral retina, however these cells were not associated with areas of detachment (Fig. 57). Immediately after retinal detachment, RPE cells did not enter the cell cycle and there was a latent period of approximately 12–18 hours followed by gradual increases in the number of Ki67 positive cells (Fig. 58). The peak in RPE cell proliferation was observed at 24 hours post detachment.

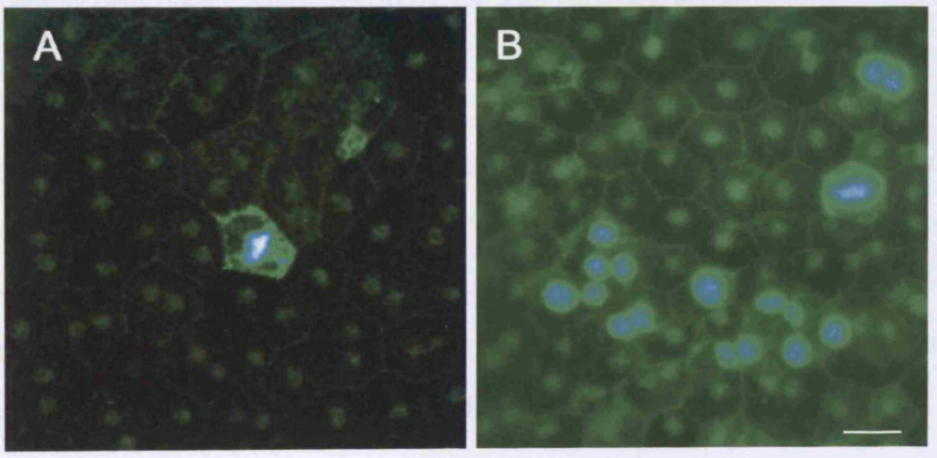

Figure 57. A. Image of a single Ki67 positive cell in a normal flat-mounted retina in pigmented animal without retinal detachment. B. Image of Ki67-positive cells located below an area of retinal detachment. Scale bar=20 μm

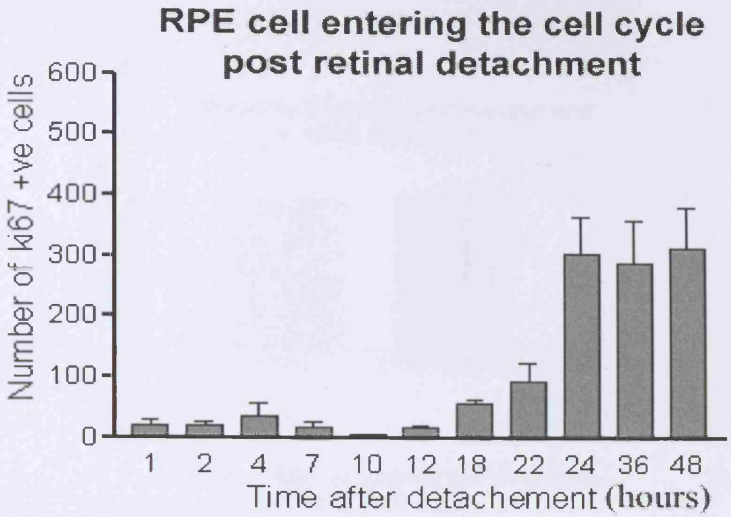

Figure 58. The association between duration of retinal detachment and RPE cell proliferation. The number of labelled cells seen after 1 to 12 hours is not significantly different than the number seen in normal non-detached retina. The increase in the number of labelled cells seen at 18 hours is the significant response to retinal detachment, ANOVA= 0.0001. (N=5 for each time point)

To analyse the contribution of newly proliferative cells to the RPE monolayer, I measured RPE cell size, regularity and density in areas with retinal detachment and compared them with non-detached areas. Figure 59 shows that there was no significant difference in RPE cell density, size or matrix of irregularity between areas with retinal detachment and areas of non-detached retinae.

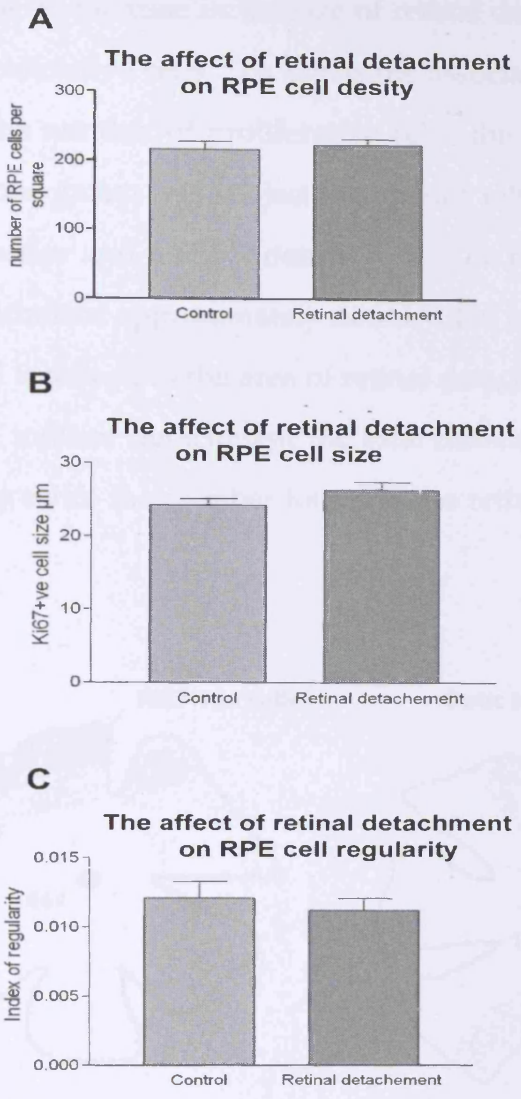

Figure 59. The contribution of newly proliferative cells to the RPE monolayer. RPE cell density was measured by counting the number of RPE cells in 150 μm^2 box below and away from retinal detachment. Within the same box the size and regularity of RPE cells were measured using MatLab. (A) The graph show no significant increase in cell density related to retinal detachment P=0.54. (B) RPE cell size also did not change under the detachment, P=0.12. (C) RPE cell regularity also was not affected by retinal detachment P=0.54. (N=5)

I hypothesised that an increase in the size of retinal detachment will also increase the number of proliferative cells. To assess the association between size of retinal detachment and the number of proliferative cells, the rats were divided into two groups, of which one group was subject to superior retinal detachment, the second group to both superior and inferior detachment. The result was that doubling the size of retinal detachment approximately doubled the number of proliferative cells. These cells are still localized to the area of retinal detachment (Fig. 60). In the retina with superior and inferior detachment the total number of proliferative RPE cells was approximately twice the number found in the retina with inferior detachment only (Fig. 61).

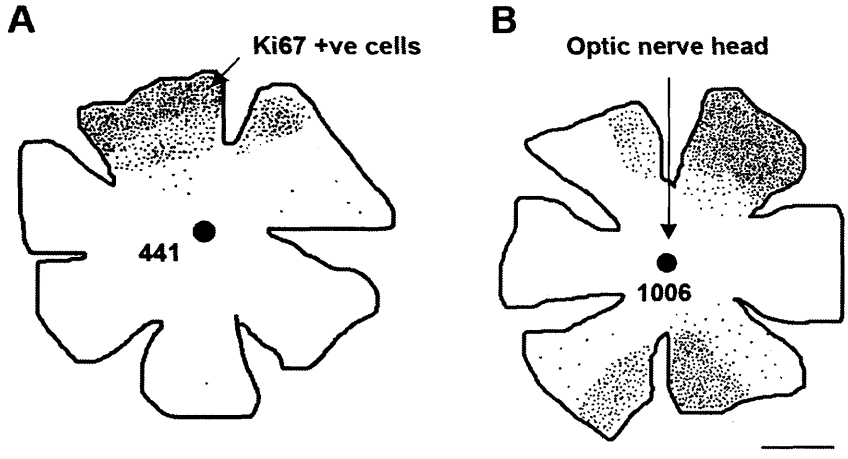

Figure 60. Outline diagram of retina with Ki67 cell density and distribution after retinal detachment. (A) Superior retinal detachment. (B) Superior and inferior retinal detachment. The approximate number and distribution of Ki67 positive cells is represented by the small black dots. The total number of proliferative RPE cells in superior retinal detachment was 441 and for superior and inferior detachment was 1006. Scale bar 2mm

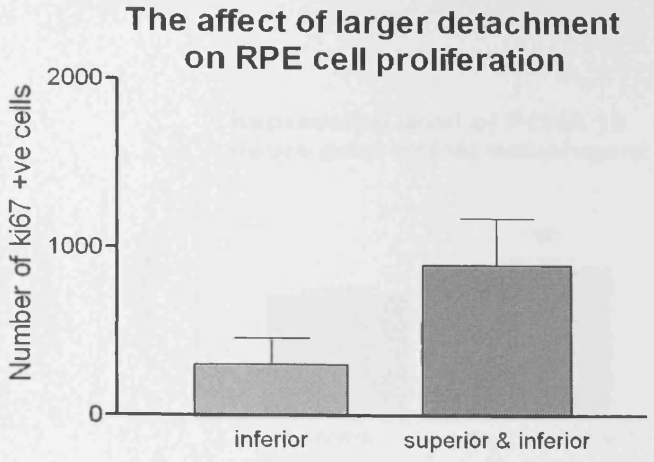

Figure 61. The size of retinal detachment affects the number of proliferative RPE cells. Retinal detachment was induced in two groups of animal. One group had superior detachment and the second group had superior and inferior detachment to increase the size of detachment. The number of Ki67 positive cells was counted for each group. The group with superior and inferior retinal detachment showed approximately increase of double the number of proliferative RPE cells of the group with superior detachment only, Ttest P=0.0005. (N=5)

6.2.2 Gene expression in retinal detachment

RPE cell gene expression level after retinal detachment was analysed using quantitative RT-PCR. Here RNA was extracted from three groups of 7 pairs of retinae at 18, 24 or 48 hours after retinal detachment and three groups of 7 RPE sheets without retinal detachment. First strand cDNA synthesis was undertaken at the same time for each group. Quantitative RT-PCR was undertaken for different proliferative and stem cell marker genes. It was found that the level of two proliferative markers (PCNA, KI67) was elevated. However the increase in PCNA was statistically significant (P= 0.016) early, within 18 hours post retinal detachment, (Fig. 62), whereas the level Ki67 was statistically significant (Ttest, P<0.0001) at 48 hours (Fig. 63).

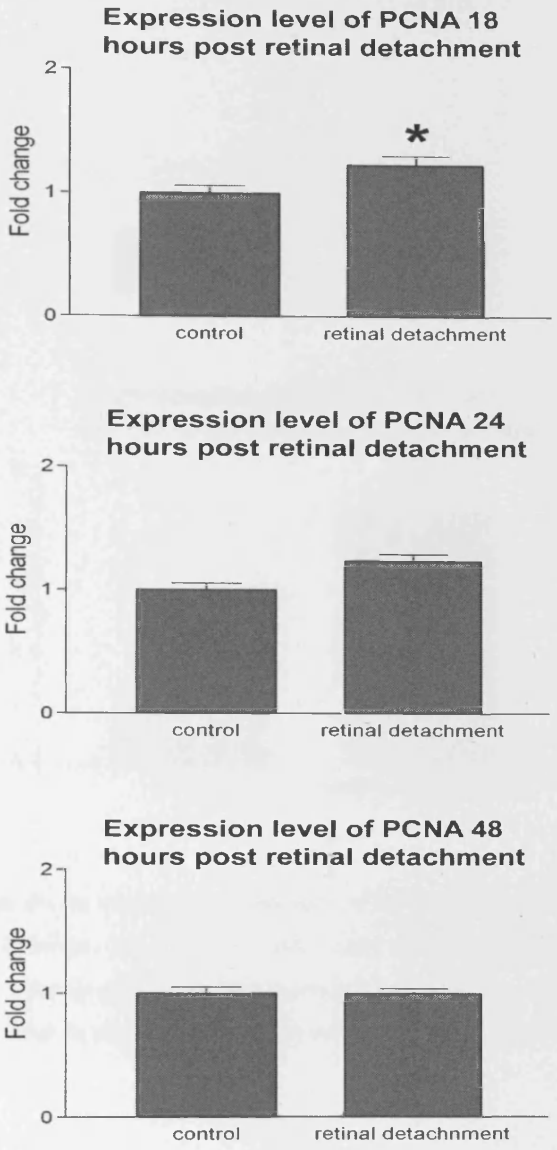

Figure 62. The graphs show the level of expression of PCNA at different times after retinal detachment; 18, 24 and 48 hours. (A) shows a statistically significant increase in the level of expression of PCNA 18 hours after retinal detachment (Ttest, P= 0.016). After 24 hours (B) and 48 hours (C) the level of expression of PCNA decreases and becomes statistically nonsignificant. (N=7)

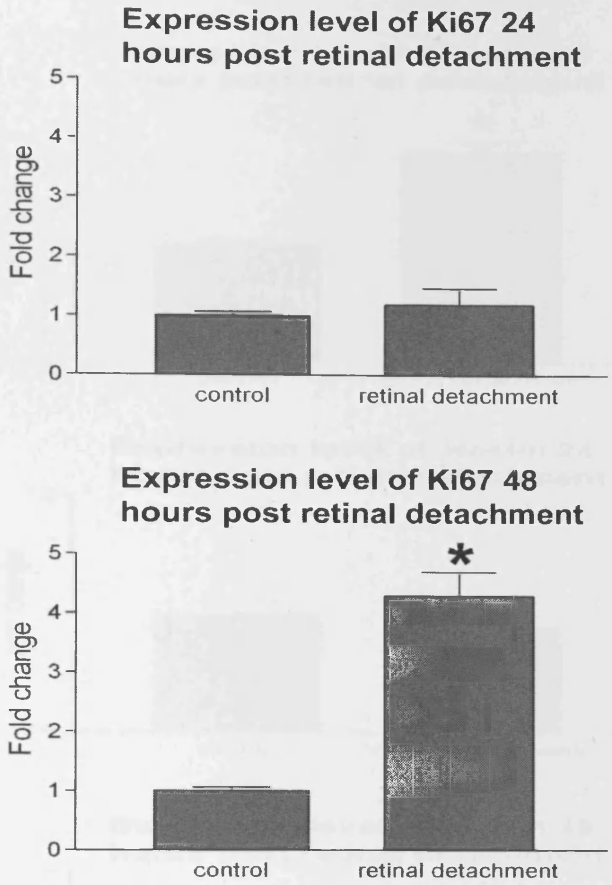

Figure 63. The graph shows the level of expression of Ki67 at different times after retinal detachment; 24 and 48 hours. (A) Shows no statistically significant increase in the level of expression of Ki67 18 hours after retinal detachment, however after 48 hours the level of Ki67 expression increases to 4 times higher than control (Ttest, $P<0.0001$). (N=7)

Furthermore Nestin, which is a stem cell marker, showed a statistically significant increase ($P=0.006$) in the level of expression within 18 hours after retinal detachment (Fig. 64). Immunohistochemical analysis also revealed the presence of Nestin 18 hours after retinal detachment (Fig. 65). The level of expression of both Nestin and PCNA was down-regulated 24 hours after retinal detachment. The expression profile of many other genes such as Crx, Dcx, Sox2, Six3, Six6, RPE65 and Otx was undertaken but failed to show any statistically significant increase after retinal detachment.

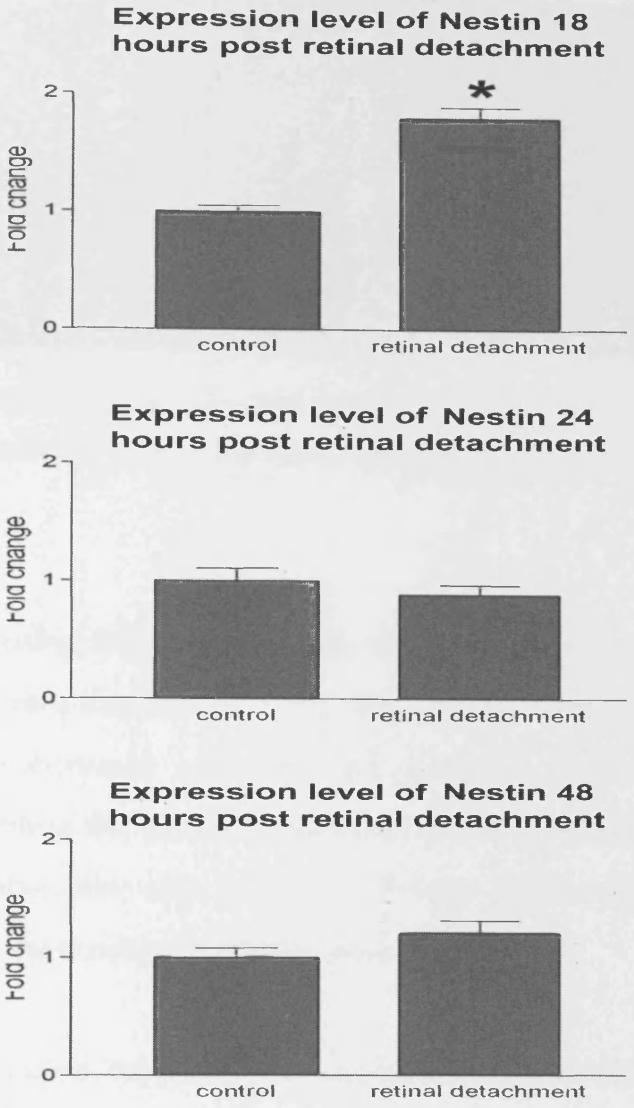

Figure 64. The graphs show the level of expression of Nestin at different times after retinal detachment; 18, 24 and 48 hours. (A) shows a statistically significant increase in the the level of expression of Nestin after 18 hours of retinal detachment (Ttest, P= 0.006). After 24 hours (B) and 48 hours (C) of retinal detachment the level of expression of Nestin decreases and becomes statistically nonsignificant. (N=7)

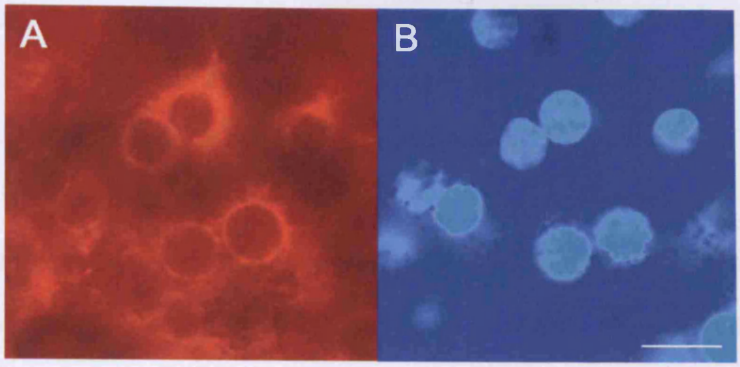

Figure 65. (A) An image of perinuclear Nestin labe'ling of RPE cells after 18 hours of retinal detachment. (B) The corresponding DAPI labelling of the same tissue.

5.6 Discussion

It has been shown using Ki67 as a cell-cycle marker that retinal detachment results in the entry of RPE cells into the cell cycle. This occurred after a latent period of 12–18 hours, but then increased gradually and peaked at 24–36 hours after retinal detachment. Doubling the size of detachment was also associated with doubling the number of proliferative cells, indicating a linear relationship between the size of detachment and the number of proliferative cells.

The newly proliferative cells did not contribute to the RPE monolayer and migrated to contribute in the formation of the subretinal membrane, which is a complication of retinal detachment or retinal tears (Kampik *et al.*, 1981; Michels, 1982; Hiscott et al., 1999). It is of interest to mention here that several studies have shown that RPE cells , which contribute to subretinal membrane, looks and behave different than the normal RPE cells on bruch's membrane (Machemer and Laqua, 1975; Machemer, 1977; Machemer *et al.*, 1978; Grierson *et al.*, 1994).

Analysis of gene expression showed an increase in the level of expression of Nestin, which is a stem cell marker, 18 hours after retinal detachment and this was

also confirmed at protein level by immunohistochemical studies. In addition there was an increase in the level of expression of two proliferative markers, PCNA after 18 hours and Ki67 after 48 hours of retinal detachment.

Several studies have shown that the adult mammalian RPE retains the capacity to proliferate under certain conditions; in response to injury (Miller et al., 1986), after cryotherapy (Laqua and Machemer, 1976), or after retinal detachment (Anderson et al., 1981a). In some species RPE cells retain the capacity to transdifferentiate into new retinal cells.

Studies of the regenerative capacity of the amphibians were the first to identify the capacity of RPE cells to act as a source for newly generated neurons. These observed that devascularization-induced retinal degeneration in the frog is followed by the formation of a new retina by increased proliferation of the marginal zone (Reh and Nagy, 1987). The regenerated retina originates primarily from the RPE cell (Keefe, 1973; Klein et al., 1990). Furthermore, complete removal of the original retina results in regeneration of a new functional retina, even in adults (Reyer, 1977; Reh and Pittack, 1995). Following retinal removal, the RPE cells begin to proliferate and quickly form two layers of cells instead of their normal single layer. These cells then begin to lose their pigmentation and down-regulate the expression level of RPE65 (Chiba *et al.*, 2006).

The trandifferentiating capacity was also identified in embryonic chick retina in a manner very similar to that observed in the amphibian (Coulombre and Coulombre, 1965). In late embryonic chiken, RPE-based retinal regeneration does not occur spontaneously but can be induced by FGF (Park and Hollenberg, 1989, , 1991) and requires cell-cell interaction (Pittack *et al.*, 1991).

As for mammals, *in vitro* transdifferentiation of RPE cells is well documented. In the presence of FGF, cultured early embryonic rat RPE cells that have not yet acquired pigment develop to form a retina-like multilayer structure containing neuronal cells that express markers of retinal ganglion, amacrine, and rod photoreceptors, however this ability was restricted to a certain age range (Zhao *et al.*, 1995).

In amphibian an attempt to find early activated genes has been made and several genes are described, although none have yet been identified as master control genes for retinal regeneration (Goto *et al.*, 2006). Recent studies have shown that many common features exist between the development and regeneration of the retina in gene expression of several transcription factors necessary for ocular development, For example *in situ* hybridization study showed that the expression of N-Notch increases during retinal regeneration of newt (Kaneko *et al.*, 2001). In addition, Pax-6, the paired homeobox-containing gene, is expressed in neuroepithelial regenerating retina during newt retinal regeneration (Kaneko *et al.*, 1999). Furthermore a recent study showed that during retinal regeneration the expression of RPE65 and Otx are down-regulated, whereas the level of expression of Pax6 is differentially up regulated (Sakami et al., 2005). In my study, an early upregulation of nestin and PCNA in proliferating RPE cells was observed 18 hours after retinal detachment, which was followed by upregulation of Ki67 48 hours after retinal detachment. This may indicate that a sequence in gene activity is required for RPE prior to differentiation.

Several studies have been undertaken to identify the factors that regulate RPE proliferation and redifferentiation *in vitro* and *in vivo.* The involvement of individual growth factors in the stimulation of RPE cell proliferation has been thoroughly investigated in different species, for example, fibroblast growth factor

(FGF), which is a mitogenic factor for a wide variety of cells derived from the mesoderm and neuroectoderm including the retina (Burgess and Maciag, 1989).

In vitro studies showed that fibroblast growth factor 2 (FGF2) is a potent factor in stimulating RPE proliferation in newts as well as in embryonic avian tissue (Park and Hollenberg, 1989, , 1991; Pittack et al., 1991; Sakaguchi *et al.*, 1997; Araki *et al.*, 1998). FGFs have been proposed as candidate regulatory molecules for the response to retinal injury and high levels of FGF1 production in proliferative RPE cells have been correlated with proliferative vitreoretinopathy (Malecaze *et al.*, 1993). However, little is known about the mechanisms underlying endogenous FGF-mediated RPE cell proliferation.

Insulin-like growth factor 1 (IGF1) is another growth factor that has been shown to play some supplementary role in the case of chick retinal regeneration (Fisher et al., 2001). Together with FGF2, IGF1 has a strong synergistic effect on RPE cell differentiation. Interestingly a recent study showed that RPE transdifferentiation into neural cells can only be seen when they were cultured with the underlying connective tissue (the choroids) and they do not proliferate if cultured alone (Mitsuda *et al.*, 2005).

In vitro studies have shown the importance of RPE and choroid interaction in RPE cell proliferation and differentiation in amphibian (Mitsuda *et al.*, 2005). This was supported by reverse transcription polymerase chain reaction (RT-PCR) of *in vivo* regenerating newt eyes showing an unregulation in the expression of both FGF2 and IGF1 in the choroids after retinal removal (Mitsuda *et al.*, 2005). This indicates that the interaction between RPE cells and the choroids is important for RPE cells proliferation.

In chicks, the process of transdifferentiation also requires interaction with some neural derivatives (Coulombre and Coulombre, 1965, , 1970). Furthermore an *in vitro* study showed that RPE cells are much less susceptible to FGF2 than those combined with the underlying periocular connective tissue (Araki *et al.*, 1998).

The above studies reveal that the tissue interaction between the RPE and the choroid plays an essential role in RPE transdifferentiation and, although the most important question has not yet been answered (why the removal of the retina triggers RPE cells to proliferate and initiate transdifferentiation), there are several possibilities to address the question. One preferable possibility is that the persistence of the interaction of the intact retina-RPE tissue may inhibit RPE cells from responding to the choroids-derived factors by suppressing the FGF signal pathway within RPE cells. Alternatively, the removal of the retina may cause the choroids cells to initiate FGF gene expression. The retina is a rich source of FGFs yet the RPE does not respond to them, and further study on this subject has to be undertaken to identify the mechanism involved.

Another factor shown to be important in RPE cell regeneration is activin, which is a TGFβ family signalling protein. Activin is an important developmental signal, important for the patterning of the optic vesicle, and inhibition of activin signalling prevents normal RPE differentiation (Fuhrmann et al., 2000). A recent study showed that activin contributes to the loss of competence of the RPE to regenerate retina (Sakami et al., 2007). The addition of activin blocks regeneration from the RPE in chick embryos, even in the presence of FGF, and activin inhibitor can reverse the developmental restriction in FGF-stimulated neural retinal regeneration. Hence, it appears that, like the amphibian RPE, the RPE of higher vertebrates has the capacity to differentiate but it is inhibited from doing so through different signalling pathways.

The precise signalling that mediates RPE cell proliferation is not yet determined. An example of these pathways is the mitogen-activated protein kinases (MAPKs) pathway. MAPKs are ubiquitous enzymes involved in numerous cellular functions, including proliferation and programmed cell death (Robinson and Cobb, 1997). Extracellular signal-regulated kinases (ERKs) 1 and 2 are the most well characterized MAPKs (Daum *et al.*, 1994). A recent study has shown that the MAPKs pathway is involved in cell growth during the induction of RPE cell proliferation (Hecquet *et al.*, 2002).

Recently Sonic hedgehog (Shh) has been implicated in regulation of RPE regeneration. Shh signalling is important in several aspects of neural development, affecting both proliferation and differentiation of cells throughout the CNS. Shh has been shown to negatively regulate regeneration from the RPE, and an antagonist to Shh can stimulate this process in the chick embryo (Spence et al., 2004). Shh has also been implicated in adult neural stem cell proliferation (Lai *et al.*, 2003). A recent study analysed the function of Shh in adult neurogenesis in the mammalian eye using mice with a single functional allele of the Shh (Moshiri and Reh, 2004). They found an increase in numbers of neural progenitors at every stage of retinal development and in addition, these mice had persistent progenitors at the retinal margin for up to 3 months of age.

Finaly, a recent study showed that E2F1, which is a transcription factor that promotes the cell cycle (Ishida et al., 2003), works as a cell cycle suppressor in differentiated neurons (Ogata et al., 2001). Hence several studies have been undertaken to analyse the proliferative capacity of RPE cells in different species.

General discussion

RPE cell loss is a characteristic feature of aging (Panda-Jonas *et al.*, 1996) and retinal diseases such as macular degeneration or retinitis pigmentosa (Adler et al., 1999). As one strategy in therapy may be tissue replacement, I have undertaken several studies in an attempt to investigate the proliferative capacity of this cell type *in vivo* using different approaches.

The first method was based on the proliferative histological features of human RPE cells, where a subpopulation of peripheral RPE cells were found to be large, irregular and binucleated. These histological features were not observed in equatorial and central regions of the retina except close to drusen, and are indicative of cell proliferation.

The second method was based on immunohistochemical studies using different proliferative markers. Here it was found that a small number of peripheral RPE cells were in the cell cycle (Ts'o and Friedman, 1967) and approximately one-third of these cells underwent complete cellular division as determined by BrdU label. This wave of proliferation was not associated with the wave of nuclear division observed in the early post-natal stage (Strova & Panova, 1983). In addition, cell proliferation was not restricted to a specific postnatal age and was found in animals up to one year old, but at a slower rate.

The third method was based on analyses of the gene expression profile of RPE cells after retinal detachment using quantitative RT-PCR. There was an early upregulation of two proliferative markers (PCNA, Ki67) and one stem cell marker (Nestin). However a key question that arises here, is can RPE cells act as neuronal stem cells in mammals?

Stem cells have the capacity to self-renew as well as to give rise to specialized cell types. They are uncommitted and remain so until they receive a signal to develop into a distinct cell type. Besides embryonic stem cells that are pluripotent and derived from the blastocyst (Thomson *et al.*, 1998), adult stem or precursor cells, which have a more limited potency to give rise to specialized cells, are found in different somatic tissues including the central nervous system (Weissman *et al.*, 2001). Irrespective of their origins, stem and precursor cells are multipotent in differentiation and transdifferentiation, responding to stimuli both *in vivo* and *in vitro (Stevenson et al., 1988;* Whittemore *and Snyder, 1996; Bjornson et al., 1999).*

In fish and amphibians, neurogenesis does not cease after the embryonic stage, but continues to take place throughout life. As a result the retina continues to grow and new cells are added continually in the stem-cell-containing zone known as the ora serrata (Straznicky and Gaze, 1971; Johns, 1977). By using a birth date indicator, such as ^{3}H thymidine, it has been shown that new rings of cells are constantly added from this zone to the retina, cells situated more peripherally being younger than those in the central region (Hollyfield, 1971; Straznicky and Gaze, 1971). In chicks, a few cells could be labelled with ^{3}H thymidine in the most peripheral region of the retina in the hatched chick (Morris *et al.*, 1976). Fischer and Reh 2000 have more recently re-examined this proliferating marginal zone in post-natal chicks and found that these cells produce neurons, however, unlike in fish and amphibians, the CMZ does not participate in the regeneration process observed following injury. Moreover, the presence of a potential retinal stem cell population within the ciliary epithelium of rodents has been reported (Ahmad *et al.*, 2000; Tropepe *et al.*, 2001).

Previous studies have found neural stem cells expressing Nestin (Cattaneo and McKay, 1990) in regions with cellular population that remain active in terms of cell

production at maturity, like the dentate gyrus or subventricular zone (Kuhn et al., 1996). Neural stem cells provide a potential cellular substrate for cell replacement strategies for diseases of the central nervous system (CNS) including the retina (Chacko *et al.*, 2000; Nishida *et al.*, 2000).

Retinal degeneration and dystrophies are a major cause of blindness and are often characterized by apoptotic death of cells of the retina as occurs in retinitis pigmentosa and AMD (Lolley *et al.*, 1994) and Stem cell therapies may hold enormous potential for replacement of degenerative cells due to the high plasticity of these cells (reviewed in Ahmad, 2001). It has been shown that retinal stem cells isolated from the embryonic retina express a photoreceptor-specific marker following transplantation into the subretinal space of rats (Chacko *et al.*, 2000). Further, it has been shown that stem cells isolated from the ciliary epithelium of adult rats and transplanted into eyes with retinal injury, will express photoreceptor markers (Chacko *et al.*, 2003). The attempt to repopulate the retina with grafted retinal derived stem cells has been relatively unsuccessful because of limited integration of donor cells into the host retina (Silverman et al., 1992; Aramant and Seiler, 1995; Berson and Jakobiec, 1999). However, a recent study showed that donor cells can integrate into the adult or degenerating retina if they are taken from the developing retina at a specific age were they are committed to a specific fate (MacLaren et al., 2006). As a result the discovery of any potential retinal stem cells would offers new perspectives for a substrate for retinal regeneration (Ahmad et al., 2000; Tropepe et al., 2000).

Retinal stem cells arise from multipotential progenitors that may provide a substrate for retinal regeneration. Although progress has been made lately we still know very little about their origin and molecular characteristics. This knowledge may help in the future to design of stem-cell-based retinal transplantation projects.

Here I found a subpopulation of RPE cells proliferating at a slow rate in the peripheral retinal zone, which could act as a source to replace apoptotic central RPE cells due to aging (Del Priore *et al.*, 2002). In the light of this result it is of interest to mention that a recent comparative study of adult rat CB- and RPE-derived cells suggested that the two cell types share certain neuronal properties *in vitro*. These two types of cells express neural progenitor markers such as Nestin, Flk-1, Hes1, and Musashi. Moreover, they have the capacity to differentiate into neuronal and glial cells (Engelhardt et al., 2005). This may suggest that RPE cells have the potential to act as neuronal stem cell.

Here I also show that post retinal detachment proliferating RPE cells express Nestin, which is a neural stem marker. Nestin can be up regulated due to tissue damage (Duggal *et al.*, 1997; Holmin *et al.*, 1997; Li and Chopp, 1999), and it is possible that this is the reason for its expression here. While this possibility can not be dismissed, there are three reasons for thinking it less likely. First, nestin up-regulation in the mature retina and brain in response to insult is almost invariably confined to glia (Kohno *et al.*, 2006; Xue *et al.*, 2006; Chang *et al.*, 2007; Pekny *et al.*, 2007; Wan *et al.*, 2008). When up-regulation is found in the RPE it is *in vitro* rather than *in vivo* (Engelhardt et al., 2005), and differences between retinal staining patterns found *in vitro* and *in vivo* have been stressed (Qiu *et al.*, 2007). Second, there was no spatial relationship between nestin labelling and the hole through which the injection was made detaching the retina. This region would experience significant local trauma, and if this were the reason for the up-regulation of this neural stem cell marker, then one would expect it to be more localised to this site, rather than diffuse label under the detachment. Finally, there was a clear temporal coincidents between nestin up regulation at both the RNA and protein level and the increase in the number of Ki67 positive cells. Hence, while it is not possible to

reject the notion that nestin up-regulation was induced by damage alone, there is a strong temporal relationship to RPE cells entering the cell cycle.

The fact that RPE cells are capable of proliferating and expressing a stem cell marker, may suggest a possible regenerative capacity of mammalian RPE cells. This partially mirrors the regenerative capacity of amphibian RPE cells, which are capable of regenerating a full functional retina post retinal detachment (Klein et al., 1990; Reh and Pittack, 1995). However , a key question that remains to be answered is what inhibits mammalian RPE cells from forming different cell types in a manner similar to amphibian and whether it is possible to regulate the signals that stimulate trans-differentiation. This might help repopulate damaged regions of the neural retina. However before this could be investigated many other question need to be answered in future studies.

In this study I found a slow rate of proliferation taking place in the peripheral retina. Approximately 25 cells were found positive for Ki67. Labelling with BrdU produced 7 cells, which represents the subset in S-phase of the cell cycle. However, as BrdU injections were given as a single pulse, it may under estimate the actual number of proliferating cells because of it short availability and its restriction to labal cells in S-phase of the cell cycle. To answer this question another experiment should be designed where BrdU pulse is given once every 3-4 hours and then count the number of proliferating RPE cells in fixed time window. Further, it would be interesting to design experiments to analyse the RPE cell cycle and duration. This could probably be achieved by counting the number of proliferative cell after single BrdU injections and compare to the number of labelled BrdU after 6, 12, 18, and 24 hours. However, this could be difficult as the number of proliferating RPE cells was small. Alternatively Caviness *et al.* (2003) have a methods using multiple markers that could be used to the cell cycle length

In this study I also show that albino rats have 10 times more proliferating RPE cells when compared with pigmented animals. Hence, it might be easier to use albinos as a model to study RPE cell-cycle. However, the reasons behind this variation should be investigated before it could be used as model to investigate RPE cell proliferation. While tentative hypothesis can be raised as to why there are so many more proliferating cells in these animals, these have still to be tested

Why is proliferative capacity preserved in peripheral but not central retina?
An important finding in this study was the difference in RPE cell capacity to proliferate between central and peripheral RPE cells. This difference may be due to a number of reasons of which variation in gene expression between the two areas could be one. This variation could be identified by using gene chip analysis to find out differences in gene expression between central and peripheral retina. However this could be difficult as extracting RNA from the RPE monolayer was one of the major difficulties faced in this project.

What happens if the retina was detached for longer period, could it have the capacity to differentiate as amphibian retina? In this study, it was shown that RPE cell proliferation continues up to 48 hours post retinal detachment. However, this period might not be sufficient for any serious attempt at transdifferentiation, and it would be more appropriate to analyse this issue at a much extended time period. Further, it would be interesting to find out if the RPE cell expresses any further neuronal cell markers after extended period of retinal detachment, which may suggest a possible capacity of these cells to differentiate.

Appendix

(Work undertaken and written by Peter Lundh von Leithner)

Data analysis (Delaunay triangulation)

Consider a microscopic image of the RPE as an almost regular tessellation (*P*) on a 2-dimensional plane that is made up of a small range of congruent regular polygons. We now construct a Delaunay triangulation for *P* such that no point in *P* is inside the circumcircle of any triangle in *DT (P).* By 'almost regular' is meant that the Delaunay triangles formed by these points are nearly equilateral, and have roughly the same size. Instead of considering distances to nearest neighbours directly, we instead use a more general definition of 'size' of certain subsets – specifically the size of the Delaunay triangles – of the point pattern.

The measurements used in this method are derived from the average squared nearest neighbour distance and its coefficient of variation, however instead of considering nearest neighbours directly (Brown, 1975; Brown and Rothery, 1978), we instead used a more general definition of size and regularity based on subsets of cell populations by using the Delaunay triangulation of the point pattern formed by the cell centroids.

We now create a coordinate system from the points P, the centroid in each RPE cell – that is, the point within each polygon that is equidistant from all vertices and which is different from the cell nucleus.

The centroid size is defined as

$$S(z)=\left\{\sum\|z_i-\bar{z}\|^2\right\}^{1/2}$$

where the centre of gravity is $\bar{z}=\frac{1}{k}\sum_{i=1}^{k}z_i$. Using this definition, the size S of a triangle with edge lengths a, b and c is determined by $3S^2=\left(a^2+b^2+c^2\right)$, and it

can be seen that the average squared size of a triangle is closely related to the average of three neighbouring squared distances (in the case of a nearly regular tessellation). The size of the triangles in a Delaunay triangulation will be closely related to the size of the corresponding Voronoi polygons, and it is this connection that has motivated this work.

Cell size and regularity measurements

The average diameter of a sub-population of sampled RPE cells *(D)* is derived from lengths of the sides of triangles.

$$D(\mu m)=\frac{1}{j}\sum_{j\in P_i}\frac{\sqrt{\left(x_j-\bar{x}_i\right)^2+\left(y_j-\bar{y}_i\right)^2}}{px/\mu m},$$

Where x and y are the coordinates of each triangle vertex in sub-population *P*.

To examine the regularity of the RPE cells we want to examine the relative sizes of the triangles. Although the pixel to micron relationship is known, it is of interest to implement a scaleless statistic so as to make the regularity measurement completely independent of cell size.

Since we are examining a nearly regular process, a squared coefficient of variation of squared sizes is well suited for detecting regular departures from a random Poisson process as defined by,

$$T=\frac{\Sigma\left(S_i^2-\overline{S^2}\right)^2}{m\left(\overline{S^2}\right)^2},$$

Where T is the coefficient of variation of squared sizes of triangles of a Delaunay triangulation and $S_i^2=\sum_{j\in P_i}\left[\left(x_j-\bar{x}_i\right)^2+\left(y_j-\bar{y}_i\right)^2\right]$, where (x_i,y_i) denotes the *i*th point co-ordinates, $\bar{x}_i=\frac{1}{3}\sum_{j\in P_i}x_j$ and $\bar{y}_i=\frac{1}{3}\sum_{j\in P_i}y_i$ with *i*=1,2.

co-ordinates, $\bar{x}_i=\frac{1}{3}\sum_{j\in P_i}x_j$ and $\bar{y}_i=\frac{1}{3}\sum_{j\in P_i}y_i$ with *i*=1,2.

The T statistic obtained from the triangulations is used to compare the regularity of sub-populations of RPE cells sampled at different radial distances from the fovea and in donor tissue from different ages.

Simulation

To test the accuracy of the user-operated software, and more specifically, the ability of the operator to define the centroid of each RPE cell a simulated RPE lattice with known centroid locations was designed. It was designed as a simple cellular automata simulation of the RPE lattice, where each iteration increased the irregularity of the lattice (Fig. 65).

An obvious criticism of the above methodology is that the underlying iterative model of perturbations from a regular hexagonal grid is not sufficiently sophisticated to accurately model the aging of the RPE lattice. However, for the purpose of having an operator locate the cell centroid it is sufficiently complex. The results from having five operators locate the centroid in cell lattices of varying degrees of regularity showed no significant difference between operator located and true centroid location ($P=0.874$).

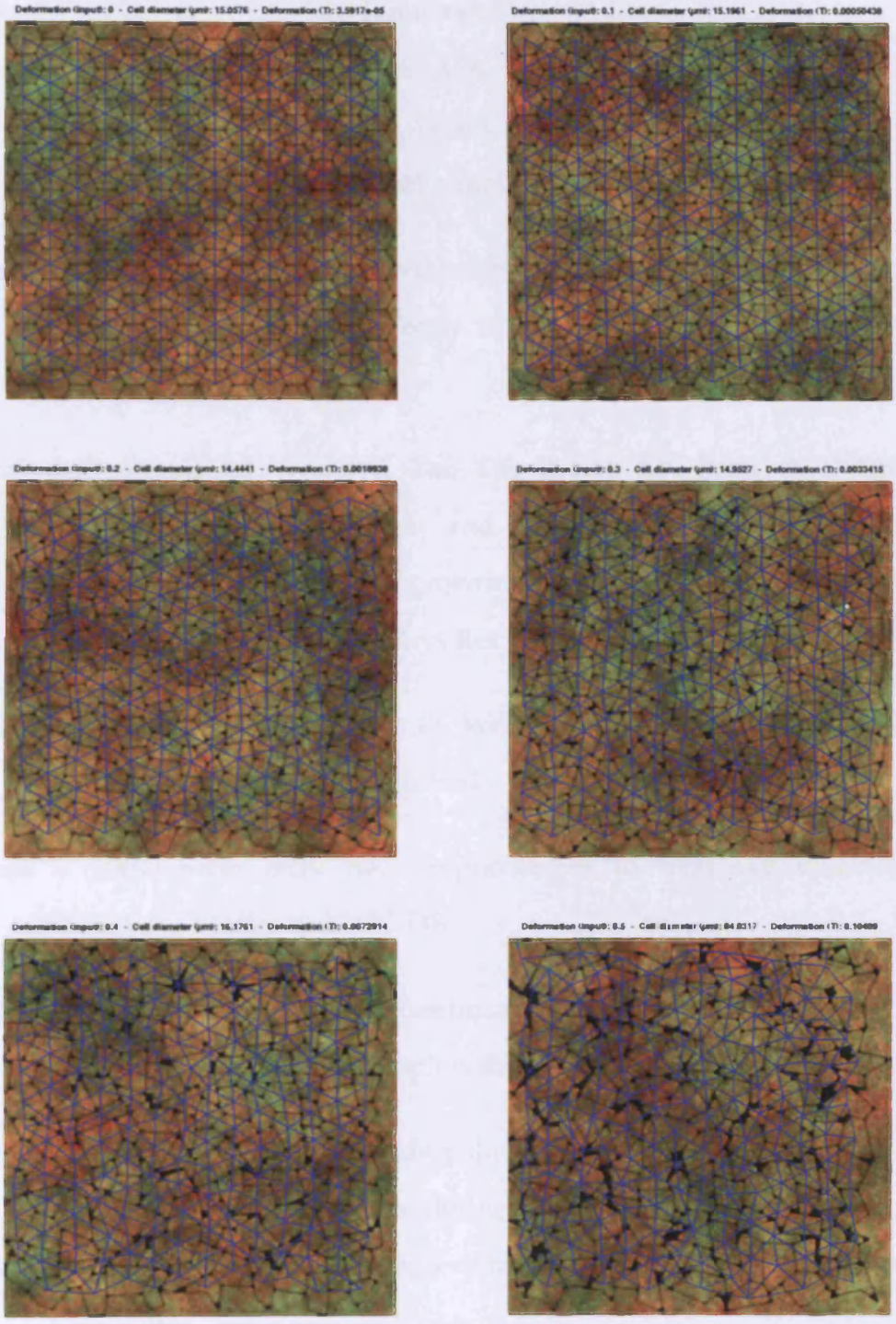

Figure 66. Delaunay triangulation of simulated tessellation of polygons with increasing degrees of deformation.

References

Abdelsalam A, Del Priore L, Zarbin MA (1999) Drusen in age-related macular degeneration: pathogenesis, natural course, and laser photocoagulation-induced regression. Surv Ophthalmol 44:1-29.

Abdouh M, Bernier G (2006) In vivo reactivation of a quiescent cell population located in the ocular ciliary body of adult mammals. Exp Eye Res 83:153-164.

Adamis AP, Shima DT, Yeo KT, Yeo TK, Brown LF, Berse B, D'Amore PA, Folkman J (1993) Synthesis and secretion of vascular permeability factor/vascular endothelial growth factor by human retinal pigment epithelial cells. Biochem Biophys Res Commun 193:631-638.

Adler R, Curcio C, Hicks D, Price D, Wong F (1999) Cell death in age-related macular degeneration. Mol Vis 5:31.

Ahmad I (2001) Stem cells: new opportunities to treat eye diseases. Invest Ophthalmol Vis Sci 42:2743-2748.

Ahmad I, Tang L, Pham H (2000) Identification of neural progenitors in the adult mammalian eye. Biochem Biophys Res Commun 270:517-521.

Ahuja P, Caffe AR, Holmqvist I, Soderpalm AK, Singh DP, Shinohara T, van Veen T (2001) Lens epithelium-derived growth factor (LEDGF) delays photoreceptor degeneration in explants of rd/rd mouse retina. Neuroreport 12:2951-2955.

Alamouti B, Funk J (2003) Retinal thickness decreases with age: an OCT study. Br J Ophthalmol 87:899-901.

Amemiya K, Haruta M, Takahashi M, Kosaka M, Eguchi G (2004) Adult human retinal pigment epithelial cells capable of differentiating into neurons. Biochem Biophys Res Commun 316:1-5.

Anderson D, Stern W, Fisher S, Erickson P, Borgula G (1981a) The onset of pigment epithelial proliferation after retinal detachment. IOVS 21:10-16.

Anderson DH, Stern WH, Fisher SK, Erickson PA, Borgula GA (1981b) The onset of pigment epithelial proliferation after retinal detachment. Invest Ophthalmol Vis Sci 21:10-16.

Araki M, Yamao M, Tsudzuki M (1998) Early embryonic interaction of retinal pigment epithelium and mesenchymal tissue induces conversion of pigment epithelium to neural retinal fate in the silver mutation of the Japanese quail. Dev Growth Differ 40:167-176.

Aramant RB, Seiler MJ (1995) Fiber and synaptic connections between embryonic retinal transplants and host retina. Exp Neurol 133:244-255.

Asami M, Sun G, Yamaguchi M, Kosaka M (2007) Multipotent cells from mammalian iris pigment epithelium. Dev Biol 304:433-446.

Barron MJ, Johnson MA, Andrews RM, Clarke MP, Griffiths PG, Bristow E, He LP, Durham S, Turnbull DM (2001) Mitochondrial abnormalities in ageing macular photoreceptors. Invest Ophthalmol Vis Sci 42:3016-3022.

Bavik CO, Eriksson U, Allen RA, Peterson PA (1991) Identification and partial characterization of a retinal pigment epithelial membrane receptor for plasma retinol-binding protein. J Biol Chem 266:14978-14985.

Bazan NG, Gordon WC, Rodriguez de Turco EB (1992) Docosahexaenoic acid uptake and metabolism in photoreceptors: retinal conservation by an

efficient retinal pigment epithelial cell-mediated recycling process. Adv Exp Med Biol 318:295-306.

Beatty S, Koh H, Phil M, Henson D, Boulton M (2000) The role of oxidative stress in the pathogenesis of age-related macular degeneration. Surv Ophthalmol 45:115-134.

Bellingham J, Chaurasia SS, Melyan Z, Liu C, Cameron MA, Tarttelin EE, Iuvone PM, Hankins MW, Tosini G, Lucas RJ (2006) Evolution of melanopsin photoreceptors: discovery and characterization of a new melanopsin in nonmammalian vertebrates. PLoS Biol 4:e254.

Bennett NT, Schultz GS (1993) Growth factors and wound healing: Part II. Role in normal and chronic wound healing. Am J Surg 166:74-81.

Berson EL, Jakobiec FA (1999) Neural retinal cell transplantation: ideal versus reality. Ophthalmology 106:445-446.

Bhutto IA, McLeod DS, Hasegawa T, Kim SY, Merges C, Tong P, Lutty GA (2006) Pigment epithelium-derived factor (PEDF) and vascular endothelial growth factor (VEGF) in aged human choroid and eyes with age-related macular degeneration. Exp Eye Res 82:99-110.

Bird AC (1992) Bruch's membrane change with age. Br J Ophthalmol 76:166-168.

Bjornson CR, Rietze RL, Reynolds BA, Magli MC, Vescovi AL (1999) Turning brain into blood: a hematopoietic fate adopted by adult neural stem cells in vivo. Science 283:534-537.

Bok D (1993) The retinal pigment epithelium: a versatile partner in vision. J Cell Sci Suppl 17:189-195.

Bost LM, Aotaki-Keen AE, Hjelmeland LM (1992) Coexpression of FGF-5 and bFGF by the retinal pigment epithelium in vitro. Exp Eye Res 55:727-734.

Bost LM, Aotaki-Keen AE, Hjelmeland LM (1994) Cellular adhesion regulates bFGF gene expression in human retinal pigment epithelial cells. Exp Eye Res 58:545-552.

Boucher CA, King SK, Carey N, Krahe R, Winchester CL, Rahman S, Creavin T, Meghji P, Bailey ME, Chartier FL, et al. (1995) A novel homeodomain-encoding gene is associated with a large CpG island interrupted by the myotonic dystrophy unstable (CTG)n repeat. Hum Mol Genet 4:1919-1925.

Boulton M, Dayhaw-Barker P (2001) The role of the retinal pigment epithelium: topographical variation and ageing changes. Eye 15:384-389.

Bovolenta P, Mallamaci A, Briata P, Corte G, Boncinelli E (1997) Implication of OTX2 in pigment epithelium determination and neural retina differentiation. J Neurosci 17:4243-4252.

Bowman GD, O'Donnell M, Kuriyan J (2004) Structural analysis of a eukaryotic sliding DNA clamp-clamp loader complex. Nature 429:724-730.

Boycott BB, Hopkins JM, Sperling HG (1987) Cone connections of the horizontal cells of the rhesus monkey's retina. Proc R Soc Lond B Biol Sci 229:345-379.

Braun N, Papadopoulos T, Muller-Hermelink HK (1988) Cell cycle dependent distribution of the proliferation-associated Ki-67 antigen in human embryonic lung cells. Virchows Arch B Cell Pathol Incl Mol Pathol 56:25-33.

Bressler NM, Silva JC, Bressler SB, Fine SL, Green WR (1994) Clinicopathologic correlation of drusen and retinal pigment epithelial abnormalities in age-related macular degeneration. Retina 14:130-142.

Bressler NM, Silva JC, Bressler SB, Fine SL, Green WR (2005) Clinicopathologic correlation of drusen and retinal pigment epithelial abnormalities in age-related macular degeneration. 1994. Retina 25:130-142.

Bressler SB, Maguire MG, Bressler NM, Fine SL (1990) Relationship of drusen and abnormalities of the retinal pigment epithelium to the prognosis of neovascular macular degeneration. The Macular Photocoagulation Study Group. Arch Ophthalmol 108:1442-1447.

Brown D (1975) A Test of Randomness of nest spacing. Wildfowl 26:102-103.

Brown D, Rothery P (1978) **Randomness and local regularity of points in a plane**. Biometrika 65:115-122.

Brown DC, Gatter KC (2002) Ki67 protein: the immaculate deception? Histopathology 40:2-11.

Bruno S, Darzynkiewicz Z (1992) Cell cycle dependent expression and stability of the nuclear protein detected by Ki-67 antibody in HL-60 cells. Cell Prolif 25:31-40.

Burgess WH, Maciag T (1989) The heparin-binding (fibroblast) growth factor family of proteins. Annu Rev Biochem 58:575-606.

Burke J, Soref C (1988) Topographical variation in growth in cultured bovine retinal pigment epithelium. Invest Ophthalmol Vis Sci 29:1784-1788.

Burke JM, Skumatz CM (1998) Autofluorescent inclusions in long-term postconfluent cultures of retinal pigment epithelium. Invest Ophthalmol Vis Sci 39:1478-1486.

Burke JM, McKay BS, Jaffe GJ (1991) Retinal pigment epithelial cells of the posterior pole have fewer Na/K adenosine triphosphatase pumps than peripheral cells. Invest Ophthalmol Vis Sci 32:2042-2046.

Burke JM, Cao F, Irving PE (2000) High levels of E-/P-cadherin: correlation with decreased apical polarity of Na/K ATPase in bovine RPE cells in situ. Invest Ophthalmol Vis Sci 41:1945-1952.

Burke JM, Skumatz CM, Irving PE, McKay BS (1996) Phenotypic heterogeneity of retinal pigment epithelial cells in vitro and in situ. Exp Eye Res 62:63-73.

Burns MS, Hartz MJ (1992) The retinal pigment epithelium induces fenestration of endothelial cells in vivo. Curr Eye Res 11:863-873.

Cabral L, Unger W, Boulton M, Lightfoot R, McKechnie N, Grierson I, Marshall J (1990) Regional distribution of lysosomal enzymes in the canine retinal pigment epithelium. Invest Ophthalmol Vis Sci 31:670-676.

Cai J, Nelson KC, Wu M, Sternberg P, Jr., Jones DP (2000) Oxidative damage and protection of the RPE. Prog Retin Eye Res 19:205-221.

Callaerts P, Halder G, Gehring WJ (1997) PAX-6 in development and evolution. Annu Rev Neurosci 20:483-532.

Campochiaro PA, Sugg R, Grotendorst G, Hjelmeland LM (1989) Retinal pigment epithelial cells produce PDGF-like proteins and secrete them into their media. Exp Eye Res 49:217-227.

Campochiaro PA, Hackett SF, Vinores SA, Freund J, Csaky C, LaRochelle W, Henderer J, Johnson M, Rodriguez IR, Friedman Z, et al. (1994) Platelet-derived growth factor is an autocrine growth stimulator in retinal pigmented epithelial cells. J Cell Sci 107 (Pt 9):2459-2469.

Cao W, Wen R, Li F, Lavail MM, Steinberg RH (1997) Mechanical injury increases bFGF and CNTF mRNA expression in the mouse retina. Exp Eye Res 65:241-248.

Cao W, Tombran-Tink J, Chen W, Mrazek D, Elias R, McGinnis JF (1999) Pigment epithelium-derived factor protects cultured retinal neurons against hydrogen peroxide-induced cell death. J Neurosci Res 57:789-800.

Cao W, Tombran-Tink J, Elias R, Sezate S, Mrazek D, McGinnis JF (2001) In vivo protection of photoreceptors from light damage by pigment epithelium-derived factor. Invest Ophthalmol Vis Sci 42:1646-1652.

Cardillo-Piccolino F, Ghiglione D, Borgia L, Zingirian M (1989) [New occult choroidal vessels in age-related macular degeneration]. J Fr Ophtalmol 12:869-876.

Caruelle D, Groux-Muscatelli B, Gaudric A, Sestier C, Coscas G, Caruelle JP, Barritault D (1989) Immunological study of acidic fibroblast growth factor (aFGF) distribution in the eye. J Cell Biochem 39:117-128.

Cattaneo E, McKay R (1990) Proliferation and differentiation of neuronal stem cells regulated by nerve growth factor. Nature 347:762-765.

Caviness VS, Jr., Goto T, Tarui T, Takahashi T, Bhide PG, Nowakowski RS (2003) Cell output, cell cycle duration and neuronal specification: a model of integrated mechanisms of the neocortical proliferative process. Cereb Cortex 13:592-598.

Chacko DM, Rogers JA, Turner JE, Ahmad I (2000) Survival and differentiation of cultured retinal progenitors transplanted in the subretinal space of the rat. Biochem Biophys Res Commun 268:842-846.

Chacko DM, Das AV, Zhao X, James J, Bhattacharya S, Ahmad I (2003) Transplantation of ocular stem cells: the role of injury in incorporation and differentiation of grafted cells in the retina. Vision Res 43:937-946.

Chaitin MH, Hall MO (1983) Defective ingestion of rod outer segments by cultured dystrophic rat pigment epithelial cells. Invest Ophthalmol Vis Sci 24:812-820.

Chalepakis G, Fritsch R, Fickenscher H, Deutsch U, Goulding M, Gruss P (1991) The molecular basis of the undulated/Pax-1 mutation. Cell 66:873-884.

Chan-Ling T (1994) Glia, neuronal and vascular interactions in the mammalian retina. Progress in Retinal and Eye Research 13:357-389.

Chang ML, Wu CH, Jiang-Shieh YF, Shieh JY, Wen CY (2007) Reactive changes of retinal astrocytes and Muller glial cells in kainate-induced neuroexcitotoxicity. J Anat 210:54-65.

Chen J, Simon MI, Matthes MT, Yasumura D, LaVail MM (1999) Increased susceptibility to light damage in an arrestin knockout mouse model of Oguchi disease (stationary night blindness). Invest Ophthalmol Vis Sci 40:2978-2982.

Chiba C, Hoshino A, Nakamura K, Susaki K, Yamano Y, Kaneko Y, Kuwata O, Maruo F, Saito T (2006) Visual cycle protein RPE65 persists in new retinal cells during retinal regeneration of adult newt. J Comp Neurol 495:391-407.

Couillard-Despres S, Winner B, Schaubeck S, Aigner R, Vroemen M, Weidner N, Bogdahn U, Winkler J, Kuhn HG, Aigner L (2005) Doublecortin expression levels in adult brain reflect neurogenesis. Eur J Neurosci 21:1-14.

Coulombre JL, Coulombre AJ (1965) Regeneration of neural retina from the pigmented epithelium in the chick embryo. Dev Biol 12:79-92.

Coulombre JL, Coulombre AJ (1970) Influence of mouse neural retina on regeneration of chick neural retina from chick embryonic pigmented epithelium. Nature 228:559-560.

Curcio CA, Owsley C, Jackson GR (2000) Spare the rods, save the cones in aging and age-related maculopathy. Invest Ophthalmol Vis Sci 41:2015-2018.

Curcio CA, Sloan KR, Kalina RE, Hendrickson AE (1990) Human photoreceptor topography. J Comp Neurol 292:497-523.

Curcio CA, Millican CL, Allen KA, Kalina RE (1993) Aging of the human photoreceptor mosaic: evidence for selective vulnerability of rods in central retina. Invest Ophthalmol Vis Sci 34:3278-3296.

Curtin B (1985) The Myopias:Basic science and clinical management. Philadelphia.

Curtis AS, Seehar GM (1978) The control of cell division by tension or diffusion. Nature 274:52-53.

Dacey DM, Lee BB, Stafford DK, Pokorny J, Smith VC (1996) Horizontal cells of the primate retina: cone specificity without spectral opponency. Science 271:656-659.

Daum G, Eisenmann-Tappe I, Fries HW, Troppmair J, Rapp UR (1994) The ins and outs of Raf kinases. Trends Biochem Sci 19:474-480.

Dawson DW, Volpert OV, Gillis P, Crawford SE, Xu H, Benedict W, Bouck NP (1999) Pigment epithelium-derived factor: a potent inhibitor of angiogenesis. Science 285:245-248.

Defoe DM, Adams LB, Sun J, Wisecarver SN, Levine EM (2007) Defects in retinal pigment epithelium cell proliferation and retinal attachment in mutant mice with p27(Kip1) gene ablation. Mol Vis 13:273-286.

Del Priore LV, Kuo YH, Tezel TH (2002) Age-related changes in human RPE cell density and apoptosis proportion in situ. Invest Ophthalmol Vis Sci 43:3312-3318.

Drager UC, Olsen JF (1981) Ganglion cell distribution in the retina of the mouse. Invest Ophthalmol Vis Sci 20:285-293.

Dreher B, Sefton AJ, Ni SY, Nisbett G (1985) The morphology, number, distribution and central projections of Class I retinal ganglion cells in albino and hooded rats. Brain Behav Evol 26:10-48.

Duggal N, Schmidt-Kastner R, Hakim AM (1997) Nestin expression in reactive astrocytes following focal cerebral ischemia in rats. Brain Res 768:1-9.

Engelhardt M, Bogdahn U, Aigner L (2005) Adult retinal pigment epithelium cells express neural progenitor properties and the neuronal precursor protein doublecortin. Brain Res 1040:98-111.

Engelhardt M, Wachs FP, Couillard-Despres S, Aigner L (2004) The neurogenic competence of progenitors from the postnatal rat retina in vitro. Exp Eye Res 78:1025-1036.

Essers J, Theil AF, Baldeyron C, van Cappellen WA, Houtsmuller AB, Kanaar R, Vermeulen W (2005) Nuclear dynamics of PCNA in DNA replication and repair. Mol Cell Biol 25:9350-9359.

Faktorovich EG, Steinberg RH, Yasumura D, Matthes MT, LaVail MM (1990) Photoreceptor degeneration in inherited retinal dystrophy delayed by basic fibroblast growth factor. Nature 347:83-86.

Feeney-Burns L, Hilderbrand E, Eldridge S (1984a) Aging human RPE: morphometric analysis of macular, equatorial, and peripheral cells. Invest Ophthalmol Vis Sci 25:195-200.

Feeney-Burns L, Hilderbrand ES, Eldridge S (1984b) Aging human RPE: morphometric analysis of macular, equatorial, and peripheral cells. Invest Ophthalmol Vis Sci 25:195-200.

Feeney L (1978) Lipofuscin and melanin of human retinal pigment epithelium. Fluorescence, enzyme cytochemical, and ultrastructural studies. Invest Ophthalmol Vis Sci 17:583-600.

Feeney L, Hogan MJ (1961) Electron microscopy of the human choroid. II. The choroidal nerves. Am J Ophthalmol 51:1072-1083.

Finnemann SC (2003) Focal adhesion kinase signaling promotes phagocytosis of integrin-bound photoreceptors. Embo J 22:4143-4154.

Finnemann SC, Silverstein RL (2001) Differential roles of CD36 and alphavbeta5 integrin in photoreceptor phagocytosis by the retinal pigment epithelium. J Exp Med 194:1289-1298.

Fischer AJ (2005) Neural regeneration in the chick retina. Prog Retin Eye Res 24:161-182.

Fischer AJ, Reh TA (2000) Identification of a proliferating marginal zone of retinal progenitors in postnatal chickens. Dev Biol 220:197-210.

Fischer AJ, Reh TA (2003) Growth factors induce neurogenesis in the ciliary body. Dev Biol 259:225-240.

Fisher AB, Chien S, Barakat AI, Nerem RM (2001) Endothelial cellular response to altered shear stress. Am J Physiol Lung Cell Mol Physiol 281:L529-533.

Fisher SK, Erickson PA, Lewis GP, Anderson DH (1991) Intraretinal proliferation induced by retinal detachment. Invest Ophthalmol Vis Sci 32:1739-1748.

Fisher SK, Lewis GP, Linberg KA, Verardo MR (2005) Cellular remodeling in mammalian retina: results from studies of experimental retinal detachment. Prog Retin Eye Res 24:395-431.

Flood MT, Haley JE, Gouras P (1984) Cellular aging of human retinal epithelium in vivo and in vitro. Monogr Dev Biol 17:80-93.

Folkman J, Moscona A (1978) Role of cell shape in growth control. Nature 273:345-349.

Freeman WM, Walker SJ, Vrana KE (1999) Quantitative RT-PCR: pitfalls and potential. Biotechniques 26:112-122, 124-115.

Friedman E, Smith TR, Kuwabara T (1963) Senile choroidal vascular patterns and drusen. Arch Ophthalmol 69:220-230.

Fuchs E, Cleveland DW (1998) A structural scaffolding of intermediate filaments in health and disease. Science 279:514-519.

Fuhrmann S, Levine EM, Reh TA (2000) Extraocular mesenchyme patterns the optic vesicle during early eye development in the embryonic chick. Development 127:4599-4609.

Gao H, Hollyfield JG (1992) Aging of the human retina. Differential loss of neurons and retinal pigment epithelial cells. Invest Ophthalmol Vis Sci 33:1-17.

Gerdes J, Schwab U, Lemke H, Stein H (1983) Production of a mouse monoclonal antibody reactive with a human nuclear antigen associated with cell proliferation. Int J Cancer 31:13-20.

Gerdes J, Lemke H, Baisch H, Wacker HH, Schwab U, Stein H (1984) Cell cycle analysis of a cell proliferation-associated human nuclear antigen defined by the monoclonal antibody Ki-67. J Immunol 133:1710-1715.

Gimenez E, Lavado A, Jeffery G, Montoliu L (2005) Regional abnormalities in retinal development are associated with local ocular hypopigmentation. J Comp Neurol 485:338-347.

Glaser T, Jepeal L, Edwards JG, Young SR, Favor J, Maas RL (1994) PAX6 gene dosage effect in a family with congenital cataracts, aniridia, anophthalmia and central nervous system defects. Nat Genet 7:463-471.

Gleeson JG, Lin PT, Flanagan LA, Walsh CA (1999) Doublecortin is a microtubule-associated protein and is expressed widely by migrating neurons. Neuron 23:257-271.

Gleeson JG, Allen KM, Fox JW, Lamperti ED, Berkovic S, Scheffer I, Cooper EC, Dobyns WB, Minnerath SR, Ross ME, Walsh CA (1998) Doublecortin, a brain-specific gene mutated in human X-linked lissencephaly and double cortex syndrome, encodes a putative signaling protein. Cell 92:63-72.

Goldman RD, Chou YH, Prahlad V, Yoon M (1999) Intermediate filaments: dynamic processes regulating their assembly, motility, and interactions with other cytoskeletal systems. Faseb J 13 Suppl 2:S261-265.

Gollapalli DR, Rando RR (2004) The specific binding of retinoic acid to RPE65 and approaches to the treatment of macular degeneration. Proc Natl Acad Sci U S A 101:10030-10035.

Gollapalli DR, Maiti P, Rando RR (2003) RPE65 operates in the vertebrate visual cycle by stereospecifically binding all-trans-retinyl esters. Biochemistry 42:11824-11830.

Goto T, Hisatomi O, Kotoura M, Tokunaga F (2006) Induced expression of hematopoietic- and neurologic-expressed sequence 1 in retinal pigment epithelial cells during newt retina regeneration. Exp Eye Res 83:972-980.

Grant MB, Guay C, Marsh R (1990) Insulin-like growth factor I stimulates proliferation, migration, and plasminogen activator release by human retinal pigment epithelial cells. Curr Eye Res 9:323-335.

Grant S, Patel NN, Philp AR, Grey CN, Lucas RD, Foster RG, Bowmaker JK, Jeffery G (2001) Rod photopigment deficits in albinos are specific to mammals and arise during retinal development. Vis Neurosci 18:245-251.

Grierson I, Hiscott P, Hogg P, Robey H, Mazure A, Larkin G (1994) Development, repair and regeneration of the retinal pigment epithelium. Eye 8 (Pt 2):255-262.

Grindley JC, Davidson DR, Hill RE (1995) The role of Pax-6 in eye and nasal development. Development 121:1433-1442.

Gruss P, Walther C (1992) Pax in development. Cell 69:719-722.

Guillaud P, du Manoir S, Seigneurin D (1989) Quantification and topographical description of Ki-67 antibody labelling during the cell cycle of normal

fibroblastic (MRC-5) and mammary tumour cell lines (MCF-7). Anal Cell Pathol 1:25-39.

Hack I, Peichl L (1999) Horizontal cells of the rabbit retina are non-selectively connected to the cones. Eur J Neurosci 11:2261-2274.

Hageman GS, Mullins RF, Russell SR, Johnson LV, Anderson DH (1999) Vitronectin is a constituent of ocular drusen and the vitronectin gene is expressed in human retinal pigmented epithelial cells. Faseb J 13:477-484.

Hageman GS, Luthert PJ, Victor Chong NH, Johnson LV, Anderson DH, Mullins RF (2001) An integrated hypothesis that considers drusen as biomarkers of immune-mediated processes at the RPE-Bruch's membrane interface in aging and age-related macular degeneration. Prog Retin Eye Res 20:705-732.

Hageman GS, Anderson DH, Johnson LV, Hancox LS, Taiber AJ, Hardisty LI, Hageman JL, Stockman HA, Borchardt JD, Gehrs KM, Smith RJ, Silvestri G, Russell SR, Klaver CC, Barbazetto I, Chang S, Yannuzzi LA, Barile GR, Merriam JC, Smith RT, Olsh AK, Bergeron J, Zernant J, Merriam JE, Gold B, Dean M, Allikmets R (2005) A common haplotype in the complement regulatory gene factor H (HF1/CFH) predisposes individuals to age-related macular degeneration. Proc Natl Acad Sci U S A 102:7227-7232.

Haimovici R, Gantz DL, Rumelt S, Freddo TF, Small DM (2001) The lipid composition of drusen, Bruch's membrane, and sclera by hot stage polarizing light microscopy. Invest Ophthalmol Vis Sci 42:1592-1599.

Haines JL, Hauser MA, Schmidt S, Scott WK, Olson LM, Gallins P, Spencer KL, Kwan SY, Noureddine M, Gilbert JR, Schnetz-Boutaud N, Agarwal A, Postel EA, Pericak-Vance MA (2005) Complement factor H variant increases the risk of age-related macular degeneration. Science 308:419-421.

Hamann S (2002) Molecular mechanisms of water transport in the eye. Int Rev Cytol 215:395-431.

Hamel CP, Tsilou E, Harris E, Pfeffer BA, Hooks JJ, Detrick B, Redmond TM (1993) A developmentally regulated microsomal protein specific for the pigment epithelium of the vertebrate retina. J Neurosci Res 34:414-425.

Hargrave PA (2001) Rhodopsin structure, function, and topography the Friedenwald lecture. Invest Ophthalmol Vis Sci 42:3-9.

Harman AM, Fleming PA, Hoskins RV, Moore SR (1997) Development and aging of cell topography in the human retinal pigment epithelium. Invest Ophthalmol Vis Sci 38:2016-2026.

Harman D (1981) The aging process. Proc Natl Acad Sci U S A 78:7124-7128.

Hayreh SS (1975) Segmental nature of the choroidal vasculature. Br J Ophthalmol 59:631-648.

Heath SK, Carne S, Hoyle C, Johnson KJ, Wells DJ (1997) Characterisation of expression of mDMAHP, a homeodomain-encoding gene at the murine DM locus. Hum Mol Genet 6:651-657.

Hecquet C, Lefevre G, Valtink M, Engelmann K, Mascarelli F (2002) Activation and role of MAP kinase-dependent pathways in retinal pigment epithelial cells: ERK and RPE cell proliferation. Invest Ophthalmol Vis Sci 43:3091-3098.

Hiscott P, Sheridan C, Magee RM, Grierson I (1999) Matrix and the retinal pigment epithelium in proliferative retinal disease. Prog Retin Eye Res 18:167-190.

Hiscott PS, Grierson I, McLeod D (1984) Retinal pigment epithelial cells in epiretinal membranes: an immunohistochemical study. Br J Ophthalmol 68:708-715.

Hockfield S, McKay RD (1985) Identification of major cell classes in the developing mammalian nervous system. J Neurosci 5:3310-3328.

Hofmann KP (1999) Signalling states of photoactivated rhodopsin. Novartis Found Symp 224:158-175; discussion 175-180.

Hogan MJ (1961) Ultrastructure of the choroid. Its role in the pathogenesis of chorioretinal disease. Trans Pac Coast Otoophthalmol Soc Annu Meet 42:61-87.

Hogan MJ, J. A Alvarado, and J. E Weddell (1971) Histology of the Human Eye. Philadelphia

Hollyfield JG (1971) Differential growth of the neural retina in Xenopus laevis larvae. Dev Biol 24:264-286.

Holmin S, Almqvist P, Lendahl U, Mathiesen T (1997) Adult nestin-expressing subependymal cells differentiate to astrocytes in response to brain injury. Eur J Neurosci 9:65-75.

Holz FG, Sheraidah G, Pauleikhoff D, Bird AC (1994) Analysis of lipid deposits extracted from human macular and peripheral Bruch's membrane. Arch Ophthalmol 112:402-406.

Ilia M, Jeffery G (1996) Delayed neurogenesis in the albino retina: evidence of a role for melanin in regulating the pace of cell generation. Brain Res Dev Brain Res 95:176-183.

Ilia M, Jeffery G (1999) Retinal mitosis is regulated by dopa, a melanin precursor that may influence the time at which cells exit the cell cycle: analysis of patterns of cell production in pigmented and albino retinae. J Comp Neurol 405:394-405.

Ilia M, Jeffery G (2000) Retinal cell addition and rod production depend on early stages of ocular melanin synthesis. J Comp Neurol 420:437-444.

Iseli HP, Wenzel A, Hafezi F, CE RE, Grimm C (2002) Light damage susceptibility and RPE65 in rats. Exp Eye Res 75:407-413.

Ishibashi K, Tian J, Handa JT (2004) Similarity of mRNA phenotypes of morphologically normal macular and peripheral retinal pigment epithelial cells in older human eyes. Invest Ophthalmol Vis Sci 45:3291-3301.

Ishida K, Panjwani N, Cao Z, Streilein JW (2003) Participation of pigment epithelium in ocular immune privilege. 3. Epithelia cultured from iris, ciliary body, and retina suppress T-cell activation by partially non-overlapping mechanisms. Ocul Immunol Inflamm 11:91-105.

Jang JH, Rives CB, Shea LD (2005) Plasmid delivery in vivo from porous tissue-engineering scaffolds: transgene expression and cellular transfection. Mol Ther 12:475-483.

Jean D, Bernier G, Gruss P (1999) Six6 (Optx2) is a novel murine Six3-related homeobox gene that demarcates the presumptive pituitary/hypothalamic axis and the ventral optic stalk. Mech Dev 84:31-40.

Jeffery G (1997) The albino retina: an abnormality that provides insight into normal retinal development. Trends Neurosci 20:165-169.

Jeffery G, Kinsella B (1992) Translaminar deficits in the retinae of albinos. J Comp Neurol 326:637-644.

Jeffery G, Darling K, Whitmore A (1994a) Melanin and the regulation of mammalian photoreceptor topography. Eur J Neurosci 6:657-667.

Jeffery G, Schutz G, Montoliu L (1994b) Correction of abnormal retinal pathways found with albinism by introduction of a functional tyrosinase gene in transgenic mice. Dev Biol 166:460-464.

Jeffery G, Brem G, Montoliu L (1997) Correction of retinal abnormalities found in albinism by introduction of a functional tyrosinase gene in transgenic mice and rabbits. Brain Res Dev Brain Res 99:95-102.

Jeon CJ, Strettoi E, Masland RH (1998) The major cell populations of the mouse retina. J Neurosci 18:8936-8946.

Johns PR (1977) Growth of the adult goldfish eye. III. Source of the new retinal cells. J Comp Neurol 176:343-357.

Kainz P (2000) The PCR plateau phase - towards an understanding of its limitations. Biochim Biophys Acta 1494:23-27.

Kamachi Y, Cheah KS, Kondoh H (1999) Mechanism of regulatory target selection by the SOX high-mobility-group domain proteins as revealed by comparison of SOX1/2/3 and SOX9. Mol Cell Biol 19:107-120.

Kampik A, Kenyon KR, Michels RG, Green WR, de la Cruz ZC (1981) Epiretinal and vitreous membranes. Comparative study of 56 cases. Arch Ophthalmol 99:1445-1454.

Kaneko Y, Matsumoto G, Hanyu Y (1999) Pax-6 expression during retinal regeneration in the adult newt. Dev Growth Differ 41:723-729.

Kaneko Y, Hirota K, Matsumoto G, Hanyu Y (2001) Expression pattern of a newt Notch homologue in regenerating newt retina. Brain Res Dev Brain Res 128:53-62.

Keefe JR (1973) An analysis of urodelian retinal regeneration. I. Studies of the cellular source of retinal regeneration in Notophthalmus viridescens utilizing 3 H-thymidine and colchicine. J Exp Zool 184:185-206.

Kiilgaard JF, Prause JU, Prause M, Scherfig E, Nissen MH, la Cour M (2007) Subretinal posterior pole injury induces selective proliferation of RPE cells in the periphery in in vivo studies in pigs. Invest Ophthalmol Vis Sci 48:355-360.

Kishi H, Mishima HK, Yamashita U (1994) Growth regulation of retinal pigment epithelial (RPE) cells in vitro. Curr Eye Res 13:661-668.

Klein LR, MacLeish PR, Wiesel TN (1990) Immunolabelling by a newt retinal pigment epithelium antibody during retinal development and regeneration. J Comp Neurol 293:331-339.

Klein RJ, Zeiss C, Chew EY, Tsai JY, Sackler RS, Haynes C, Henning AK, SanGiovanni JP, Mane SM, Mayne ST, Bracken MB, Ferris FL, Ott J, Barnstable C, Hoh J (2005) Complement factor H polymorphism in age-related macular degeneration. Science 308:385-389.

Kliffen M, van der Schaft TL, Mooy CM, de Jong PT (1997) Morphologic changes in age-related maculopathy. Microsc Res Tech 36:106-122.

Kobayashi M, Toyama R, Takeda H, Dawid IB, Kawakami K (1998) Overexpression of the forebrain-specific homeobox gene six3 induces rostral forebrain enlargement in zebrafish. Development 125:2973-2982.

Kohno H, Sakai T, Kitahara K (2006) Induction of nestin, Ki-67, and cyclin D1 expression in Muller cells after laser injury in adult rat retina. Graefes Arch Clin Exp Ophthalmol 244:90-95.

Kralj-Hans I, Tibber M, Jeffery G, Mobbs P (2006) Differential effect of dopamine on mitosis in early postnatal albino and pigmented rat retinae. J Neurobiol 66:47-55.

Kubota R, Hokoc JN, Moshiri A, McGuire C, Reh TA (2002) A comparative study of neurogenesis in the retinal ciliary marginal zone of homeothermic vertebrates. Brain Res Dev Brain Res 134:31-41.

Kubrusly RC, Guimaraes MZ, Vieira AP, Hokoc JN, Casarini DE, de Mello MC, de Mello FG (2003) L-DOPA supply to the neuro retina activates dopaminergic communication at the early stages of embryonic development. J Neurochem 86:45-54.

Kuhn HG, Dickinson-Anson H, Gage FH (1996) Neurogenesis in the dentate gyrus of the adult rat: age-related decrease of neuronal progenitor proliferation. J Neurosci 16:2027-2033.

Kvanta A (1994) Expression and secretion of transforming growth factor-beta in transformed and nontransformed retinal pigment epithelial cells. Ophthalmic Res 26:361-367.

La Vail MM, Rapaport DH, Rakic P (1991) Cytogenesis in the monkey retina. The Journal of Comparitive Neurology 309:86-114.

Lagutin O, Zhu CC, Furuta Y, Rowitch DH, McMahon AP, Oliver G (2001) Six3 promotes the formation of ectopic optic vesicle-like structures in mouse embryos. Dev Dyn 221:342-349.

Lai K, Kaspar BK, Gage FH, Schaffer DV (2003) Sonic hedgehog regulates adult neural progenitor proliferation in vitro and in vivo. Nat Neurosci 6:21-27.

Laqua H, Machemer R (1976) Repair and adhesion mechanisms of the cryotherapy lesion in experimental retinal detachment. Am J Ophthalmol 81:833-846.

LaVail MM (1976) Rod outer segment disk shedding in rat retina: relationship to cyclic lighting. Science 194:1071-1074.

LaVail MM (1980) Circadian nature of rod outer segment disc shedding in the rat. Invest Ophthalmol Vis Sci 19:407-411.

LaVail MM (1983) Outer segment disc shedding and phagocytosis in the outer retina. Trans Ophthalmol Soc U K 103 (Pt 4):397-404.

Lendahl U (1997) Transgenic analysis of central nervous system development and regeneration. Acta Anaesthesiol Scand Suppl 110:116-118.

Lendahl U, Zimmerman LB, McKay RD (1990) CNS stem cells express a new class of intermediate filament protein. Cell 60:585-595.

Lengyel I, Tufail A, Hosaini HA, Luthert P, Bird AC, Jeffery G (2004) Association of drusen deposition with choroidal intercapillary pillars in the aging human eye. Invest Ophthalmol Vis Sci 45:2886-2892.

Leonardi E, Girlando S, Serio G, Mauri FA, Perrone G, Scampini S, Dalla Palma P, Barbareschi M (1992) PCNA and Ki67 expression in breast carcinoma: correlations with clinical and biological variables. J Clin Pathol 45:416-419.

Leschey KH, Hackett SF, Singer JH, Campochiaro PA (1990) Growth factor responsiveness of human retinal pigment epithelial cells. Invest Ophthalmol Vis Sci 31:839-846.

Leschey KH, Hines J, Singer JH, Hackett SF, Campochiaro PA (1991) Inhibition of growth factor effects in retinal pigment epithelial cells. Invest Ophthalmol Vis Sci 32:1770-1778.

Lewis GP, Charteris DG, Sethi CS, Leitner WP, Linberg KA, Fisher SK (2002) The ability of rapid retinal reattachment to stop or reverse the cellular and molecular events initiated by detachment. Invest Ophthalmol Vis Sci 43:2412-2420.

Lewis H, Straatsma BR, Foos RY (1986) The prevalence of macular drusen in postmortem eyes. Am J Ophthalmol 102:801-803.

Li CM, Clark ME, Rudolf M, Curcio CA (2007) Distribution and composition of esterified and unesterified cholesterol in extra-macular drusen. Exp Eye Res 85:192-201.

Li Y, Chopp M (1999) Temporal profile of nestin expression after focal cerebral ischemia in adult rat. Brain Res 838:1-10.

Linberg KA, Sakai T, Lewis GP, Fisher SK (2002) Experimental retinal detachment in the cone-dominant ground squirrel retina: morphology and basic immunocytochemistry. Vis Neurosci 19:603-619.

Lolley RN, Rong H, Craft CM (1994) Linkage of photoreceptor degeneration by apoptosis with inherited defect in phototransduction. Invest Ophthalmol Vis Sci 35:358-362.

Loosli F, Koster RW, Carl M, Krone A, Wittbrodt J (1998) Six3, a medaka homologue of the Drosophila homeobox gene sine oculis is expressed in the anterior embryonic shield and the developing eye. Mech Dev 74:159-164.

Lopez-Rios J, Gallardo ME, Rodriguez de Cordoba S, Bovolenta P (1999) Six9 (Optx2), a new member of the six gene family of transcription factors, is expressed at early stages of vertebrate ocular and pituitary development. Mech Dev 83:155-159.

Lothian C, Lendahl U (1997) An evolutionarily conserved region in the second intron of the human nestin gene directs gene expression to CNS progenitor cells and to early neural crest cells. Eur J Neurosci 9:452-462.

Machemer R (1977) Massive periretinal proliferation: a logical approach to therapy. Trans Am Ophthalmol Soc 75:556-586.

Machemer R, Laqua H (1975) Pigment epithelium proliferation in retinal detachment (massive periretinal proliferation). Am J Ophthalmol 80:1-23.

Machemer R, van Horn D, Aaberg TM (1978) Pigment epithelial proliferation in human retinal detachment with massive periretinal proliferation. Am J Ophthalmol 85:181-191.

MacLaren RE, Pearson RA, MacNeil A, Douglas RH, Salt TE, Akimoto M, Swaroop A, Sowden JC, Ali RR (2006) Retinal repair by transplantation of photoreceptor precursors. Nature 444:203-207.

Malecaze F, Mascarelli F, Bugra K, Fuhrmann G, Courtois Y, Hicks D (1993) Fibroblast growth factor receptor deficiency in dystrophic retinal pigmented epithelium. J Cell Physiol 154:631-642.

Mann I (1964) The development of the human eye. New York: Grune & Stratton.

Marlhens F, Bareil C, Griffoin JM, Zrenner E, Amalric P, Eliaou C, Liu SY, Harris E, Redmond TM, Arnaud B, Claustres M, Hamel CP (1997) Mutations in RPE65 cause Leber's congenital amaurosis. Nat Genet 17:139-141.

Marmor MF, Wolfensberger TJ (1998) The Retinal Pigment Epithelium: Oxford University Press.

Marshall J, Mellerio J (1971) Disappearance of retino-epithelial scar tissue from ruby laser photocoagulations. Exp Eye Res 12:173-174.

Martin DM, Yee D, Carlson RO, Feldman EL (1992) Gene expression of the insulin-like growth factors and their receptors in human neuroblastoma cell lines. Brain Res Mol Brain Res 15:241-246.

Martin PR (1986) The projection of different retinal ganglion cell classes to the dorsal lateral geniculate nucleus in the hooded rat. Exp Brain Res 62:77-88.

Martinez-Morales JR, Rodrigo I, Bovolenta P (2004) Eye development: a view from the retina pigmented epithelium. Bioessays 26:766-777.

Martinez-Morales JR, Signore M, Acampora D, Simeone A, Bovolenta P (2001) Otx genes are required for tissue specification in the developing eye. Development 128:2019-2030.

Masland RH (2001) Neuronal diversity in the retina. Curr Opin Neurobiol 11:431-436.

Mata NL, Weng J, Travis GH (2000) Biosynthesis of a major lipofuscin fluorophore in mice and humans with ABCR-mediated retinal and macular degeneration. Proc Natl Acad Sci U S A 97:7154-7159.

Mata NL, Moghrabi WN, Lee JS, Bui TV, Radu RA, Horwitz J, Travis GH (2004) Rpe65 is a retinyl ester binding protein that presents insoluble substrate to the isomerase in retinal pigment epithelial cells. J Biol Chem 279:635-643.

Matsuo T, Osumi-Yamashita N, Noji S, Ohuchi H, Koyama E, Myokai F, Matsuo N, Taniguchi S, Doi H, Iseki S, et al. (1993) A mutation in the Pax-6 gene in rat small eye is associated with impaired migration of midbrain crest cells. Nat Genet 3:299-304.

McKay BS, Burke JM (1994) Separation of phenotypically distinct subpopulations of cultured human retinal pigment epithelial cells. Exp Cell Res 213:85-92.

Miceli MV, Liles MR, Newsome DA (1994) Evaluation of oxidative processes in human pigment epithelial cells associated with retinal outer segment phagocytosis. Exp Cell Res 214:242-249.

Michels RG (1982) A clinical and histopathologic study of epiretinal membranes affecting the macula and removed by vitreous surgery. Trans Am Ophthalmol Soc 80:580-656.

Miller H, Miller B, Ryan SJ (1986) The role of retinal pigment epithelium in the involution of subretinal neovascularization. Invest Ophthalmol Vis Sci 27:1644-1652.

Miller MW, Nowakowski RS (1988) Use of bromodeoxyuridine-immunohistochemistry to examine the proliferation, migration and time of origin of cells in the central nervous system. Brain Res 457:44-52.

Miller SS, Edelman JL (1990) Active ion transport pathways in the bovine retinal pigment epithelium. J Physiol 424:283-300.

Mitsuda S, Yoshii C, Ikegami Y, Araki M (2005) Tissue interaction between the retinal pigment epithelium and the choroid triggers retinal regeneration of the newt Cynops pyrrhogaster. Dev Biol 280:122-132.

Mizuseki K, Kishi M, Matsui M, Nakanishi S, Sasai Y (1998) Xenopus Zic-related-1 and Sox-2, two factors induced by chordin, have distinct activities in the initiation of neural induction. Development 125:579-587.

Morgan DO (1997) Cyclin-dependent kinases: engines, clocks, and microprocessors. Annu Rev Cell Dev Biol 13:261-291.

Morris VB, Wylie CC, Miles VJ (1976) The growth of the chick retina after hatching. Anat Rec 184:111-113.

Moshiri A, Reh TA (2004) Persistent progenitors at the retinal margin of ptc+/- mice. J Neurosci 24:229-237.

Muller H (1856) Untersuchungen uber die gladuatees des auges, insbesondere die glaslamelle der choroidea und ihr senilen veranderungen. Arch Ophthalmol 2:1.

Mullins RF, Aptsiauri N, Hageman GS (2001) Structure and composition of drusen associated with glomerulonephritis: implications for the role of complement activation in drusen biogenesis. Eye 15:390-395.

Mullins RF, Russell SR, Anderson DH, Hageman GS (2000) Drusen associated with aging and age-related macular degeneration contain proteins common to extracellular deposits associated with atherosclerosis, elastosis, amyloidosis, and dense deposit disease. Faseb J 14:835-846.

Namiki J, Tator CH (1999) Cell proliferation and nestin expression in the ependyma of the adult rat spinal cord after injury. J Neuropathol Exp Neurol 58:489-498.

Nawrot M, West K, Huang J, Possin DE, Bretscher A, Crabb JW, Saari JC (2004) Cellular retinaldehyde-binding protein interacts with ERM-binding phosphoprotein 50 in retinal pigment epithelium. Invest Ophthalmol Vis Sci 45:393-401.

Neveu MM, Jeffery G, Burton LC, Sloper JJ, Holder GE (2003) Age-related changes in the dynamics of human albino visual pathways. Eur J Neurosci 18:1939-1949.

Newman E, Reichenbach A (1996) The Muller cell: a functional element of the retina. Trends Neurosci 19:307-312.

Nicoletti A, Wong DJ, Kawase K, Gibson LH, Yang-Feng TL, Richards JE, Thompson DA (1995) Molecular characterization of the human gene encoding an abundant 61 kDa protein specific to the retinal pigment epithelium. Hum Mol Genet 4:641-649.

Ogata N, Wada M, Otsuji T, Jo N, Tombran-Tink J, Matsumura M (2002) Expression of pigment epithelium-derived factor in normal adult rat eye and experimental choroidal neovascularization. Invest Ophthalmol Vis Sci 43:1168-1175.

Ogata N, Wang L, Jo N, Tombran-Tink J, Takahashi K, Mrazek D, Matsumura M (2001) Pigment epithelium derived factor as a neuroprotective agent against ischemic retinal injury. Curr Eye Res 22:245-252.

Oliver G, Mailhos A, Wehr R, Copeland NG, Jenkins NA, Gruss P (1995) Six3, a murine homologue of the sine oculis gene, demarcates the most anterior border of the developing neural plate and is expressed during eye development. Development 121:4045-4055.

Panda-Jonas S, Jonas JB, Jakobczyk-Zmija M (1996) Retinal pigment epithelial cell count, distribution, and correlations in normal human eyes. Am J Ophthalmol 121:181-189.

Park CM, Hollenberg MJ (1989) Basic fibroblast growth factor induces retinal regeneration in vivo. Dev Biol 134:201-205.

Park CM, Hollenberg MJ (1991) Induction of retinal regeneration in vivo by growth factors. Dev Biol 148:322-333.

Pauleikhoff D, Harper CA, Marshall J, Bird AC (1990a) Aging changes in Bruch's membrane. A histochemical and morphologic study. Ophthalmology 97:171-178.

Pauleikhoff D, Barondes MJ, Minassian D, Chisholm IH, Bird AC (1990b) Drusen as risk factors in age-related macular disease. Am J Ophthalmol 109:38-43.

Peirson S, Foster RG (2006) Melanopsin: another way of signaling light. Neuron 49:331-339.

Peirson SN, Bovee-Geurts PH, Lupi D, Jeffery G, DeGrip WJ, Foster RG (2004) Expression of the candidate circadian photopigment melanopsin (Opn4) in the mouse retinal pigment epithelium. Brain Res Mol Brain Res 123:132-135.

Pekny M, Wilhelmsson U, Bogestal YR, Pekna M (2007) The role of astrocytes and complement system in neural plasticity. Int Rev Neurobiol 82:95-111.

Pevny LH, Lovell-Badge R (1997) Sox genes find their feet. Curr Opin Genet Dev 7:338-344.

Pittack C, Jones M, Reh TA (1991) Basic fibroblast growth factor induces retinal pigment epithelium to generate neural retina in vitro. Development 113:577-588.

Prada C, Puga J, Perez-Mendez L, Lopez And R, Ramirez G (1991) Spatial and Temporal Patterns of Neurogenesis in the Chick Retina. Eur J Neurosci 3:1187.

Qiu G, Seiler MJ, Thomas BB, Wu K, Radosevich M, Sadda SR (2007) Revisiting nestin expression in retinal progenitor cells in vitro and after transplantation in vivo. Exp Eye Res 84:1047-1059.

Rapaport DH, Rakic P, Yasamura D, LaVail MM (1995) Genesis of the retinal pigment epithelium in the macaque monkey. J Comp Neurol 363:359-376.

Rattner A, Smallwood PM, Nathans J (2000) Identification and characterization of all-trans-retinol dehydrogenase from photoreceptor outer segments, the visual cycle enzyme that reduces all-trans-retinal to all-trans-retinol. J Biol Chem 275:11034-11043.

Raymond SM, Jackson IJ (1995) The retinal pigmented epithelium is required for development and maintenance of the mouse neural retina. Curr Biol 5:1286-1295.

Redmond TM, Yu S, Lee E, Bok D, Hamasaki D, Chen N, Goletz P, Ma JX, Crouch RK, Pfeifer K (1998) Rpe65 is necessary for production of 11-cis-vitamin A in the retinal visual cycle. Nat Genet 20:344-351.

Reh TA, Nagy T (1987) A possible role for the vascular membrane in retinal regeneration in Rana catesbienna tadpoles. Dev Biol 122:471-482.

Reh TA, Pittack C (1995) Transdifferentiation and retinal regeneration. Semin Cell Biol 6:137-142.

Reyer RW (1977) Repolarization of reversed, regenerating lenses in adult newts, Notophthalmus viridescens. Exp Eye Res 24:501-509.

Rizzolo LJ (1997) Polarity and the development of the outer blood-retinal barrier. Histol Histopathol 12:1057-1067.

Robb RM (1982) Increase in retinal surface area during infancy and childhood. J Pediatr Ophthalmol Strabismus 19:16-20.

Robb RM (1985) Regional changes in retinal pigment epithelial cell density during ocular development. Invest Ophthalmol Vis Sci 26:614-620.

Roberts WG, Palade GE (1995) Increased microvascular permeability and endothelial fenestration induced by vascular endothelial growth factor. J Cell Sci 108 (Pt 6):2369-2379.

Robinson MJ, Cobb MH (1997) Mitogen-activated protein kinase pathways. Curr Opin Cell Biol 9:180-186.

Rodieck RW (1998) The First Steps in Seeing: Sinauer Associates Inc, Sunderland, Massachusetts.

Ryeom SW, Sparrow JR, Silverstein RL (1996) CD36 participates in the phagocytosis of rod outer segments by retinal pigment epithelium. J Cell Sci 109 (Pt 2):387-395.

Saari JC (1982) Isolation of cellular retinoid-binding proteins from bovine retina with bound endogenous ligands. Methods Enzymol 81:819-826.

Saari JC, Bredberg DL (1990) Acyl-CoA:retinol acyltransferase and lecithin:retinol acyltransferase activities of bovine retinal pigment epithelial microsomes. Methods Enzymol 190:156-163.

Saari JC, Bredberg DL, Noy N (1994) Control of substrate flow at a branch in the visual cycle. Biochemistry 33:3106-3112.

Saari JC, Garwin GG, Van Hooser JP, Palczewski K (1998) Reduction of all-trans-retinal limits regeneration of visual pigment in mice. Vision Res 38:1325-1333.

Saari JC, Nawrot M, Kennedy BN, Garwin GG, Hurley JB, Huang J, Possin DE, Crabb JW (2001) Visual cycle impairment in cellular retinaldehyde binding protein (CRALBP) knockout mice results in delayed dark adaptation. Neuron 29:739-748.

Sakaguchi DS, Janick LM, Reh TA (1997) Basic fibroblast growth factor (FGF-2) induced transdifferentiation of retinal pigment epithelium: generation of retinal neurons and glia. Dev Dyn 209:387-398.

Sakami S, Etter P, Reh TA (2007) Activin signaling limits the competence for retinal regeneration from the pigmented epithelium. Mech Dev.

Sakami S, Hisatomi O, Sakakibara S, Liu J, Reh TA, Tokunaga F (2005) Downregulation of Otx2 in the dedifferentiated RPE cells of regenerating newt retina. Brain Res Dev Brain Res 155:49-59.

Sambrook J, Russell D (2000) Molecular cloning: A laboratory manual, Third Edition. New York: Cold Spring Harbour laboratory press.

Sarks JP, Sarks SH, Killingsworth MC (1994) Evolution of soft drusen in age-related macular degeneration. Eye 8 (Pt 3):269-283.

Sarna T, Burke JM, Korytowski W, Rozanowska M, Skumatz CM, Zareba A, Zareba M (2003) Loss of melanin from human RPE with aging: possible role of melanin photooxidation. Exp Eye Res 76:89-98.

Sarraf D, Gin T, Yu F, Brannon A, Owens SL, Bird AC (1999) Long-term drusen study. Retina 19:513-519.

Schluter C, Duchrow M, Wohlenberg C, Becker MH, Key G, Flad HD, Gerdes J (1993) The cell proliferation-associated antigen of antibody Ki-67: a very large, ubiquitous nuclear protein with numerous repeated elements, representing a new kind of cell cycle-maintaining proteins. J Cell Biol 123:513-522.

Scholzen T, Gerdes J (2000) The Ki-67 protein: from the known and the unknown. J Cell Physiol 182:311-322.

Seki T, Arai Y (1995) Age-related production of new granule cells in the adult dentate gyrus. Neuroreport 6:2479-2482.

Semo M, Peirson S, Lupi D, Lucas RJ, Jeffery G, Foster RG (2003) Melanopsin retinal ganglion cells and the maintenance of circadian and pupillary responses to light in aged rodless/coneless (rd/rd cl) mice. Eur J Neurosci 17:1793-1801.

Sethi CS, Lewis GP, Fisher SK, Leitner WP, Mann DL, Luthert PJ, Charteris DG (2005) Glial remodeling and neural plasticity in human retinal detachment with proliferative vitreoretinopathy. Invest Ophthalmol Vis Sci 46:329-342.

Shamsi FA, Boulton M (2001) Inhibition of RPE lysosomal and antioxidant activity by the age pigment lipofuscin. Invest Ophthalmol Vis Sci 42:3041-3046.

Silverman MS, Hughes SE, Valentino TL, Liu Y (1992) Photoreceptor transplantation: anatomic, electrophysiologic, and behavioral evidence for the functional reconstruction of retinas lacking photoreceptors. Exp Neurol 115:87-94.

Simeone A, Puelles E, Acampora D (2002) The Otx family. Curr Opin Genet Dev 12:409-415.

Simeone A, Acampora D, Gulisano M, Stornaiuolo A, Boncinelli E (1992) Nested expression domains of four homeobox genes in developing rostral brain. Nature 358:687-690.

Simeone A, Acampora D, Mallamaci A, Stornaiuolo A, D'Apice MR, Nigro V, Boncinelli E (1993) A vertebrate gene related to orthodenticle contains a homeodomain of the bicoid class and demarcates anterior neuroectoderm in the gastrulating mouse embryo. Embo J 12:2735-2747.

Sparrow JR, Boulton M (2005) RPE lipofuscin and its role in retinal pathobiology. Exp Eye Res 80:595-606.

Spence JR, Madhavan M, Ewing JD, Jones DK, Lehman BM, Del Rio-Tsonis K (2004) The hedgehog pathway is a modulator of retina regeneration. Development 131:4607-4621.

Spraul CW, Grossniklaus HE (1997) Characteristics of Drusen and Bruch's membrane in postmortem eyes with age-related macular degeneration. Arch Ophthalmol 115:267-273.

Spraul CW, Kaven C, Amann J, Lang GK, Lang GE (2000) Effect of insulin-like growth factors 1 and 2, and glucose on the migration and proliferation of bovine retinal pigment epithelial cellsin vitro. Ophthalmic Res 32:244-248.

Stevenson B, Anderson J, Bullivant S (1988) The epithelial tight junction: structure, function and preliminary biochemical characterization. Mol Cell Biochem 83:129-145.

Strauss O (2005) The retinal pigment epithelium in visual function. Physiol Rev 85:845-881.

Straznicky K, Gaze RM (1971) The growth of the retina in Xenopus laevis: an autoradiographic study. J Embryol Exp Morphol 26:67-79.

Streeten BW (1969) Development of the human retinal pigment epithelium and the posterior segment. Arch Ophthalmol 81:383-394.

Stroeva OG, Panova IG (1976) [Growth of the eye and pigment epithelium of the retina during postnatal development of rats]. Ontogenez 7:170-177.

Stroeva OG, Panova IG (1983) Retinal pigment epithelium: pattern of proliferative activity and its regulation by intraocular pressure in postnatal rats. J Embryol Exp Morphol 75:271-291.

Stroeva OG, Mitashov VI (1983) Retinal pigment epithelium: proliferation and differentiation during development and regeneration. Int Rev Cytol 83:221-293.

Takahashi T, Nowakowski RS, Caviness VS, Jr. (1992) BUdR as an S-phase marker for quantitative studies of cytokinetic behaviour in the murine cerebral ventricular zone. J Neurocytol 21:185-197.

Teakle EM, Wildsoet CF, Vaney DI (1993) The spatial organization of tyrosine hydroxylase-immunoreactive amacrine cells in the chicken retina and the consequences of myopia. Vision Res 33:2383-2396.

Thompson DA, Gal A (2003) Vitamin A metabolism in the retinal pigment epithelium: genes, mutations, and diseases. Prog Retin Eye Res 22:683-703.

Thomson JA, Itskovitz-Eldor J, Shapiro SS, Waknitz MA, Swiergiel JJ, Marshall VS, Jones JM (1998) Embryonic stem cell lines derived from human blastocysts. Science 282:1145-1147.

Tibber MS, Whitmore AV, Jeffery G (2006) Cell division and cleavage orientation in the developing retina are regulated by L-DOPA. J Comp Neurol 496:369-381.

Tropepe V, Hitoshi S, Sirard C, Mak TW, Rossant J, van der Kooy D (2001) Direct neural fate specification from embryonic stem cells: a primitive mammalian neural stem cell stage acquired through a default mechanism. Neuron 30:65-78.

Tropepe V, Coles BL, Chiasson BJ, Horsford DJ, Elia AJ, McInnes RR, van der Kooy D (2000) Retinal stem cells in the adult mammalian eye. Science 287:2032-2036.

Ts'o MO, Friedman E (1967) The retinal pigment epithelium. I. Comparative histology. Arch Ophthalmol 78:641-649.

Ts'o MO, Friedman E (1968) The retinal pigment epithelium. 3. Growth and development. Arch Ophthalmol 80:214-216.

Vandesompele J, De Preter K, Pattyn F, Poppe B, Van Roy N, De Paepe A, Speleman F (2002) Accurate normalization of real-time quantitative RT-PCR

data by geometric averaging of multiple internal control genes. Genome Biol 3:RESEARCH0034.

Verheijen R, Kuijpers HJ, Schlingemann RO, Boehmer AL, van Driel R, Brakenhoff GJ, Ramaekers FC (1989a) Ki-67 detects a nuclear matrix-associated proliferation-related antigen. I. Intracellular localization during interphase. J Cell Sci 92 (Pt 1):123-130.

Verheijen R, Kuijpers HJ, van Driel R, Beck JL, van Dierendonck JH, Brakenhoff GJ, Ramaekers FC (1989b) Ki-67 detects a nuclear matrix-associated proliferation-related antigen. II. Localization in mitotic cells and association with chromosomes. J Cell Sci 92 (Pt 4):531-540.

Verma AS, Fitzpatrick DR (2007) Anophthalmia and microphthalmia. Orphanet J Rare Dis 2:47.

Vernay B, Koch M, Vaccarino F, Briscoe J, Simeone A, Kageyama R, Ang SL (2005) Otx2 regulates subtype specification and neurogenesis in the midbrain. J Neurosci 25:4856-4867.

Vinding T (1990) Occurrence of drusen, pigmentary changes and exudative changes in the macula with reference to age-related macular degeneration. An epidemiological study of 1000 aged individuals. Acta Ophthalmol (Copenh) 68:410-414.

Vugler AA, Semo M, Jospeh A, Jeffery G (In Press) Survival and remodelling of melanopsin cells in retinal dystrophy. Visual Neuroscience.

Wallman J (1993) Retinal control of the eye growth and refraction. Prog Retin Eye Res 12:133-153.

Wallow IH, Tso MO (1973) Repair after xenon arc photocoagulation. 2. A clinical and light microscopic study of the evolution of retinal lesions in the rhesus monkey. Am J Ophthalmol 75:610-626.

Wan J, Zheng H, Chen ZL, Xiao HL, Shen ZJ, Zhou GM (2008) Preferential regeneration of photoreceptor from Muller glia after retinal degeneration in adult rat. Vision Res 48:223-234.

Wassle H, Boycott BB, Rohrenbeck J (1989) Horizontal Cells in the Monkey Retina: Cone connections and dendritic network. Eur J Neurosci 1:421-435.

Watzke RC, Soldevilla JD, Trune DR (1993) Morphometric analysis of human retinal pigment epithelium: correlation with age and location. Curr Eye Res 12:133-142.

Weissman IL, Anderson DJ, Gage F (2001) Stem and progenitor cells: origins, phenotypes, lineage commitments, and transdifferentiations. Annu Rev Cell Dev Biol 17:387-403.

Weiter J, Delori F, Wing G, Fitch K (1986a) Retinal pigment epithelial lipofuscin and melanin and choroidal melanin in human eyes. Invest Ophthalmol Vis Sci 27:145-152.

Weiter JJ, Delori FC, Wing GL, Fitch KA (1986b) Retinal pigment epithelial lipofuscin and melanin and choroidal melanin in human eyes. Invest Ophthalmol Vis Sci 27:145-152.

Wenzel A, Reme CE, Williams TP, Hafezi F, Grimm C (2001) The Rpe65 Leu450Met variation increases retinal resistance against light-induced degeneration by slowing rhodopsin regeneration. J Neurosci 21:53-58.

Wetts R, Fraser SE (1988) Multipotent precursors can give rise to all major cell types of the frog retina. Science 239:1142-1145.

Whittemore SR, Snyder EY (1996) Physiological relevance and functional potential of central nervous system-derived cell lines. Mol Neurobiol 12:13-38.

Williams RW (1991) The human retina has a cone-enriched rim. Vis Neurosci 6:403-406.

Wirz-Justice A, Da Prada M, Reme C (1984) Circadian rhythm in rat retinal dopamine. Neurosci Lett 45:21-25.

Xue LP, Lu J, Cao Q, Kaur C, Ling EA (2006) Nestin expression in Muller glial cells in postnatal rat retina and its upregulation following optic nerve transection. Neuroscience 143:117-127.

Young RW (1978) The daily rhythm of shedding and degradation of rod and cone outer segment membranes in the chick retina. Invest Ophthalmol Vis Sci 17:105-116.

Young RW (1985) Cell proliferation during postnatal development of the retina in the mouse. Brain Res 353:229-239.

Young RW, Bok D (1969) Participation of the retinal pigment epithelium in the rod outer segment renewal process. J Cell Biol 42:392-403.

Zhang HR (1994) "Scanning electron-microscopic study of corrosion casts on retinal and choroidal angioarchitecture in man and animals." ProgReteye Res 13 243-270.

Zhao S, Thornquist SC, Barnstable CJ (1995) In vitro transdifferentiation of embryonic rat retinal pigment epithelium to neural retina. Brain Res 677:300-310.

Zimmerman L, Parr B, Lendahl U, Cunningham M, McKay R, Gavin B, Mann J, Vassileva G, McMahon A (1994) Independent regulatory elements in the nestin gene direct transgene expression to neural stem cells or muscle precursors. Neuron 12:11-24.

Zinn KM MM (1979) The Retinal Pigment Epithelium. Cambridge, MA: Harvard University Press.

Znoiko SL, Crouch RK, Moiseyev G, Ma JX (2002) Identification of the RPE65 protein in mammalian cone photoreceptors. Invest Ophthalmol Vis Sci 43:1604-1609.

Zuber ME, Perron M, Philpott A, Bang A, Harris WA (1999) Giant eyes in Xenopus laevis by overexpression of XOptx2. Cell 98:341-352.